Optimal Control Methods for PV-integrated Shading Devices

by

Sung Kwon Jung

A dissertation submitted in partial fulfillment
of the requirements for the degree of
Doctor of Philosophy
(Architecture)
in the University of Michigan
2014

Doctoral Committee:

Associate Professor Jong-Jin Kim, Chair
Professor George Michailidis
Professor Kazuhiro Saitou
Professor Peter von Bülow

ACKNOWLEDGEMENTS

I dedicate this dissertation to my parents, whose support in every aspect was crucial during the entire course of my study. I also thank to my fiancée, Jeewon Kim, who has been waiting for me with priceless supports and few complaints. I owe a lot to Lux, who has been relieving my solitude with his unceasing love.

Encouragement from my friends including Gun Phil Jung, Seung Ho Lee, Ji Hoon Park, and Jin Goo Park, was of great help. I also thank to valuable friends of DC91: Hee Jong Lee, Moya Kim, Sang Yeon Jo, Sang Min Kim, Sung Woo Choi, and Youn Je Kim.

I am grateful to previous and current colleagues at the University of Michigan. Prof. Soo Young Kim, Prof. Sung Hoon Yoon, and Prof. Jin Woo Moon helped me since I arrived at Ann Arbor. Their research advices were precious assets to my study. Prof. Youngchu Kim, Dr. Yongha Hwang, and Nuri Bae provided kind help in the dissertation research and presentation. Dr. Yoonseok Choi, a visiting scholar, played an important role in the early stage of my dissertation research.

I sincerely appreciate inspirations and advices from many professors: Prof. Jean Wineman, Prof. James Turner, and Prof. Yong Yee Kim. I also thank to Prof. Jeongtae Kim; his short story kept me focused on my dissertation.

TABLE OF CONTENTS

LIST OF TABLES

Table

LIST OF FIGURES

Figure

LIST OF APPENDICES

Appendix

ABSTRACT

The main reason for the under-utilization of natural light is glare caused by excessive admission of daylight into interior spaces. Absence of a dynamic and effective shading control system entails leaving shading devices at a closed position for glare prevention. For increasing building energy efficiency, it is imperative to develop shading control methods that provide both visual comfort and electric lighting energy savings.

A tracking PV system has higher light-to-electricity conversion efficiency than its fixed counterpart. Previous studies on louver controls indicate that louver slat surfaces blocking sunlight receive higher solar radiation than a vertical or tilted-up position. As such, a louver coated with photovoltaics cells, when appropriately controlled, has potentials to achieve high energy production efficiency and visual comfort simultaneously. This is the motivation of the development of a novel hybrid of PV system and shading device: a PV-integrated shading device (PVIS).

The performance of a PVIS, whose louvers are coated with photovoltaic cells, was evaluated in terms of electricity production, daylight admission, and occupant visual comfort. Three different shading control methods were developed and tested: 1) maximizing the louver PV output only, 2) maximizing the PV output while meeting an indoor daylight level requirement, and 3) maximizing the PV output while satisfying an indoor daylight level and daylight glare criteria.

An artificial neural network was developed to predict the effect of solar radiation and slat tilt angle on PV output and visual comfort.

Through experimental testings, it was found that artificial neural network can effectively incorporated in the optimization of shading control. It was also found that the control method with the visual comfort criteria resulted in 9% reduction of PV output compared to that without them. The total building energy benefits of the control method with visual comfort criteria was at least 36% higher than that without due to the reduction of electric lighting energy consumption. Due to the PV-output criterion, the daylight glare remained within the comfortable range. For this reason, the glare criterion made no difference in louver tilt angle control.

CHAPTER 1: INTRODUCTION

PV-integrated shading devices (PVIS) have the potential to provide multiple benefits to buildings and occupants: they can shade windows to prevent glare and heat gain in the cooling seasons, produce electricity from PV cells, and bring in natural light. However, these potential benefits sometimes conflict, as increasing one beneficial outcome can reduce another. For instance, to maximize the energy production from the integrated PV cells, the shading device must be angled perpendicularly to the incident sunlight, which reduces the amount of daylight admitted to interior spaces. On the other hand, increasing the benefit of indoor lighting by allowing in more daylight decreases the shading effect of the device. Glare will increase, the occupants' visual comfort may be compromised, and the PV cells will produce less electricity.

In recent years, a variety of PVIS have been developed as building integrated photovoltaics (BIPV) typically installed on building facades and windows, but their multiple potential benefits have not been optimized. Most PV panels are installed on building envelopes to make a symbolic statement, not to provide an economically viable energy alternative. Thus the electricity produced by PV panels is prohibitively expensive, and their energy, thermal, and natural lighting benefits have been under-utilized.

This research is motivated by the under-utilization of PVIS. Optimal control methods for PVIS are developed and evaluated in this study.

CHAPTER 2: BACKGROUND

2.1 Photovoltaic (PV) systems

Solar power is one of the most promising, reliable, and environmentally friendly renewable energy technologies. It has the potential to significantly reduce reliance on fossil fuels, a resource that is quickly nearing exhaustion. Additionally, the substantial increase in the consumption of these fossil fuels has resulted in significant CO_2 emissions, accelerating the greenhouse effect: the cause of global warming. To confront this issue, it is necessary to replace fossil fuels with renewable resources such as wind and solar energy and to develop strategies for the effective use of natural resources. Although photovoltaics have traditionally been more expensive than grid power, the cost of PV cells has declined drastically in recent years. However, in densely populated metropolitan areas it is impractical to install large ground-based solar arrays. Therefore, urban PV systems must be integrated into buildings, which present an opportunity to pair energy supply with local energy demands. Building integrated photovoltaic (BIPV) systems have increasingly been incorporated into elements of recent building enclosure systems. Building-integrated PV can provide sufficient energy for small-scale buildings while producing significant energy savings (Kim and Gerow, 2013). Furthermore, building-integrated PV systems can be installed at cost equal to that of many current façade cladding systems. The advantages of BIPVs are significant, and, due to the potentially large savings, more and more countries are starting to develop and construct BIPV systems on a large scale (Schoen, 2001).

Advantages and disadvantages

Each kWp of PV installed as part of a BIPV system prevents the emission of approximately one ton of CO_2 per year (Archer and Hill, 2001). The advantages of BIPVs are further enhanced when PV panels are effectively utilized for multiple functions within the building system. A BIPV system that functions as a shading device, for example, will produce electricity and will also decrease building operational power usage by reducing heating and cooling loads.

BIPV systems can be a cost-effective alternative energy source. According to Lin and Carlson (2000), at peak power, a large-scale BIPV system has the potential to produce electricity at a cost comparable to that offered by a large, centralized power plant (less than 10 cents per kWh). They argue that as the cost of electricity storage keeps decreasing, a networked BIPV system could provide a reliable and cost-effective power source.

However, the energy production from BIPV systems is subject to climatic variations. If we are to rely on PV systems as an energy source, it is necessary to estimate their daily and seasonal power generation. Additionally, BIPV systems are expensive to install and construct; consequently, their development has depended upon government subsidies and tax benefits. As technology improves and systems become more widespread, competition and improvements in technology should drive these costs down.

The average Performance Ratio of BIPV system is 0.75 - 0.80 due to partial shadows, temperature effects, PV inverter losses, thermal losses, and various other factors. Furthermore, cell performance fluctuates due to variations in the working temperature, the inclination or

orientation angles, I-V characteristics resulting from the manufacturing process, etc. Thus, the output power of a complete BIPV system is lower than the sum of the total power-producing potential of each PV module (Roman et al., 2008).

Efficiency

The efficiency of BIPV systems depends on a number of factors. The factors include the energy conversion efficiency of the PV cells, cell temperature, irradiation, orientation of PV panels, and the efficiency of the system's electrical components such as the inverter and batteries. The theoretical maximum conversion efficiency for unconcentrated solar radiation is around 43% (Brendel, Werner, and Queisser, 1996). New technologies would further raise the maximum efficiency and actual efficiency. In 2011, the highest PV efficiency measured under standard conditions was 22.9±0.6% for crystalline, and 15.7±0.5% for copper indium gallium selenide (CIGS) thin film (Green, Emery, Hishikawa, and Warta, 2011). In 2013, the efficiency of multi-junction cells without concentrator, crystalline cells, and thin film reached 37.7%, 27.6%, and 20.4%, respectively (NREL, 2013). The fill factor, an indicator of cell efficiency, is the ratio of maximum power, which occurs at the maximum power point (MPP), to $I_{sc}*V_{oc}$. A higher cell temperature decreases fill factor. The fill factor of silicon crystalline cells without concentrator ranges between 68.5% and 90.3%, according to lab measurements (Kazmerski, 1997).

BIPV efficiency

When PV panels are integrated into a building, factors such as aesthetics often compete with efficiency. Many BIPV systems operate below their maximum electricity production potential because of a sub-optimal orientation due to design constraints. PV panels vertically installed on

a south wall had a yearly average efficiency of 10.3%, 9.7%, 6.0%, and 5.9% for single crystalline, poly crystalline, silicon film, and triple-junction amorphous, respectively. The results are based on BIPV efficiency measurement at the National Institute of Standards and Technology (NIST) (Fanney, Dougherty, and Davis, 2002). A case study on a grid-connected BIPV system in Hong Kong, located at the latitude of 22°16'N, reports a yearly average efficiency of 9%. The system consists of 21m^2 roof cladding and 34m^2 cladding on east, south, and west walls. It is capable of providing 41% of the electric lighting energy for a 250m^2 floor (Yang, Zheng, Lou, An, and Burnett, 2004).

Operational energy savings from BIPV

BIPV is a component of building envelope. Therefore, any evaluation of a BIPV system's cost effectiveness should consider the reduction in operational energy (heating, cooling, and lighting) from the use of PV panels, as well as the energy harvested by PV. Many BIPV systems often operate below their maximum electricity production potential because of their sub-optimal orientation. However, savings in operational energy can offset that loss.

Reduction in building operational energy can significantly shorten the payback time of BIPV systems. Rahdi (2010) examines three BIPV systems in the UAE. If PV electricity production is the sole criterion considered, the three systems have an average of 13 years of payback time. Because PV panels act as an additional insulation layer, however, they decrease cooling energy consumption. With the heat gain reduced by 27%, total energy for cooling decreases by 5.8% on average. This saving shortens payback time from 13 years to 3.3 years. Shading devices contribute much more to cooling load reduction than wall insulation, which has a greater effect

on heating load. Simulations of BIPV systems in London show that heating load decreases by 30% when the U-value of walls changes from 0.62 to 0.24. In the simulations, the use of external shading devices reduces cooling demand by 50% for a building with a window ratio of 0.6 (Yun, McEvoy, and Steemers, 2007). The PV atrium at Southampton University uses semi-transparent PV panels to reduce heat gain. The energy savings resulting from the use of photovoltaics as a shading system reduces the CO_2 payback time by anywhere from several months to three or more years (James, Jentsch, and Bahaj, 2009). When PV panels serve multiple purposes—e.g., electricity source, building envelope, and shading device—they become more cost effective (Yoon, Song, and Lee, 2011). BIPVs are a cost-effective alternative to conventional cladding systems (CIBSE, 2000).

BIPV as shading device

Using a BIPV system as a shading device offers significant benefits because of the system's dual nature. While a PV shading system produces electricity, it also decreases cooling load, further reducing energy consumption. However, simulations show that in temperate climates, the efficiency of a BIPV system as a shading device is highly dependent upon the season (Yoo, 2011). Although the solar irradiance in August (summer) is higher than in February (winter), energy generation is significantly higher in February due to PV cell surface temperature, partial shading, and the effective solar radiation (ESR) (Yoo and Lee, 2011). The shaded area, the reflectance factor of the wall surface, the transmission factor of the semi-transparent PV module, and the earth surface albedo significantly influence the effective solar radiation. Of these, shading on a solar cell is the critical factor in the operation of a BIPV, and therefore various approaches have been investigated to minimize its disadvantages (Hachem, Athienitis, and Fazio,

2011; Ishaque ans Salam, 2011; Reinders, van Dijk, Wiemken, and Turkenburg, 1999). According to a field measurement study, the maximum power generation of the BIPV as a shading device is not at due south, but at southeast or southwest in summer. Due to the highly variable influence of PV tilt angle, building azimuth and albedo on power generation, a dynamic BIPV shading system that reacts to the seasonal variation of environmental conditions would be the most effective application of BIPVs, having an even greater impact than improvements in cell efficiency (Yoo and Manz, 2011). Using windows with a electrochromatic layer, which changes its transmittance according to the electric load across it, combined with PV systems is an example of BIPV-based daylight transmission control (Ma and Chen, 2011). Windows with thermotropic glass are another example of daylight transmission control, but the transmittance of such windows depends on glass temperature instead of electric load (Inoue, 2003). Under irradiance of 400W/m^2, PV efficiency significantly decreases (Stamenic, Smiley, and Karim, 2004). Thus, when daylight availability is low, it is more effective to utilize daylight as natural lighting rather than as an electricity source.

The performance of BIPV systems can be improved through continued integration of sensors and responsive systems that maximize solar energy production and help to regulate thermal gains or losses, while still maintaining and providing optimal visual comfort. Proper orientation is the essential factor in PV performance. Simulations on a BIPV system installed on a building in Korea show that electricity generation can be increased considerably by correctly orienting the PV panels to the sun position (Yoon et al., 2011). Thus, BIPV systems must be able to respond to sensor inputs and the occupants' thermal needs to make real-time decisions regarding the

operation of a building and its subsystems (Kolokosta, Rovas, Kosmatopoulos, and Kalaitzakis, 2011).

2.2 Shading device control

Natural lighting has many advantages. Psychological benefits of natural lighting include satisfaction with work environment and the well-being of occupants (Edwards and Torcellini, 2002; Boyce, Hunter, and Howlett, 2003). In a survey of office workers, respondents reported higher job satisfaction with more sunlight penetration (Leather, Pyrgas, Beale, and Lawrence, 1998). Occupants' strong preference for windows, which provide natural lighting and a view to the outdoors, has been repeatedly documented (Nicol, Wilson, and Chiancarella, 2006). Despite the advantages of natural lighting, however, excessive admission of solar radiation into interior space is visually and thermally uncomfortable. For this reason, shading devices are often used.

Dynamic control systems are more efficient than fixed systems in terms of electric lighting energy consumption (Nielsen, Svendsen, and Jensen, 2011). A dimmable electric lighting system responding to daylight availability showed significant energy savings. Such a system can potentially reduce annual electric lighting energy consumption by 60%, according to simulations and field measurements (Roisin, Bodart, Deneyer, and D'herdt, 2008; Ihm, Nemri, and Krarti, 2009). Using adjustable window blinds combined with a dimmable lighting system can result in electric lighting energy savings of up to 60% (Reinhart, 2004). Li, Lam, and Wong (2006) estimate an annual lighting energy reduction of 33%, based on their field measurements. However, insufficient consideration of glare led occupants to manually set the system at a position where no uncomfortable glare occurred.

Despite the advantages of natural lighting, occupants often leave manually controlled window blinds in the closed position (Rubin, Collins, and Tibbott, 1978; Rea, 1984; Maniccia, Rutledge, Rea, and Morrow, 1999). When excessive daylight enters the interior space, occupants tend to sacrifice the benefits of daylight to avoid the discomfort glare (Boyce et al., 2003). They adjust shading devices when their surroundings become too dark or too bright, or when uncomfortable circumstances occur (e.g., distinct shadows, thermal discomfort, insufficient privacy). When shading devices can be controlled only manually, occupants tend to leave them in a closed position even after the uncomfortable condition no longer exists. The higher adjustment frequency of user-controllable automated blinds indicates that when occupants have easy access to shading device controls, they are willing to manipulate shading devices to suit their preferences (Reinhart and Voss, 2003).

BIPV systems, especially those that also function as shading systems, provide benefits beyond energy production and reductions in heating and cooling loads. They can also control and admit the appropriate levels of daylight into interior spaces, providing shading and glare reduction (Kim and Gerow, 2013). Visual comfort is imperative to occupant satisfaction and productivity, especially in an office setting. Consequently, glare reduction is an essential part of a successful BIPV system. Predicting glare is complex because of the variability of external lighting sources. The daylight glare index (DGI), an effective, empirically driven formula, has been developed in order to better anticipate glare. The DGI is a function of lighting source size and location, source and background luminance, and direction of view. DGI is calculated using the Hopkinson-Cornell large source glare formula, which takes into account the effect of the light source

luminance, background luminance, and the size and position of the light source in relation to the observer (Fisekis, Davies, Kolokotroni, and Langford, 2003).

Although a PV-integrated shading device has not yet been extensively studied, it has the potential to simultaneously achieve PV efficiency and occupant visual comfort. Vine, Lee, Clear, DiBartolomeo, and Selkowitz (1998) tested three control systems for an adjustable louver system combined with dimmable electric lighting. They found that when the sky was clear, the louver slats were usually at a tilted-down position regardless of whether the controls were automatic, semi-automatic, or manual. The majority of the occupants were satisfied with all three control methods (Vine et al., 1998). If PV modules were mounted on the tilted-down slats, they would have a high conversion efficiency due to their position, and the occupants' satisfaction with their visual environment would not be compromised. Although the post-experiment evaluation of daylight glare revealed no uncomfortable glare levels, Vine et al. did exclude glare from their lighting system control criteria. Systems with sensors that incorporate DGI data can precisely modulate daylight to reduce glare and improve occupant visual comfort. A pilot study on a PV-integrated louver also suggests that such a device can be controlled to achieve both visual comfort and the efficient energy conversion of PV modules installed on the shading device (Kim, Jung, Choi, and Kim, 2010).

Standard for acceptable light level

An acceptable light level of a work plane is 500 lux for general office tasks. Among the nine activity types defined by IESNA, the type of visual tasks involving medium contrast or small size corresponds to illuminance category E. The category E ranges from 500 lux to 1000 lux,

with a nominal illuminance of 750 lux. Therefore, 500 lux is the minimum acceptable value for office space (Murdoch, Harrold, and Goldsbury, 1996). A desirable light level can be achieved by natural lighting, by electric lighting, or by a combination of the two.

CHAPTER 3: RESEARCH SCOPE

3.1 Problems

Lack of shading control

Lack of shading control leads to occupant discomfort and waste of energy. In an office environment, worker comfort is of utmost importance in order to maximize productivity, and lighting conditions greatly influence occupant satisfaction. In addition, office workers prefer daylight to artificial lighting and desire easy access to the shading and lighting control systems that affect natural light transmittance (Galasiu and Veitch, 2006). However, occupants prefer not to adjust shading and control systems frequently. For these reasons, there is a need for shading systems with easy access and automatic control capability. When occupants have to rely on manual controls, they often use electric lighting even when abundant natural light is available to light interior space at an acceptable level (Galasiu, Atif, and MacDonald, 2004). The primary method of resolving this problem is illuminance-driven automatic lighting control. However, such a system is incapable of preventing daylight glare, which causes visual discomfort. When workers experience visual discomfort, their productivity inevitably decreases. Therefore, an automatic, easily accessible shading control system that considers daylight glare as well as illuminance is needed. However, even an advanced shading control system such as this can waste energy by reflecting or absorbing a large portion of the solar radiation that falls on the

shading device. This study considers a possible solution: integrating PV modules into a controlled shading device as a means of using this wasted energy.

Efficiency of building-integrated PV (BIPV) systems

To be efficient, BIPV systems must use adjustable PV panels that change orientation in response to exterior inputs such as sun azimuth and altitude, as opposed to fixed panels. BIPVs installed on walls lose efficiency due to their fixed orientation. Further loss in conversion efficiency and irradiance occurs at higher sun altitudes, especially during the summer, for south-facing BIPVs. Adjustable PV panels can serve a dual function; their louvers can control daylight admission into interior space while simultaneously converting light into electricity.

3.2 Hypotheses and research questions

This research tests the hypothesis that an optimal louver slat angle can maximize the combined benefits of a PVIS: visual comfort and electricity generation. Relative to passive systems such as fixed louvers or PVs mounted on walls, a dynamically controlled PVIS can increase both visual comfort and energy efficiency. In so doing, a PVIS control system faces conflicts regarding how best to use the solar radiation. Should it use the incoming solar radiation to provide natural lighting or to generate electricity? Should it adjust the slat angle to provide a bright work plane or to reduce daylight glare? Office workers can tolerate a wide range of illuminance levels but generally require 500 to 1,000 lux of light level on the work surface. When a space is naturally lighted, increasing daylight admission to achieve such a high work plane light level can cause excessive glare and visual discomfort; it would also decrease the electricity production of the PV modules installed on the louver slats. In short, the goal of increasing the work plane light level

conflicts with the goals of increasing PV output and reducing glare. On the other hand, decreasing daylight admission usually increases louver PV output. However, too little daylight admission into interior spaces can lead occupants to use energy-consuming electric lighting to prevent visual strain, especially when the work plane light level is unacceptable. These conflicts can be resolved with the use of PVIS devices dynamically controlled to an optimal tilt angle. PV-integrated shading devices should be controlled in ways that not only generate electricity but also achieve visual comfort.

3.3 Research objectives

The principal purpose of this study is to develop and evaluate optimal control methods for PVIS. Because PVIS is a hybrid PV system and shading device, it combines the benefits of these two systems. Maximizing these benefits is the aim of optimal control. This research investigates methods of achieving the maximum benefits of PVIS.

The objectives of this research and their corresponding research questions are as follows:

As a PV system,

1) does PVIS generate more electricity than wall-mounted BIPVs?

As a shading device,

2) can PVIS provide a comfortable lighting environment for occupants?

As a hybrid of both,

3a) does PVIS offer energy-saving benefits, and if so, what are they?

3b) what control method should PVIS employ to gain maximum benefits?

To answer these questions, optimal control methods to maximize PVIS benefits were devised and evaluated. The specific research objectives were as follows:

1) Develop a prototype motorized PV-integrated exterior louver with adjustable slat angles.
2) Develop ANN-based optimal control methods for a PV-integrated shading system.
3) Develop a wireless system for controlling motorized shading devices that can be operated from either a computer or a wireless node.
4) After building a scale model of a typical office space, experimentally measure the performance of a louver-type PV-integrated shading device using the criteria of electricity production and visual comfort. The wall PV output is compared to the louver PV output (Question 1). The work plane illuminance and DGI levels are evaluated in terms of the duration of acceptable level (Question 2). Energy benefits comprising electricity production and electric lighting energy savings are also evaluated (Question 3a). Optimal control methods are compared in terms of PV output, visual comfort, and their combined benefits (Question 3b).

3.4 Scope

In determining the optimal operation of the PVIS device, this research considers various energy and visual comfort factors:

1) PV electricity output
2) Work plane illuminance
3) Daylight glare

These three factors are dependent on other factors such as the louver slat tilt angle; therefore, they are the dependent variables in this study. Visual comfort is evaluated according to two

criteria: work plane illuminance and daylight glare. Daylight glare is estimated using the daylight glare index (DGI).

3.4.1 Factors affecting PV output, illuminance, and glare

Louver PV electricity output

The electricity output of the louver PV modules on a louver slat depends on solar availability, louver slat tilt angle, and the physical configuration of the louver. The factors affecting the solar radiation on a louver slat include sun position, sky condition, and reflectance of surrounding objects. The factors involving PV modules include PV efficiency, orientation, and PV coating fraction with regard to slat area. The PV module orientation depends on the slat tilt angle, which is the controlled variable in this study. The sky condition and the sun position are variables, but they are uncontrollable. The other factors are constants.

Visual comfort

Visual comfort can be defined as a state of mind caused by the luminous environment perceived by human eyes. The evaluation of visual comfort is quite subjective; therefore, precise estimation of an individual's visual comfort is almost impossible. However, several quantifiable and controllable factors can be used as general guidelines for the general population. These factors include the work plane illuminance and the daylight glare index (DGI), which are used to estimate visual comfort in this research.

The work plane illuminance depends on many factors. When a shading device is present, it has a major effect on the daylight admission into the interior space. A louver, which comprises multiple horizontal slats, controls the daylight admission by the slat tilt angle. Therefore, the work plane illuminance depends on solar availability and the slat tilt angle of the louver. The solar availability depends on the sky condition and the sun position. Other factors affecting the work plane illuminance include the reflectance of interior surfaces, the room geometry, the transmittance of windows, the number and size of windows, and electric lighting. These factors remain constant in this research.

The daylight glare index also depends on solar availability and louver slat tilt angle. The DGI equation considers four factors: window luminance, background luminance, window size subtended by an observer, and the viewing direction of the observer. The window luminance and the background luminance depend on the solar availability and slat tilt angle. The window size and the viewing direction are constants.

To summarize, the dependent variables are the PV electricity output, the work plane illuminance, and DGI. The independent variables affecting these dependent variables are the slat tilt angle, solar availability as estimated by exterior vertical illuminance, and sun position. The slat tilt angle is the only controlled variable. The other two variables are uncontrollable and thus measured or calculated. The other factors affecting the dependent variables are constants (See Table 3.1).

This study excludes the thermal factors associated with the use of a shading device (e.g., solar heat gain and heating/cooling load control). The PV module temperature, which significantly affects PV efficiency, is also excluded.

Independent variables	
Slat tilt angle	Controlled
Exterior illuminance	Measured
Sun position	Calculated
Dependent variables	
PV electricity output	Measured
Work plane illuminance	Measured
Daylight glare index	Measured
Constants	
Surface reflectances	
PV coating fraction	
Louver slat size and spacing	
Building geometry and location	
Window configuration	
Occupant position and viewing direction	
…	

Table 3.1 Variables and constants in this research

CHAPTER 4: RESEARCH METHOD

4.1 Overview

The research procedure has three steps: pre-experiment, experiment, and post-experiment; the components of each step are described below. Figure 4.1 illustrates the flow of activities and data between the components. Rectangles in the figure represent activities, and rounded rectangles represent algorithms, objects, or data.

Pre-experiment step

Before experiments were conducted, a test building and a PV-integrated louver were developed (see Section 4.6). A wireless data acquisition system consisting of sensors, microcontrollers, transceivers, and a PC software program was developed. A step motor controller was integrated into the data acquisition system (see Section 4.7).

An artificial neural network was configured before it was initially trained. A swing control was used to acquire initial ANN training data (see Sections 4.4 and 4.5). Optimal control methods (control goals) to be tested were devised (see Section 4.2). Each optimal control method has its own algorithms to be used during experiments.

Experiment step

Experiment procedures consist of estimating an optimal angle using an ANN and finding an actual optimum. The ANN was trained using the swing control in the pre-experiment step. No additional training took place during the experiments to avoid biased comparisons between control methods. Section 4.3.1 describes the optimization algorithm using an ANN, and Section 4.3.2 describes the control direction evaluation algorithm for finding an actual optimum.

Post-experiment step

The data collected during experiments were analyzed to evaluate the performance of PVIS and its control methods. The accuracy of the ANN was evaluated as well. Section 4.8 describes the analysis of results.

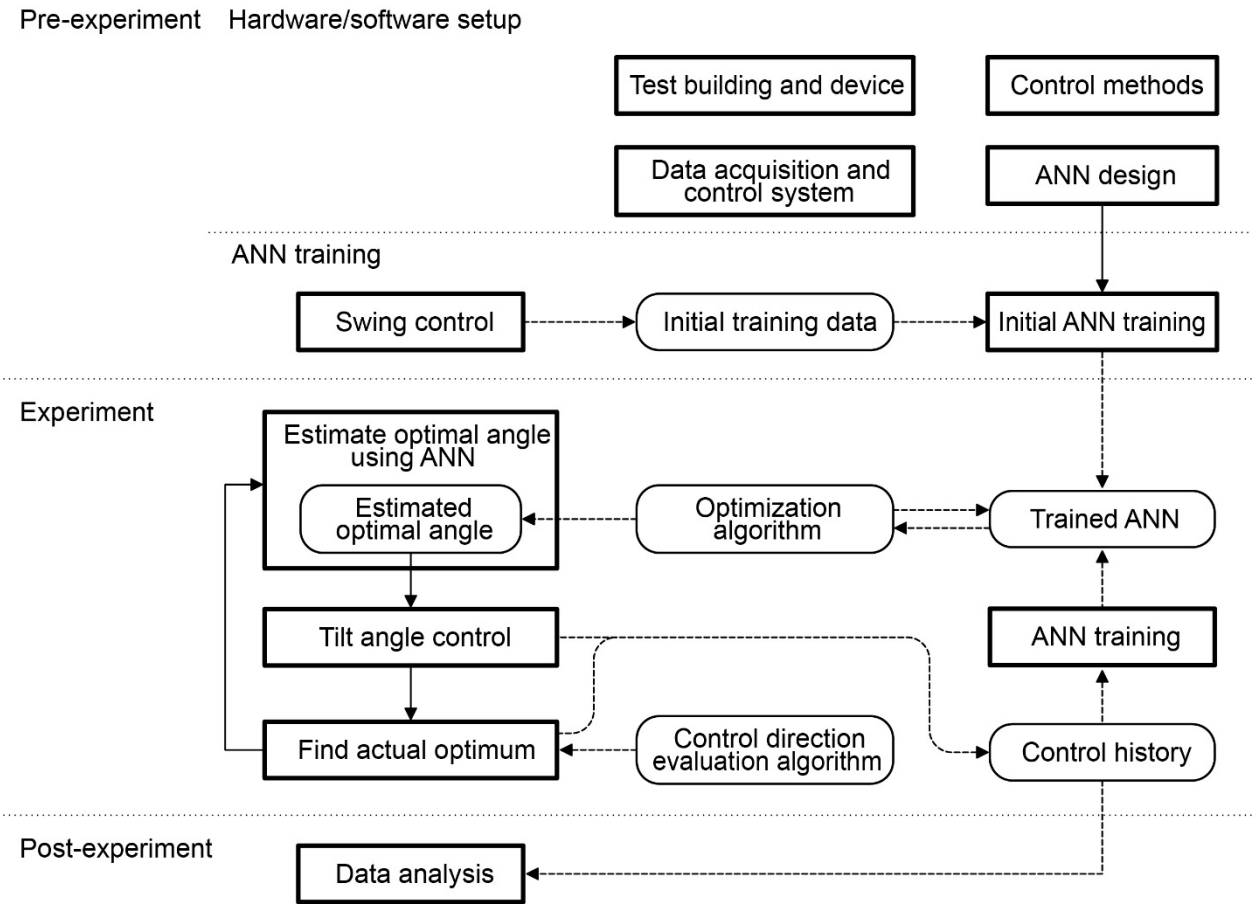

Figure 4.1 Research method overview

4.2 Optimal control methods

Optimization is generally defined as a process of finding one or more states of variables at which the objective function of the variables is minimized or maximized without violating given constraints. Thus an optimization problem consists of two parts: a domain or a search space, which depends on variable scopes and constraining functions, and an objective function to be minimized or maximized within the domain.

Depending on the criteria for optimization, three control methods were devised:

- PV output only

- PV output and work plane illuminance
- PV output, work plane illuminance and daylight glare index (DGI)

In this research, the objective is to maximize PV output because electricity generation is one of the key features of PVIS. Minimizing or maximizing any one of the three criteria (PV output, work plane illuminance, and DGI) could be an optimization objective. However, maximizing the work plane illuminance, an alternative optimization objective for PVIS control, has a few disadvantages. When a PVIS is controlled based on this objective, PV modules on the louver receive little daylight, while most daylight is utilized to illuminate the work plane. Such slat angle control leads to undesirable results: low louver PV output and high DGI. Minimizing DGI also has disadvantages. A lower source luminance and a higher background luminance cause a lower DGI, provided that the source size and the observation position are constant. For an adjustable louver, a tilt angle with minimal DGI usually results in low work plane illuminance due to low source luminance. For these reasons, these two criteria are used as constraints. Three combinations of the two constraints are used: no constraints, work plane illuminance only, and work plane illuminance and DGI. The control methods corresponding to each combination are referred to as **PV-only**, **PV+WP**, and **PV+WP+DGI**, respectively. It is also possible to use DGI alone as a constraint, but this study does not do so. However, Chapter 5 discusses the estimated results of the DGI-only method. These control methods are described below.

4.2.1 Optimal control method 1: PV-only

The only criterion of the PV-only method is the electricity output from PV cells on the louver slats. In addition to this criterion, the physical limits of the slat angle were used during optimization. The theoretical maximum range of the slat angle is between -90 and +90 degrees.

However, to avoid the mechanical malfunction caused by slat friction, a smaller range between -78 and +78 degrees was used in this study. The optimization problem can be formulated as follows:

Maximize PV output

Subject to

$-78^{\circ} \leq slat\ angle \leq 78^{\circ}$

This method is used to achieve the maximum electricity output of the shading device. Such optimization is useful particularly when a space is unoccupied and attaining visual comfort is therefore unnecessary.

4.2.2 Optimal control method 2: PV+WP

This method uses two criteria: PV output and work plane illuminance. The control goal is to maximize PV output while maintaining the work plane illuminance above 500 lux. The optimization problem of this method can be formulated as follows:

Maximize PV output

Subject to

$E_{WP} \geq 500$ lux

$-78^{\circ} \leq slat\ angle \leq 78^{\circ}$

Keeping the work plane illuminance, which depends on available daylight, above 500 lux may be impossible regardless of slat tilt angles. In that case, the control goal is to maximize the work plane illuminance, because the work plane illuminance criterion has higher priority. Maximizing PV output does not ensure that the work plane illuminance, one of the visual comfort criteria, stays above the acceptable level of 500 lux. To prevent such an unacceptable

situation, a work plane illuminance criterion is added to the PV output criterion. This method was compared with the PV-only method to evaluate the effect of the work plane illuminance criterion on PV output.

4.2.3 Optimal control method 3: PV+WP+DGI

In this method, the optimal angle is determined based on three criteria: PV output, work plane illuminance, and daylight glare. The control goal is to maximize PV output while keeping work plane illuminance above 500 lux and DGI below 22. When the work plane illuminance and DGI are both unacceptable, reducing DGI is the first goal.

Maximize PV output

Subject to

$E_{WP} \geq 500$ lux

$\text{DGI} \leq 22$

$-78^{\circ} \leq \textit{slat angle} \leq 78^{\circ}$

Daylight glare is one of the major reasons that occupants rely on artificial lighting. Concerns about glare often lead occupants to keep shading devices nearly closed throughout the day, which eliminates the benefits of daylight from windows. Therefore, suppressing daylight glare is crucial in automated shading device control. Because achieving an acceptable work plane illuminance does not necessarily prevent daylight glare, the DGI criterion was added to the PV+WP method. This method was compared with the PV-only and the PV+WP methods to identify the effect of the DGI criterion on PV output.

4.3 Optimal control of slat tilt angle

One cycle of the optimal angle control in this study consists of two steps. The first step uses an optimal angle estimated by an ANN. Estimation of optimal angle uses a grid search algorithm and a comparison algorithm. The slat tilt angle is adjusted to the estimated optimal angle; this procedure is described in Section 4.3.3. In the second step, the slat angle is adjusted from the estimated optimum to an actual optimum by exploring adjacent angles. A control direction evaluation algorithm is used after each angle adjustment to determine the direction of the next adjustment; this procedure is described in Section 4.3.4. The angle comparison algorithm and the control direction evaluation algorithm depend on the active control method in use: the PV-only, the PV+WP, or the PV+WP+DGI method (see Figure 4.2).

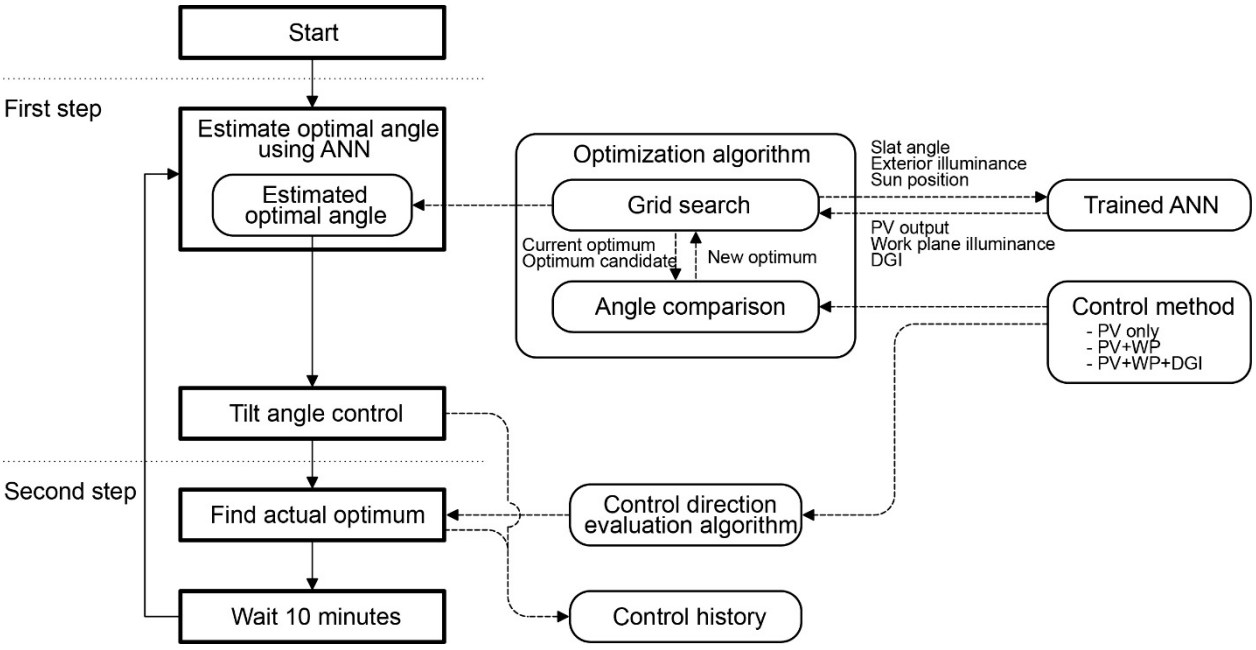

Figure 4.2 Flow of optimal angle control

4.3.1 Combination of logical global search and physical local search

As described above, a slat angle control cycle consists of a logical global search followed by a physical local search. Because the objective of the optimal control is to find a physical optimal angle, a physical search performed by adjusting slat angle is crucial in reaching an optimum. The search for an optimum can be performed on either the entire domain (global search) or a partial domain (local search). Each search method has advantages and disadvantages.

Physical local search

A physical local search requires fewer angle adjustments than a global search, resulting in a shorter search time. However, due to the nature of a local search, there is no guarantee that a local maximum found by the local search is always a global optimum.

Physical global search

In contrast, a physical global search finds a global optimum if it examines the entire search space before its termination. However, it also has a few disadvantages. A global search visits every angle between the lower and upper bounds of the slat angle; therefore, the number of angle adjustments is greater than in a local search. In addition, daylight admitted into an interior space is repeatedly changed during the search, which makes multiple slat angle adjustments. This also occurs during a local search, but the magnitude of change is often greater in a global search. Frequent angle adjustment can cause visual discomfort. Moreover, a global search results in a longer duration of non-optimal slat angle than a local search. This leads to a decrease in the louver PV output. For these reasons, this study employed a logical global search using an ANN to avoid the disadvantages of a physical search.

Logical search using an ANN

Estimating an optimum using an ANN is a logical search. Because the search space is small (there is a single discrete variable with 53 candidate solutions), it is possible to perform a global search that yields a global optimum. The difference between the estimated global optimum and a physical optimum depends on the accuracy of the ANN, but there is no guarantee that the two optima always coincide regardless of the ANN's accuracy. As discussed above, a physical optimum can be found only by a physical search, local or global. In addition, even when the slat angle is to be controlled to the logical optimum without a physical search, it is necessary to find a physical optimum to evaluate the accuracy of the estimated optimum for research purposes. For these reasons, the logical global search using an ANN is combined with a physical local search.

Combination of logical global search and physical local search

Estimation of an optimum using an ANN is followed by a physical local search. This process can be described as a 'physical local search starting at a logical global optimum.' The goal of using an estimated optimum in the first step of the optimal control is to reduce the number of angle adjustments. Such a reduction is achieved by performing a physical local search. The ANN-based logical optimization assists the physical local search in finding an optimum. Beginning a local search at a logical optimum that was estimated using a well-trained ANN raises the probability that the local search will reach a global optimum. However, using an ANN to reach a global optimum can result in a suboptimal local maximum, especially when the ANN is incorrectly trained and multiple local maxima exist.

4.3.2 Status of optimal control

The first step of the physical local search by the trial-and-error control is to evaluate the current status of an optimization problem according to the status of dependent variables (PV output, work plane illuminance, and DGI). There are four possible statuses, which fall into two categories:

- Intermediate status
  - Acceptable but suboptimal
  - Unacceptable but improvable
- Terminal status
  - Acceptable and optimal
  - Unacceptable and non-improvable

The acceptable status implies that every constraining criterion is satisfied. In other words, the slat angle is in a feasible domain: the range of the slat angle satisfies given constraints, if any. The unacceptable status occurs when any constraining criterion is violated. For the PV-only method, the status of variables is always acceptable because no constraining criteria exist. For the PV+WP method, the unacceptable status occurs when the work plane illuminance is below 500 lux. For the PV+WP+DGI method, it occurs when the work plane illuminance is below 500 lux and/or DGI is higher than 22. If the slat angle can be adjusted toward a feasible domain (that is, if the work plane illuminance can be increased or DGI can be decreased), the unacceptable status is ‘unacceptable but improvable.’ Otherwise, it is ‘unacceptable and non-improvable,’ which occurs when no feasible domain exists. A status in which PV output can further be increased within the domain is ‘acceptable but suboptimal.’

An optimization problem status is deemed ‘acceptable and optimal’ when PV output is at maximum and the constraining factors are acceptable. The ‘acceptable but suboptimal’ status occurs when PV output is not at maximum but the constraining factors are acceptable. In the ‘acceptable but suboptimal’ status, an additional angle adjustment can increase PV output while other criteria remain acceptable. The trial-and-error control terminates when the dependent variables reach a terminal state: either ‘acceptable and optimal’ or ‘unacceptable and non-improvable’ (see Figure 4.3).

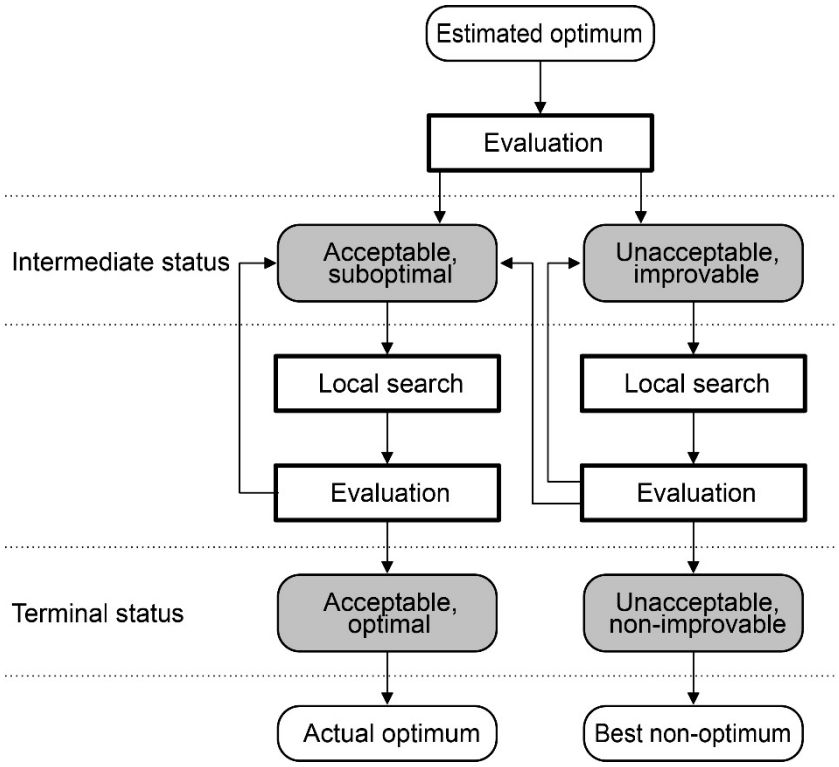

Figure 4.3 Change of optimization problem status

4.3.3 Estimation of optimal angle using ANN

In this study, the goal of the optimization process was to find the value of a single discrete variable, slat tilt angle, that maximized the louver PV output. The number and type of

constraining functions differ depending on the control method used (see Section 4.2 for details). Because PV output, work plane illuminance, and DGI depend on daylight availability, which continuously changes, and on other surrounding conditions, which are specific to a building site, predicting these variables before a louver is actually installed is almost impossible. Acquiring their mathematical expressions to use in optimization is also difficult due to the complexity of their relation to daylight availability and surrounding conditions. For these reasons, using an ANN is a reasonable strategy for optimal control.

Global search (grid search) algorithm using an ANN

The optimization in this research uses the grid search algorithm, also known as brute-force search or exhaustive search. The grid search algorithm explores every possible combination of variables. For any given maximization problem, the combination with the highest objective function value is found after repeated comparisons between one combination and another. If a combination of variables violates a constraint of the optimization, it is excluded from the candidate solutions. In general, grid search algorithm is inefficient in terms of computation time if the search space is large. Fortunately, the search space in this research is very small; there are only 53 candidate angles. Slat tilt angle ranges between -78 and +78 degrees. It has a step size of 3 degrees. Therefore, it can have 53 discrete values. The ANN output variables are calculated by feed-forwarding the input variables. The slat tilt angle, one of the input variables, is changed from -78 to +78 degrees in increments of 3. The other three variables are current exterior vertical illuminance, solar altitude, and solar azimuth. Of the 53 sets of input variables, one that yields output variables closest to an optimum is selected. The tilt angle of the selected set is an

optimal angle. Because the tilt angle is a discrete variable, a higher PV output may occur at an angle between two discrete angles. However, the difference is assumed to be negligible.

The grid search algorithm using an ANN in this study is as follows:

Let n be the size of the set of slat angle, S_i the set of ANN output variables associated with the i-th slat angle, $comp(S_i, S_j)$ a function that compares the i-th output variable set with the j-th and returns the index of the one that wins the competition, OPT the index of current optimal angle, and $CAND$ the index of an optimum candidate. The set of output variables consists of PV output, work plane illuminance, and DGI. The elements of the i-th set are denoted as PV_i, WP_i, and DGI_i. The grid search is performed in the following steps:

Step 1: $OPT \leftarrow 1$, $CAND \leftarrow 2$

Step 2: $OPT \leftarrow comp(S_{CAND}, S_{OPT})$

Step 3: $CAND \leftarrow CAND+1$

Step 4: if $CAND > n$ return OPT, else go to *Step* 2

In the first step, the first index of the slat angle is assigned to the current optimum (*OPT*), and the second index is assigned to the optimum candidate (*CAND*). The current optimum is updated to the index selected by a comparison function in the second step. The index of the optimum candidate is increased by one in the next step. Steps 2 and 3 are repeated until the index of the optimum candidate exceeds n, the total number of slat angles to be examined. When the grid search terminates, the angle corresponding to the current optimum index (*OPT*) is optimal.

Comparison functions

The comparison function used in the second step of the grid search algorithm, $comp(S_{CAND}, S_{OPT})$, differs according to the type of optimal control method. The three control methods (PV only, PV+WP, and PV+WP+DGI) have their own comparison functions. The comparison function for the PV-only control method, $comp_{PV}$, is as follows:

$comp_{PV}(S_{CAND}, S_{OPT})$

if ($PV_{CAND} \geq PV_{OPT}$) return *CAND*

else return *OPT*

The function returns the index of the variable set with a PV value greater than or equal to that of the other set. If the new candidate is selected from the comparison, it replaces the current optimum. Otherwise, the current optimum remains unchanged. By performing such comparisons for the entire range of slat angles, the optimization algorithm can find the optimal slat angle with the maximum PV output.

The comparison function for the PV+WP method, $comp_{PV+WP}$, is as follows:

$comp_{PV+WP}(S_{CAND}, S_{OPT})$

if ($WP_{CAND} \geq 500$ AND $WP_{OPT} \geq 500$), return $comp_{PV}(S_{CAND}, S_{OPT})$

else if ($WP_{CAND} \geq WP_{OPT}$) return *CAND*

else return *OPT*

This function checks whether the work plane illuminance of each variable set is greater than or equal to 500 lux. If both sets satisfy the criterion, the function compares their PV output by calling the PV comparison function $comp_{PV}(S_{CAND}, S_{OPT})$. Otherwise, it returns the index of the variable set with a work plane illuminance value greater than or equal to that of the other set. If

the new candidate is selected from the comparison, it replaces the current optimum. Otherwise, the current optimum remains unchanged.

The comparison function for the PV+WP+DGI method, $comp_{PV+WP+DGI}$, is as follows:

$comp_{PV+WP+DGI}(S_{CAND}, S_{OPT})$

if ($DGI_{CAND} \leq 22$ AND $DGI_{OPT} \leq 22$) return $comp_{PV+WP}(S_{CAND}, S_{OPT})$

else if ($DGI_{CAND} \leq DGI_{OPT}$) return *CAND*

else return *OPT*

It is similar to $comp_{PV+WP}(S_{CAND}, S_{OPT})$, except that it compares DGI first. If the DGIs of both sets are smaller than or equal to 22, it compares their work plane illuminance by calling $comp_{PV+WP}$ with the same parameters. The called function, $comp_{PV+WP}(S_{CAND}, S_{OPT})$, then evaluates their work plane illuminance and either returns a solution or calls the PV comparison function, $comp_{PV}$. Otherwise, it returns the index of the set with a DGI value smaller than or equal to that of the other set.

The comparison functions select the first (left) parameter when two parameters have identical elements. For example, $comp_{PV}(S_{CAND}, S_{OPT})$ chooses *CAND* when PV_{CAND} is equal to PV_{OPT}. Placing the current optimum (S_{OPT}) in the second argument enables the function to select a new candidate when the element being compared is identical to that of the current optimum.

4.3.4 Slat control to an optimum estimated by ANN

The first step is to set the louver slats to an estimated optimal angle obtained from the optimization algorithm. If the slats are already at the optimal angle, this step is skipped. The

current slat angle is adjusted toward the new estimated optimal angle by a step size (three degrees). Because multiple steps exist between the current angle and the new angle, a step angle adjustment is repeated until the slat angle reaches the estimated optimal angle with an interval of ten seconds. The next step is to perform a physical local search starting from the current angle using the trial-and-error method. This step is described in Section 4.3.2. The slat angle set by the trial-and-error control stays for an idle period of 10 minutes before a new control cycle begins (see Figure 4.4). The slat angle is controlled between 8am and 6pm Eastern Standard Time (EST). For the sake of consistency, Eastern Standard Time is used instead of Eastern Daylight Time (EDT) during the daylight saving period. When the exterior vertical illuminance is below 5,000 lux after 5pm, the slat angle control is forced to terminate because no higher daylight level is expected after the moment. When such a low illuminance occurs before 5pm due to heavy cloud cover, the angle control remains active. According to the pretests, the vertical PV output was insignificant (below 0.5mA), and the work plane illuminance was very low (below 100 lux) when the exterior vertical illuminance was below 5,000 lux. Because the louver control offers little benefit when daylight is insufficient for electricity generation and interior lighting, it terminates after setting the slats at the horizontal position.

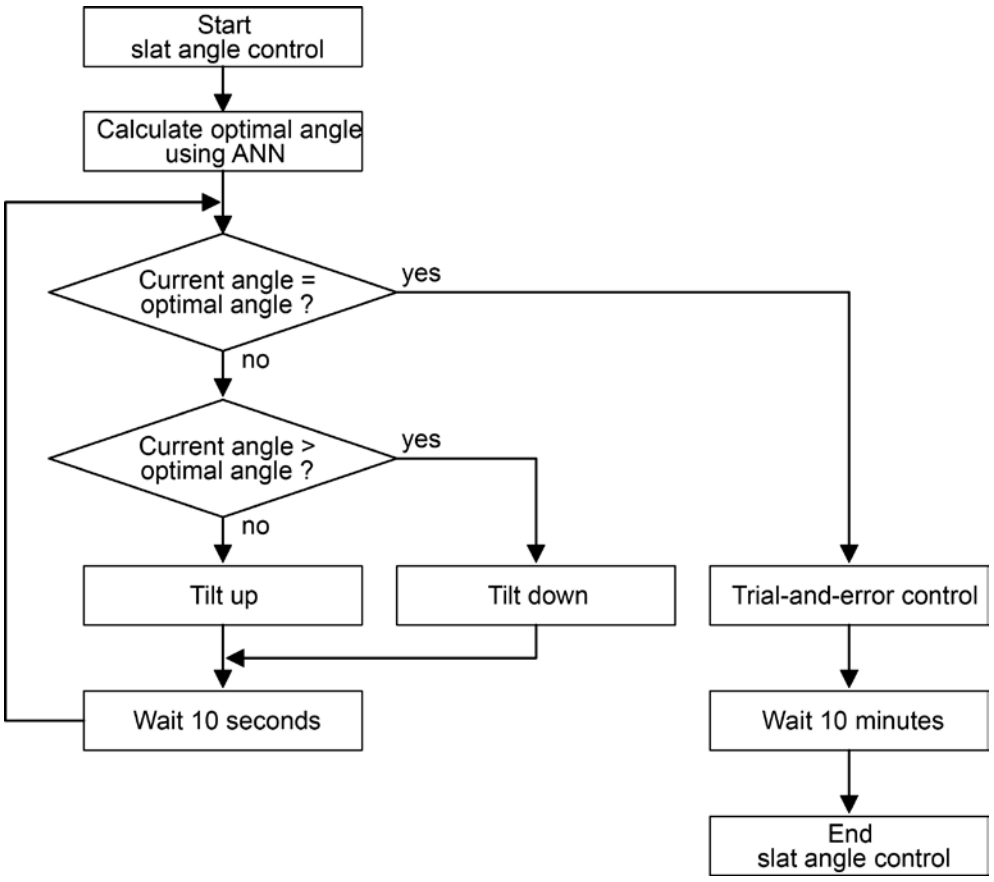

Figure 4.4 Flow of slat angle control

4.3.5 Trial-and-error control

The trial-and-error control performs a physical local search by actually adjusting the slat angle. It tests whether a better solution exists by searching angles adjacent to the logical optimum estimated using an ANN. This test is necessary because there is no guarantee that the estimated optimum coincides with the physical optimum. In other words, the ANN-based estimated optimum is valid only within the model of inter-variable relations constructed in the ANN through training. In addition, the accuracy of the ANN should be evaluated by comparing it to the actual optimum. Only after the estimated optimum based on the ANN proves to be close to

the actual optimum should the estimated optimum be used without correction using the trial-and-error control.

The trial-and-error control starts by determining an initial control direction. When the current slat angle is in an infeasible domain, where any criterion is violated, a direction that moves the angle toward a feasible domain is selected. For example, if the work plane illuminance is below 500 lux when the criterion is included in the control method (PV+WP or PV+WP+DGI), a direction increasing the work plane illuminance is selected. For the PV-only method, a tilt-down direction is selected because no constraints are present and the ANN already estimates the current angle as an optimum. However, a higher PV output may exist at a different slat angle. The initial direction is determined by using the comparison functions for the ANN-based optimization algorithm (see Section 4.3.3). When no constraints are violated, a direction increasing the louver PV output is selected.

Because the initial direction is based on the ANN's logical estimation, the physical angle adjustment can have opposite results. For example, the louver PV output can decrease after an angle adjustment for a higher PV output. Therefore, each adjustment is evaluated to check whether the adjustment coincides with the estimation. If the adjustment is incorrect, the opposite control direction is selected for consequent adjustments. Otherwise, the next angle in the current direction is checked.

A variable, *reverse count*, is used to check the control termination conditions. It represents the number of incorrect control directions. After an incorrect control direction, the control direction

is reversed and the reverse count is incremented by one. Two incorrect directions followed by a final adjustment ends a trial-and-error control cycle. Because two incorrect directions are allowed, the sequence of directions is as follows: an initial direction, the opposite direction, and the initial direction (see Figure 4.5).

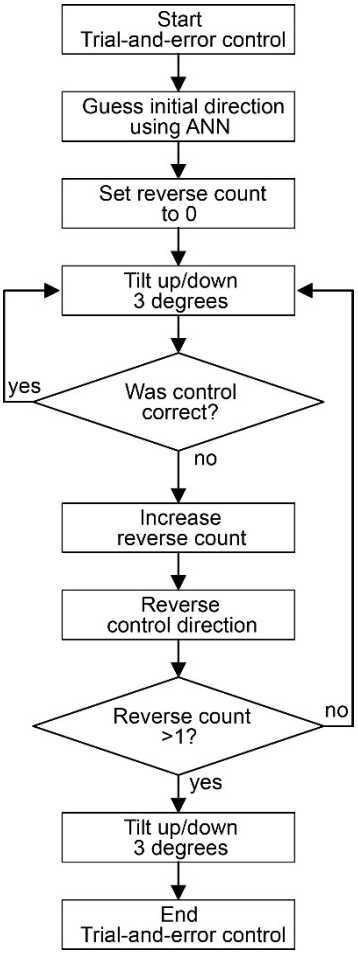

Figure 4.5 Process of trial-and-error control

At the beginning of a control cycle, a logical global optimum is acquired using the ANN. The current exterior illuminance and sun position are used for ANN feed-forwarding. After the slat angle is adjusted to the estimated optimum, the trial-and-error control begins. The trial-and-error

starts at the estimated optimum, which serves as a best-guess initial angle for the physical search. Each angle adjustment is followed by a 10-second idle period for sensor data acquisition. Two measurements are acquired with an interval of 5 seconds during the period. The trial-and-error control terminates after the control direction is reversed twice. A control cycle terminates on the completion of the trial-and-error control. Each control cycle is followed by a 10-minute idle period. During the idle period, the slat angle stays unchanged. The error of the ANN is the difference between the estimated optimum and the actual optimum found by the trial-and-error control. This error is used to evaluate the accuracy of the ANN. The error of an accurate ANN is expected to be small in magnitude and frequency. Figure 4.6 illustrates the change of slat angle during an angle control cycle.

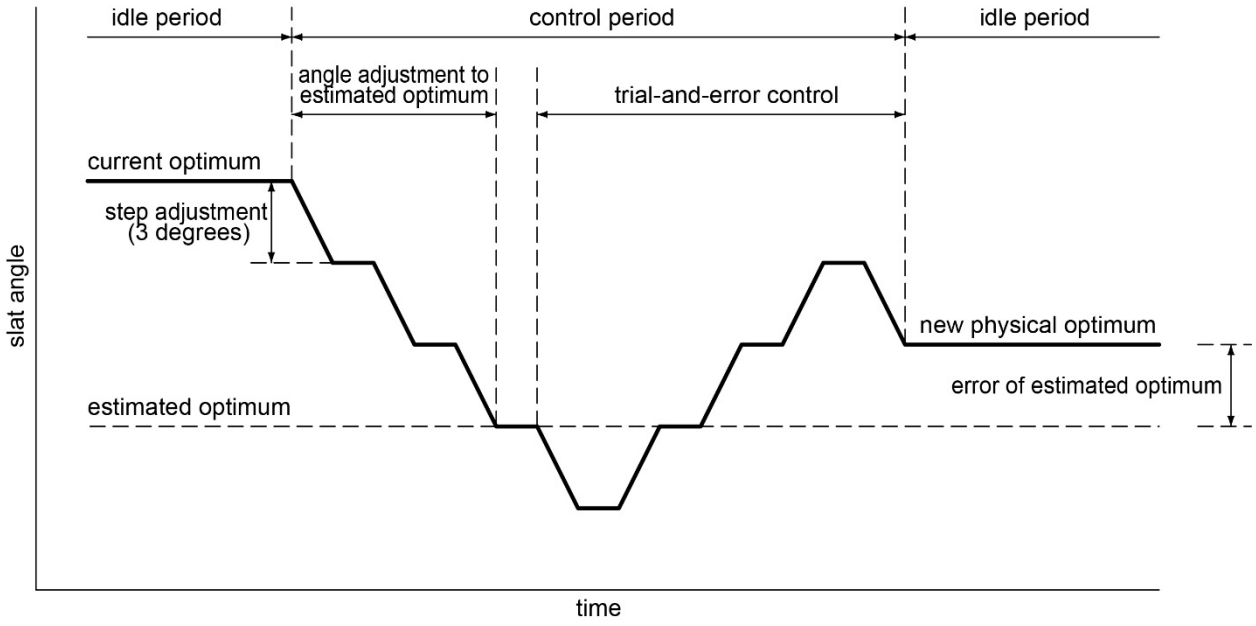

Figure 4.6 Change of slat angle during an angle control cycle

4.3.6 Evaluation of control direction

4.3.6.1 PV-only method

In this method, an angle adjustment is considered incorrect if it decreases PV output; otherwise, it is correct. A higher PV output is always preferred. This method does not use the work plane illuminance or DGI criteria (see Figure 4.7).

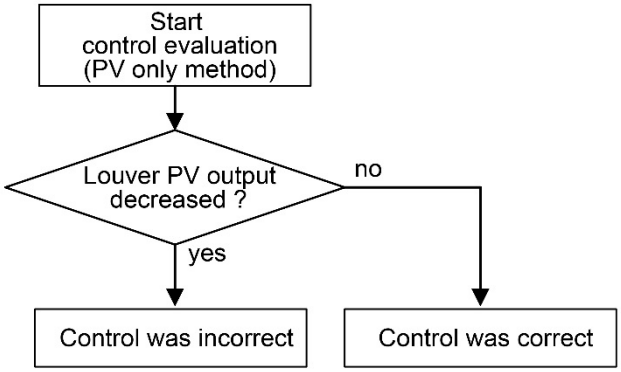

Figure 4.7 Evaluation of control direction (PV-only method)

4.3.6.2 PV+WP method

In this method, maintaining the light level of the work plane above an acceptable level takes priority. Increasing PV output is attempted only when the work plane illuminance is acceptable. The work plane illuminance before adjustment is compared with that after adjustment. The comparison leads to one of four cases: both are acceptable, change from unacceptable to acceptable, change from acceptable to unacceptable, and both unacceptable. In the first case (both acceptable), change of PV output is considered. The process is identical to that described in the section on the PV-only mode. In the second case (from unacceptable to acceptable), the adjustment is correct because the slat angle has entered a feasible domain. In the third case (from acceptable to unacceptable), the adjustment is incorrect because the slat angle has become

out-of-domain. In the last case (both unacceptable), increasing the work plane illuminance is a correct adjustment (see Figure 4.8).

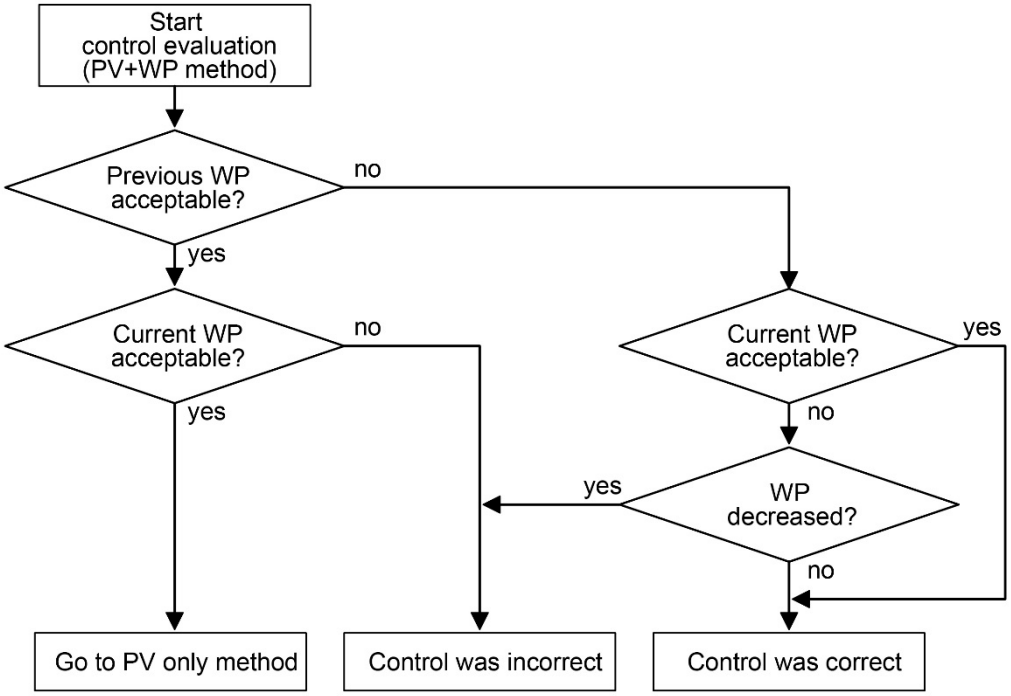

Figure 4.8 Evaluation of control direction (PV+WP method)

4.3.6.3 PV+WP+DGI method

The evaluation method for this mode is similar to that for the PV+WP mode, except that DGI has the highest priority. The DGI before adjustment is compared with that after adjustment. The comparison leads to one of four cases: both are acceptable, change from unacceptable to acceptable, change from acceptable to acceptable, or both unacceptable. In the first case (both acceptable), the method for PV+WP mode is used because the DGI criterion is inactive (see Section 4.3.3.2). In the second case (from unacceptable to acceptable), the adjustment is correct.

In the third case (from acceptable to unacceptable), the adjustment is incorrect. In the last case, neither is acceptable. In that case, decreasing DGI is a correct adjustment (see Figure 4.9).

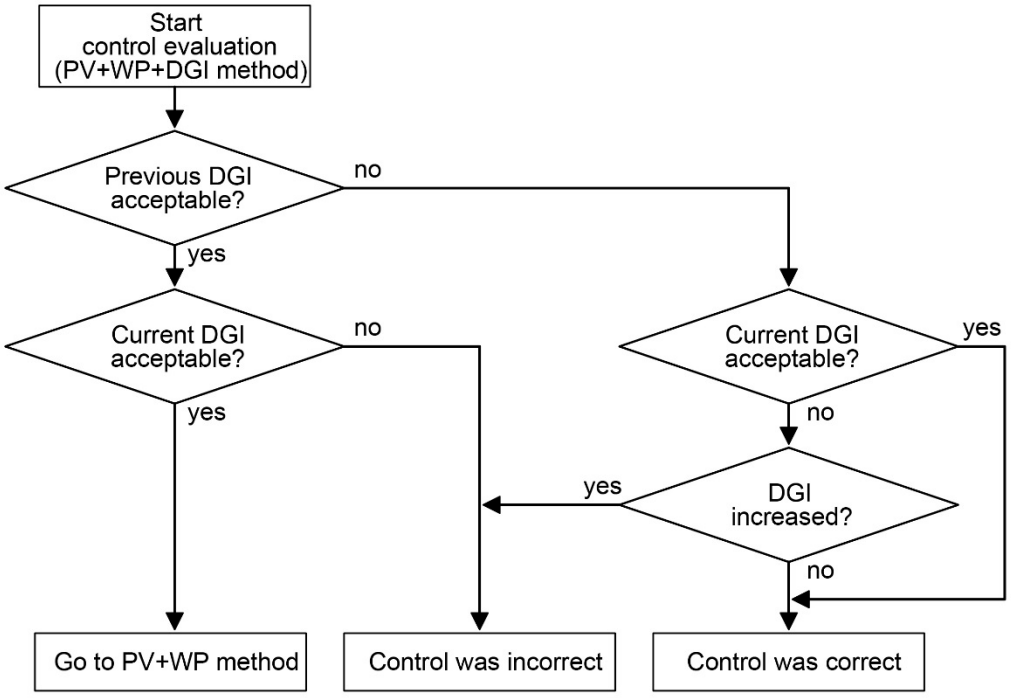

Figure 4.9 Evaluation of control direction (PV+WP+DGI method)

4.4 Artificial Neural Network (ANN)

Artificial neural networks are often used for building control and PV systems (Chen, Duan, Cai, and Liu, 2011; Kalogirou, 2001; Kalogirou and Bojic, 2000; Moon and Kim, 2010; Mozer, 1998). An artificial neural network was used to estimate the objective function value (louver PV output) and the status of the constraints (work plane illuminance and DGI) at a slat angle. The estimation is also based on the measured exterior illuminance and calculated sun position at the moment of estimation.

4.4.1 ANN configuration

There are several guidelines regarding the number of hidden layers, the number of hidden units, training methods, and many other ANN parameters. Reed and Marks (1999) list the following factors that must be considered in the design of an ANN:

- Selection of input and output variables
- Preparation of training data
- Structure of the ANN (number of hidden layers, number of neurons)
- Type of error function
- Weight updating method (learning rate, momentum, etc.)
- Use of heuristics
- Evaluation of the ANN's generalization capability

4.4.2 Input and output variables

The input variables of the ANN used for the experiments were exterior vertical illuminance, louver slat tilt angle, solar altitude, and solar azimuth. Additional variables that might increase ANN accuracy include solar profile angle, source luminance, and background luminance, which are functions of the four input variables. For this reason, they were excluded from the ANN. The output variables were louver PV output, work plane illuminance and DGI. The ANN is trained with the actual value of the variables.

4.4.3 Preparation of training data

The training data were acquired using the swing control before the optimal control experiments. The period for the training data collection was between 3/24/2012 and 3/27/2012, two weeks prior to the optimal control experiments.

4.4.4 Selection of ANN training data

ANN training data should represent input and output variables as closely as possible. In this study, training the ANN with swing control data without filtering presented a few problems. The slat tilt angle controlled using optimal control methods can stay within only a small range. This causes a bias in training data, as a few similar angles dominate in number. The bias decreases the accuracy of ANN output for slat tilt angles with fewer training data entries. Furthermore, the size of training data can grow very large, but data storage is limited. In addition, sensor measurements acquired during daylight fluctuation had errors due to the time gap between measurements. For these reasons, the training data were selected from the sensor measurement data with some selection criteria. The size of the training data was also limited at the pre-determined value.

Criteria of training data selection

Each ANN input variable is divided into small segments and each polyhedron represents a combination of segmented input variables. Each polyhedron has a finite number, three in this study, of sensor measurement data of dependent variables. Two samples are in the same polyhedron if:

the difference in slat angle < 3 degrees and

the difference in exterior vertical illuminance < 2,500 lux and

the difference in solar altitude < 2.5 degrees and

the difference in solar azimuth < 5.0 degrees.

When a new training data is to be added to the training dataset, it is processed based on the following algorithm:

If the number is greater than or equal to a maximum number of similar samples

update the oldest similar sample with the given one

Else if the dataset is in its maximum size

update the oldest sample with the given one

Else

add the given sample to the dataset

This algorithm updates the training dataset with the most recent sensor measurements while keeping the size of training data within the predetermined limit.

4.4.5 Weight update method

Back propagation learning algorithms

Learning algorithms that can be applied in artificial neural networks include supervised learning, unsupervised learning, reinforcement learning, and temporal learning (Golden, 1996). This study used the back propagation method, which is one of the supervised learning methods for ANN. Because the experiment data have input (stimulus) and output (desired response), an ANN can be trained with the supervised learning method. Back propagation is the most common method for training multilayer perceptrons.

On-line back-propagation algorithm

The on-line back propagation method is a general form of the classic ANN algorithm. It uses differentiable functions. A differentiable nonlinear non-decreasing function is commonly used as an activation function. Typically, sigmoid ($1/(1+e^{-x})$) is used as an activation function in the

on-line back propagation method (see Figure 4.10). The hyperbolic tangent (tanh) function is another common activation function. In this study, the classic on-line back propagation was used.

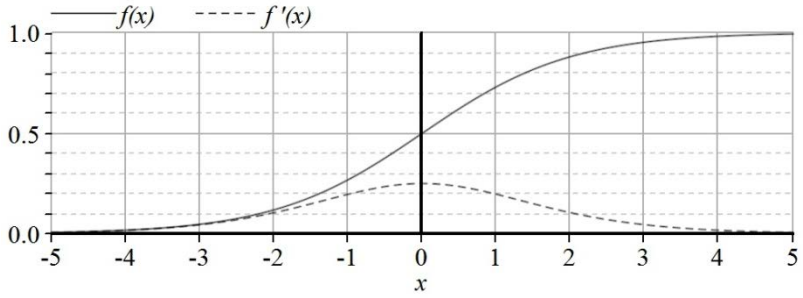

Figure 4.10 Sigmoid function ($f(x)$) and its derivative ($f'(x)$)

Classical on-line back propagation algorithm

The on-line back propagation algorithm comprises the following steps. A three-layer neural network with a hidden layer is used as an example. Each layer has two neurons.

(1) Initialization

(a) Initialize weights and biases of neurons with random values within a small range. Every random value is between -1 and 1 in this study.

(2) Feed-forward (see Figure 4.11)

(a) Randomly pick training data from the training dataset and apply it to the input layer

(b) Compute neuron values of the next layer

Let $n_{(2,1)}$ be the value of the first neuron in the second layer (the first hidden layer), $n_{(1,1)}$ the value of the first neuron in the first layer (the input layer), $n_{(1,2)}$ the value of the second neuron in the first layer, $w_{(1,1),(2,1)}$ the weight between $n_{(1,1)}$ and $n_{(2,1)}$, $w_{(1,2),(2,1)}$ the weight between $n_{(1,2)}$ and $n_{(2,1)}$, $b_{(2,1)}$ the bias for $n_{(2,1)}$, and f the activation function. The

input stimuli, $n_{(1,2)}$ and $n_{(1,2),}$ are propagated to the next layer based on the following equation:

$n_{(2,1)} = f(n_{(1,1)} * w_{(1,1),(2,1)} + n_{(1,2)} * w_{(1,2),(2,1)} + b_{(2,1)})$

(c) Repeat (a) and (b) until the last layer is computed

(3) Back propagation (see Figure 4.12)

(a) Compute error for the output layer

Let $d_{(3,1)}$ be the difference between the target value (t_1) and the output neuron value ($n_{(3,1)}$). The error of the neuron ($e_{(3,1)}$) is defined as the difference multiplied by the derivative of the activation function evaluated at the neuron value. This process can be expressed as:

$e_{(3,1)} = f'(n_{(3,1)}) * d_{(3,1)} = f'(n_{(3,1)}) * (n_{(3,1)} - t_1)$

If the sigmoid is used as the activation function, the error can be expressed as:

$e_{(3,1)} = n_{(3,1)} * (1 - n_{(3,1)}) * d_{(3,1)}$

because the derivative of the sigmoid $f'(x)$ is $f(x) * (1 - (f(x))$.

(b) Back-propagate error to the previous layer

The error of the second layer (the only hidden layer), $e_{(2,1)}$, is calculated as

$e_{(3,1)} = f'(n_{(2,1)}) * d_{(2,1)}$

$d_{(2,1)} = w_{(2,1)(3,1)} * e_{(3,1)} + w_{(2,1)(3,2)} * e_{(3,2)}$

(4) Update weights and biases (see Figure 4.13)

The weight between the first neuron of the second layer ($n_{(2,1)}$) and the first neuron of the third layer ($n_{(3,1)}$), $w_{(2,1)(3,1)}$, is updated as follows:

$w_{(2,1)(3,1)} = w_{(2,1)(3,1)} + \alpha * e_{(3,1)} * n_{(2,1)}$

where α is the learning rate of the neural network.

(5) Check termination criteria

If algorithm has not converged, continue learning by repeating steps (2) through (4). Otherwise, stop training. ANN training terminates when one of the following criteria is satisfied:

- the number of iterations is greater than the specified maximum number of iterations
- the computed error is smaller than the target error. The error is the average of the sum of squared errors of each iteration

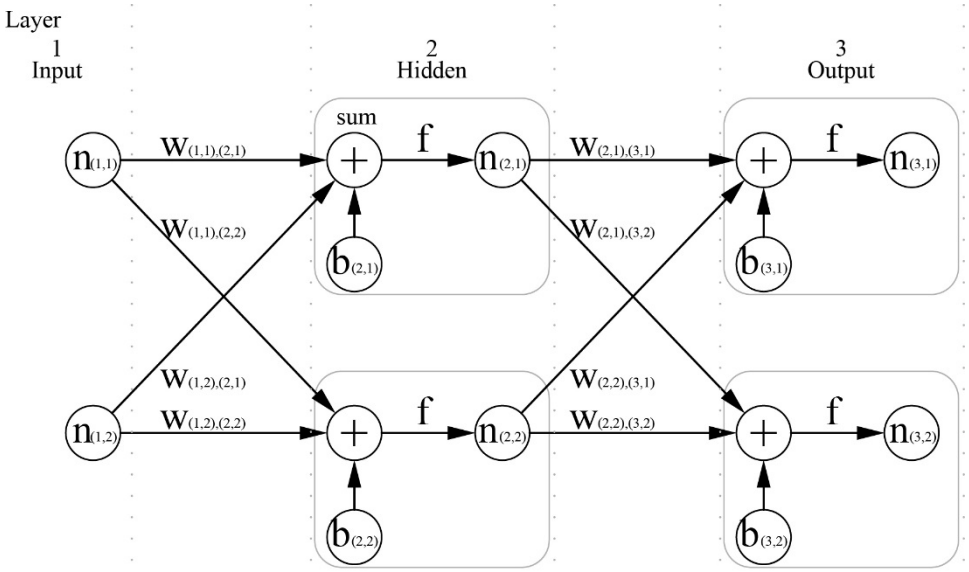

Figure 4.11 Feed-forward process of ANN

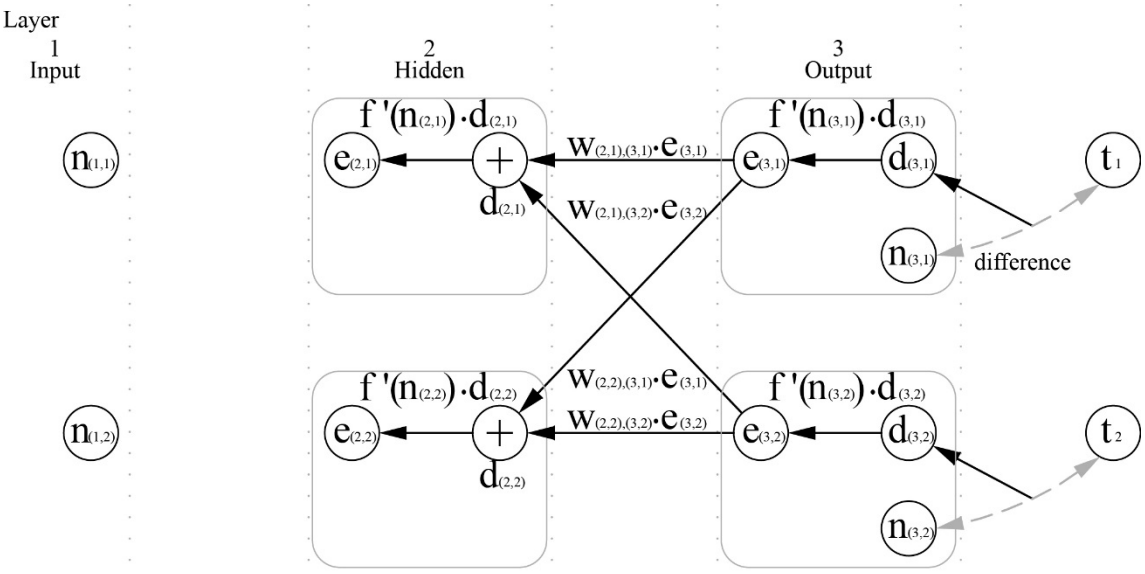

Figure 4.12 Back-propagation of error

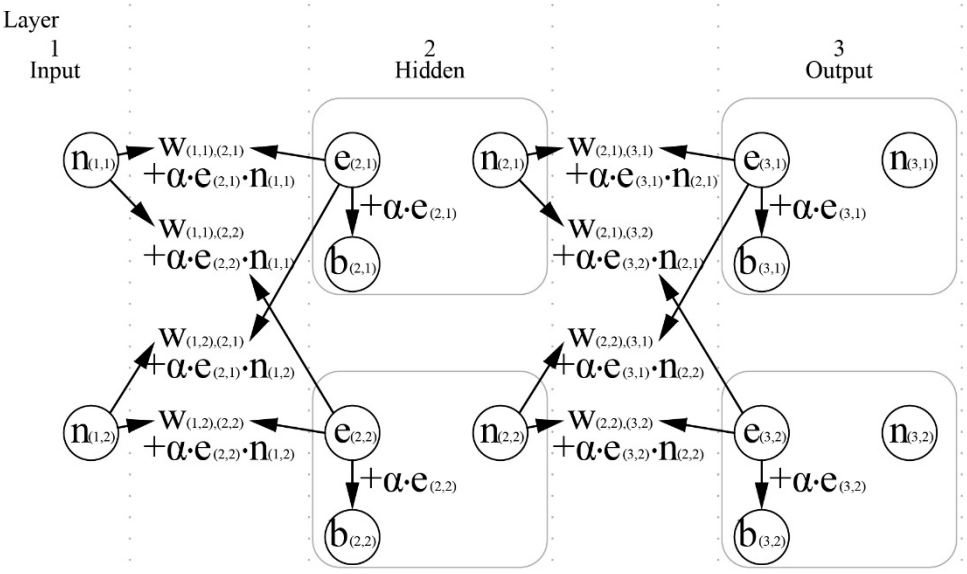

Figure 4.13 Update of weight and bias of ANN

Reasons not to use optimum angle as an output variable

The optimal slat angle is excluded from the training data because it has a few disadvantages.

Because an optimization objective can change during PVIS operation, training ANN with

optimal angle requires multiple ANNs, each of which is trained with a different control objective. Alternatively, a single ANN that has optimization objective as an input variable is also possible. This method requires less memory than using multiple ANNs. Either method requires training data for each control objective. When an optimization objective is modified or a new objective is added, an optimum-dependent ANN needs to be re-trained. To avoid this inflexibility, optimization-related variables are excluded from ANN training. A separate optimizer performs optimization while communicating with an ANN.

4.4.6 Structure of ANN

Notation of ANN structure

Let S_i be the number of nodes in the i-th layer. An ANN with n layers including input and output layers is denoted as $S_1/S_2/.../S_{n-1}/S_n$. For example, a one-hidden-layer ANN with four input variables, five nodes in the hidden layer, and three output variables is denoted as 4/5/3.

ANN structure

A two-hidden-layer ANN was used, with five neurons in each hidden layer (4/5/5/3). This structure was selected from various ANN configurations. The ANN training tests were conducted with actual measurement data acquired between 3/24/2012 and 3/27/2012. The test ANN configurations included 4/9/3, 4/24/3, 4/73/3, 4/146/3, 4/5/5/3, 4/10/10/3, 4/20/20/3, and 4/30/30/3.

Learning rate and momentum

The learning rate of the ANN was set to 0.01, and the momentum was 0.9. These values were also determined from the ANN training tests described above.

Adaptive learning rate

A constant learning rate was used in this research. Because the ANN controller was developed in a PC platform, the memory storage size was not a critical concern. However, because the ANN might be used in an embedded platform, which usually has a small memory, no adaptive learning rate methods were considered. With some additional memory, adaptive learning rate methods might speed up back-propagation training time. Many methods are available, such as Vogl's method, the Delta-Bar-Delta method, Silva and Almeida's method, and the SuperSAB method. A disadvantage of adaptive learning rate methods is that they require larger memory storage. For ANNs to run on hardware with a small storage such as microcontrollers, the size of the required storage can be a concern. On-line back-propagation using a constant learning rate requires the smallest storage (Reed and Marks, 1999).

4.5 Test building

The test building is a typical office space with a strip window. It measures 4 meters wide, 6 meters deep and 2.4 meters high. The test building has an aperture located in the south wall. The window is 3.4 meters wide and 1.6 meters high. It has no glass. A 1/6 scale model of the building measuring 0.67 meters wide, 1 meter deep, and 0.4 meters high was constructed and used for experiments (see Figures 4.14 and 4.15). The scale model was placed in the Taubman College of Architecture and Urban Planning's Art and Architecture Building, located at approximately 42.289° north and 83.717° west.

4.5.1 Interior wall reflectance

The interior ceiling, walls, and floor of the model were painted with semi-matte gray paints with a reflectance of 65%, 35%, and 13%, respectively. The reflectance of a surface was calculated by dividing the illuminance of the surface by that incident on the surface. The reflectance of each surface was determined by averaging 10 measurements.

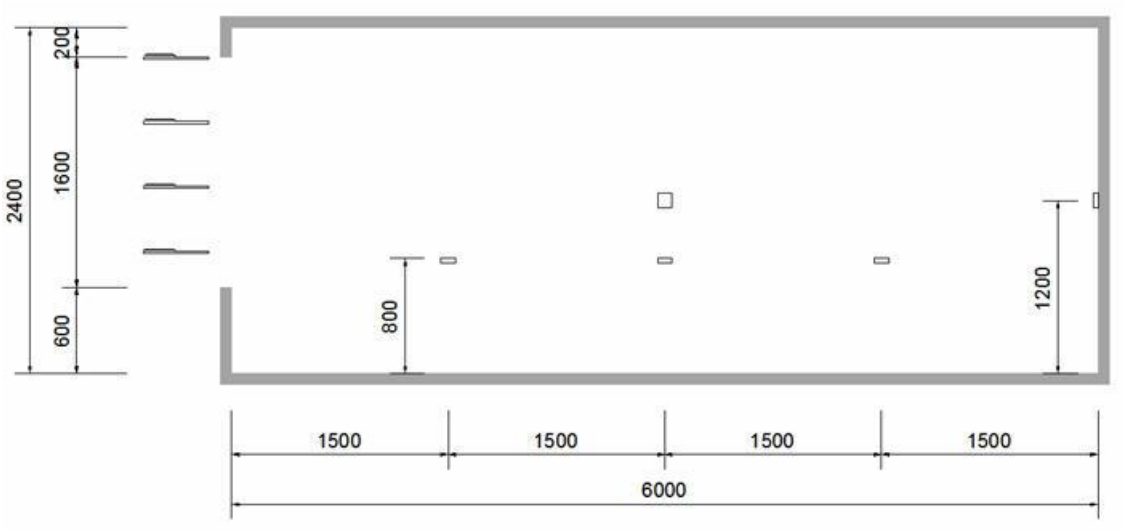

Figure 4.14 Section of test building (unit: mm)

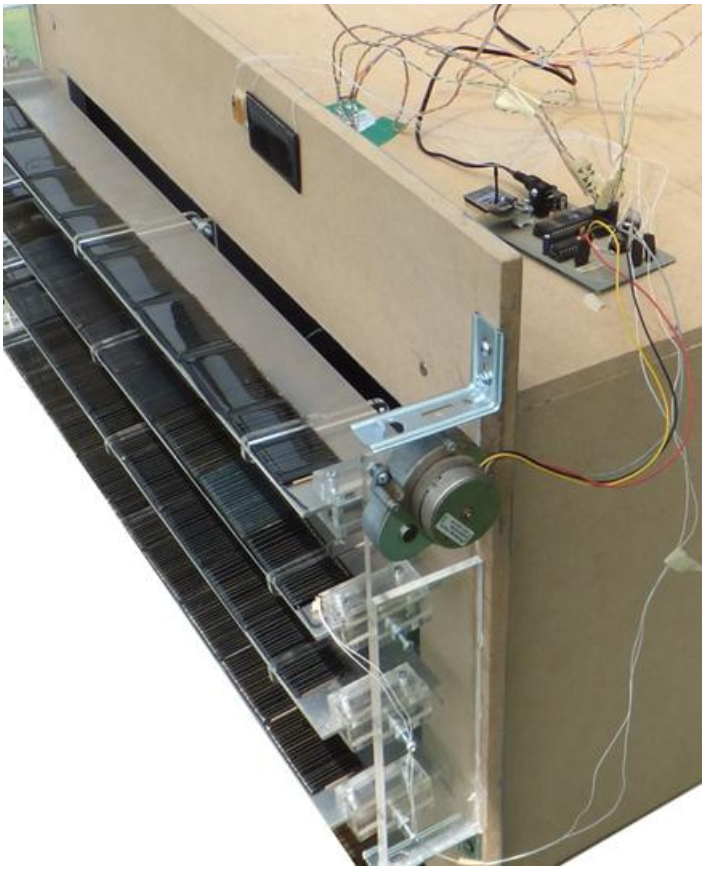

Figure 4.15 Test device installed on the window of the scale model of test building

4.6 Test device (PVIS)

A louver-type shading device was installed on the exterior of the south-facing window. The louver had four horizontal slats with a spacing of 45cm. The spacing was the same as the depth of a louver slat to allow the louver to thoroughly block the window. The louver slats were coated with polycrystalline PV cells, each of which were 6.6cm wide and 3.6cm deep (40cm wide and 21.6cm deep in actual size). To avoid low PV efficiency due to self-shading among louver slats, PV cells were installed only on the outer half (48%) of the slats. The other half (52%) was uncovered (see Figure 4.16). Nine PV cells were attached to each louver slat and connected in parallel. A single cell was capable of a maximum of 8.0V open circuit voltage with

44mA short circuit current. The fill factor of the cell was approximately 0.65. Thus, one slat had a theoretical maximum power of 2.06W. Considering the scale of the test building (1:6), the output power of the slat is equivalent to 74.1W for a full-scale device. The total peak power of the full-scale device is 296.6W (see Table 4.1). Actual electricity output depends on sky conditions and the solar irradiance on the PV cells.

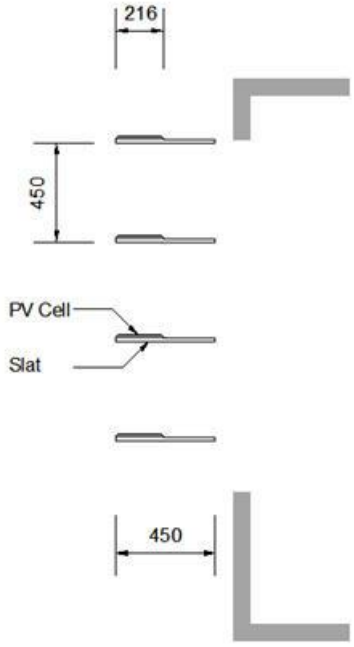

Figure 4.16 Section of PV integrated horizontal louver (unit: mm)

	1/6 scale model	Real building
Floor area	0.67 m^2	24 m^2
PV area per slat	196 cm^2	7,056 cm^2
PV area (total)	784 cm^2	28,224 cm^2
Peak power per slat	2.06 W	74.1 W
Peak power (total)	8.24 W	296.6 W

Table 4.1 Specifications of scale model and actual building

4.6.1 Estimated performance of PVIS

Estimating the performance of a BIPV indicates how much energy the PVIS will potentially save. To this end, the performance of a BIPV mounted on a south wall with the same PV area was estimated as described below.

Office buildings in the US consumed 72.9 kWh/m^2 (23.1 kBtu/ft^2) for lighting in 2003 (US EIA, 2003), 24.9% of their total energy consumption, which was 293.1 kWh/m^2 (92.9 kBtu/ft^2). Based on this, a 24m^2 office space consumes 4.79 kWh per day for artificial lighting. A south-facing vertical surface in Detroit receives, on average, 2.93kWh/m^2 of irradiance per day (NREL, 2014). When the conversion efficiency of a PV cell is 12%, a PV system mounted on a south-facing wall can produce 0.99 kWh, which is 20.1% of daily lighting energy consumption (see Table 4.2).

Supply		Demand	
PV area	2.82 m^2	Floor area	24 m^2
Orientation	South, vertical	Daily lighting energy per unit area	0.20 kWh/m^2
PV efficiency*	12%	Total daily lighting energy	4.79 kWh
Irradiance	2.93 kWh/m^2/day		
Electricity output	0.99 kWh/day		

*Approximate

Table 4.2 Estimated daily average electricity output from a wall-mounted PV system and lighting energy demand (climate data: Detroit, MI)

4.7 Data acquisition and slat tilt angle control system

Two wireless sensor/controller nodes were used. A wireless node includes a microcontroller, a wireless transceiver, and other supporting parts. The wireless transceiver (B in Figure 4.17) sends measurement data to a PC and receives control commands from the PC. The microcontroller (C) translates messages between the node and the PC. The motor driver (E)

amplifies motor control signals from the microcontroller and supplies electricity to the step motor. The 5V voltage regulator (A) supplies ripple-less electricity to the microcontroller and sensors. The 6V regulator (F) is the power source for the amplifier for the PV sensors (G).

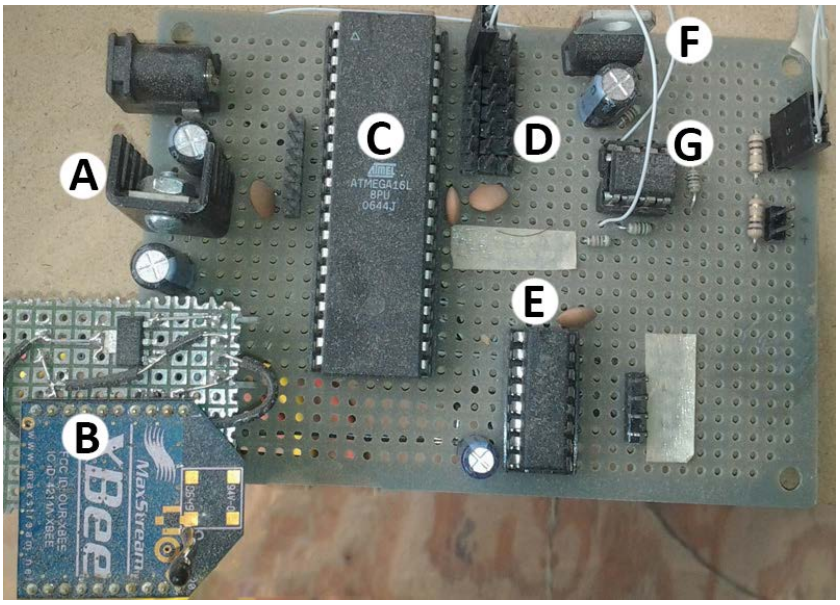

A: Voltage regulator, 5V
B: Wireless transceiver
C: Microcontroller
D: Sensor connector
E: Motor driver
F: Voltage regulator, 6V
G: Amplifier for PV sensors

Figure 4.17 Wireless sensor/controller node

4.7.1 Slat tilt angle control

A step motor controls louver slat tilt angle. Because the motor has a constant step angle, slat tilt angle can be determined based on the initial angle and the number and direction of steps. This allows the open-loop control of the slat tilt angle. In other words, it is unnecessary for the control system to check whether the slats are at an intended position after it modifies slat angle. The initial slat angle is zero (horizontal), and the slats return to the initial position when the controller is inactive.

The step adjustment of the slat tilt angle is 3 degrees. Each slat angle adjustment consists of five revolutions of the step motor cycle. The step size of the motor is 7.5 degrees, and a revolution consists of four steps. Therefore, the motor shaft rotates 30 degrees per revolution. The motor connects to the louver slats via a gear with a ratio of 1:50. As a result, the louver slats rotate 0.6 degrees per revolution of the step motor.

The louver slats have 53 discrete tilt angles between -78 and +78 degrees. The physical limits of the slat tilt angle are -84 degrees and +84 degrees. Six degrees at each limit are unused to prevent the controller from damaging the slats by mistakenly attempting to rotate them beyond the physical bounds.

4.7.2 PV output measurement

Electricity production from PVs was measured using two groups of PV modules. One group was installed on the second-highest slat of the test louver. The other group was installed on the south wall of the test building. Because the open circuit voltage (V_{OC}) is almost constant during daytime, the short circuit current (I_{SC}) is measured to estimate the electricity output of PV cells. The PV output at the maximum power point (MPP) can be calculated using the fill factor, the ratio of MPP to $V_{OC} * I_{SC}$. The fill factor of the PV module used in the experiments was 0.65, according to its specifications. The PV module used for experiments is shown in Figure 4.18.

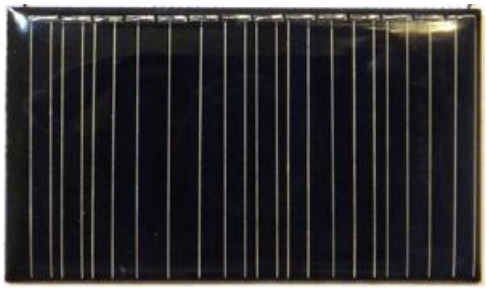

Figure 4.18 PV module used for experiments

4.7.3 Illuminance measurement

Two types of light sensors were used to measure illuminance levels. Narrow range sensors (0 ~ 3,630 lux) were used to measure work plane illuminance and background luminance (Figure 4.19) (Texas Instruments, 2003). The other wide-range type was for exterior light levels (Figure 4.20); it measures up to 230,000 lux. The wide-range light sensors were used for measurement points where a large dynamic range of light level was expected. Exterior daylight level was measured by a wide-range light sensor attached on the south wall.

A vertical sensor was used instead of a horizontal one because a vertical surface directly represents solar radiation on the window. In addition, a horizontal sensor without an appropriate shield receives light reflected by the adjacent surfaces and ignores light from the ground. Therefore, a horizontal sensor does not accurately represent the solar radiation on the window.

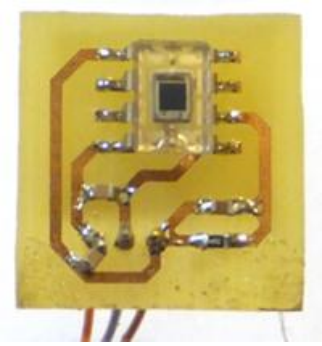

Figure 4.19 Narrow-range light sensor installed in the test building

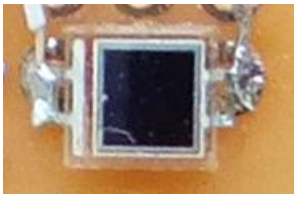

Figure 4.20 Wide-range light sensor installed on the south wall of the test building

4.7.4 Daylight glare index (DGI) measurement

DGI is calculated using background luminance, window luminance, and the solid angle of the window in relation to a hypothetical occupant. Hopkinson defines Daylight Glare Index (DGI) as the luminance of background and light sources, and the solid angle of the sources (Hopkinson, 1963). The definition is as follows:

$$\mathrm{DGI} = 10 \log_{10} \sum_{i=1}^{n} \frac{0.478 L_i^{1.6} \Omega_i^{0.8}}{L_b + 0.07 \omega_i^{0.5} L_i} \quad (1)$$

where n is the number of light sources, L_i is the luminance of the i-th light source, ω_i is the solid angle of the i-th light source subtended by the viewer, Ω_i is the modified solid angle of the i-th light source, and L_b is the background luminance.

A modified equation based on Hopkinson's equation is used. The test building has a single window. Therefore, no summing up procedure is necessary. The factors of *i*-th light source (L_i, ω_i, and Ω_i) are replaced with the factors of the single light source (L_s, ω, and Ω). The modified solid angle of the light source (Ω) is a function of the solid angle of the light source (ω) and the Guth's position index *P*. The equation of the modified solid angle is

$$\Omega = \omega/P^2 \quad (2)$$

It was hypothesized that the occupant was facing toward the window, sitting at the center of the test building (three meters from the window). The eye level of the occupant was 1.2m. The smallest possible value of *P* is 1, which occurs when an observer looks at the center of the light source. In other words, the line-of-sight coincides with the source-to-observer line. Therefore, Ω is always smaller than or equal to ω ($\Omega \leq \omega$). Because the direction of the line-of-sight may change, the worst case of DGI (maximum possible value) was considered in this research. In the modified equation, ω substitutes for Ω. In sum, the modified DGI equation calculated the highest possible DGI of a single light source. The modified equation is as follows:

$$\mathrm{DGI} = 10 \log_{10} \frac{0.478 L_s^{1.6} \omega^{0.8}}{L_b + 0.07 \omega^{0.5} L_s} \quad (3)$$

DGI scale

DGI values are interpreted based on the descriptive scale. The five thresholds in the scale define six states of daylight glare: non-perceptible (below 16), perceptible (16-20), acceptable (20-22), slightly uncomfortable (22-24), uncomfortable (24-28), and intolerable (over 28) (see Table 4.3). When DGI is below the borderline between comfort and discomfort (BCD), 22, the daylight glare is considered acceptable.

DGI value	Description
16	Just perceptible
20	Just acceptable
22	Borderline between comfort and discomfort (BCD)
24	Just uncomfortable
28	Just intolerable

Table 4.3 DGI scale

Background luminance

The luminance of a diffuse surface was calculated based on the illuminance of the surface and its reflectance, using the following equation:

$$\textit{Surface luminance} = \textit{Illuminance} * \textit{Reflectance} / \pi \quad (4)$$

Background luminance was the smaller of two luminance values measured near the left and right edges of the window (see Figure 4.21). Instead of the average of the two, the smaller value was used to represent the worst situation.

Window luminance was calculated based on the illuminance measured using a shielded sensor. A circular area in the center of the window was used for window luminance measurement. Although it would be ideal to use the entire area of the window, it is difficult to precisely align a rectangular shield that confines the sensor's field of view to the window. If the sensor is not precisely aligned, measurements are highly prone to errors. For this reason, the luminance of a partial area of the window was measured using a sensor with a circular shield. The solid angle of the circular area with regard to the shielded sensor was 0.02 sr. The window luminance sensor was calibrated using a commercial light meter.

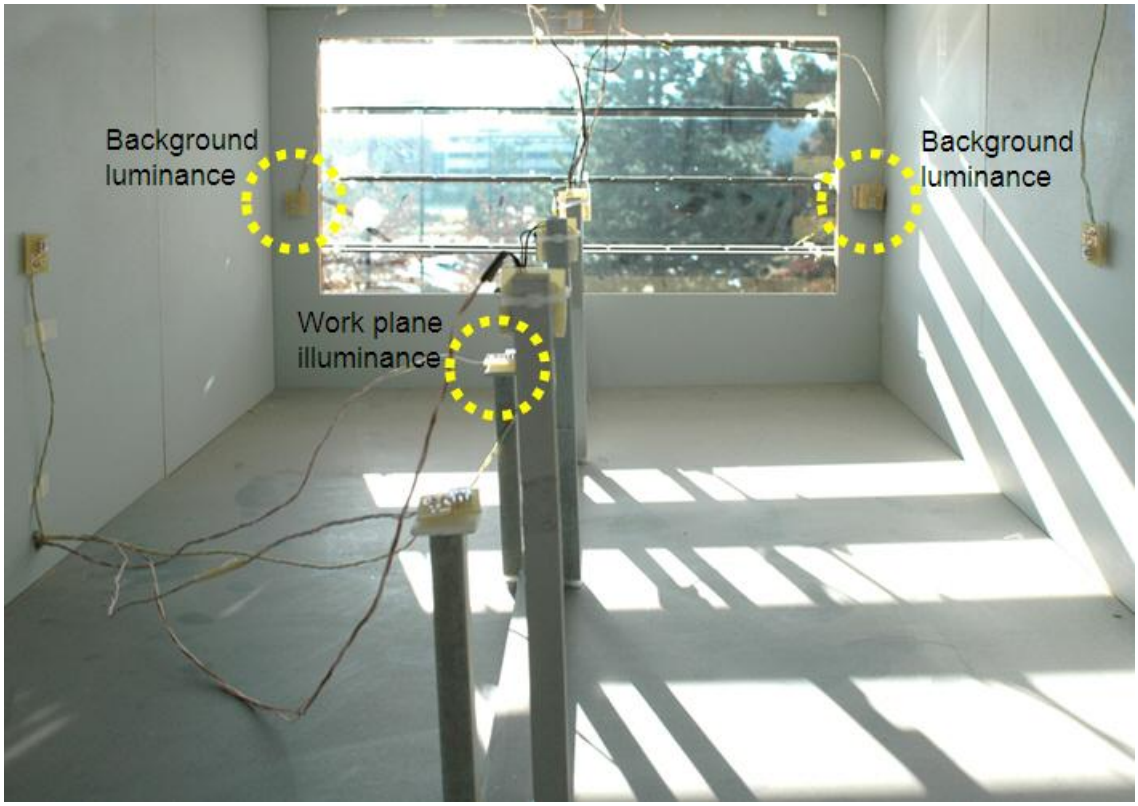

Figure 4.21 Position of background luminance sensors and work plane illuminance sensor

4.7.5 Sun position

The position of the sun consists of two factors: altitude (elevation) and azimuth. The two factors are calculated based on the latitude and the longitude of a location, as well as the local time. The sun position was calculated based on the sun position equations available at the National Oceanic and Atmospheric Administration (NOAA) website (NOAA, 2014). The sun altitude was calculated using the following equation:

$$\theta_{AL} = \pi/2 - \cos^{-1}(\sin\theta_{LAT} * \sin\theta_D + \cos\theta_{LAT} * \cos\theta_D * \cos\theta_H) \quad (5)$$

where

θ_{AL} is sun altitude,

θ_{LAT} is the latitude of a location,

θ_D is sun declination angle, and

θ_H is sun hour angle, which is a conversion of solar time from 24 hours to 360 degrees.

The sun azimuth (θ_{AZ}) was calculated using the following equation:

$$\theta_{AZ} = \cos^{-1}\left(\frac{\sin\theta_{LAT} * \cos(\pi/2 - \theta_{ALT}) - \sin\theta_D}{\cos\theta_{LAT} * \sin(\pi/2 - \theta_{ALT})}\right) \quad (6)$$

Figures 4.22 and 4.23 show the sun position and the solar profile angle at Ann Arbor, MI, USA, where the experiments were conducted. Note that the solar profile angle is almost constant at the spring and fall equinoxes. In addition, between the spring equinox and the fall equinox, the solar profile angle is always greater than 47 degrees.

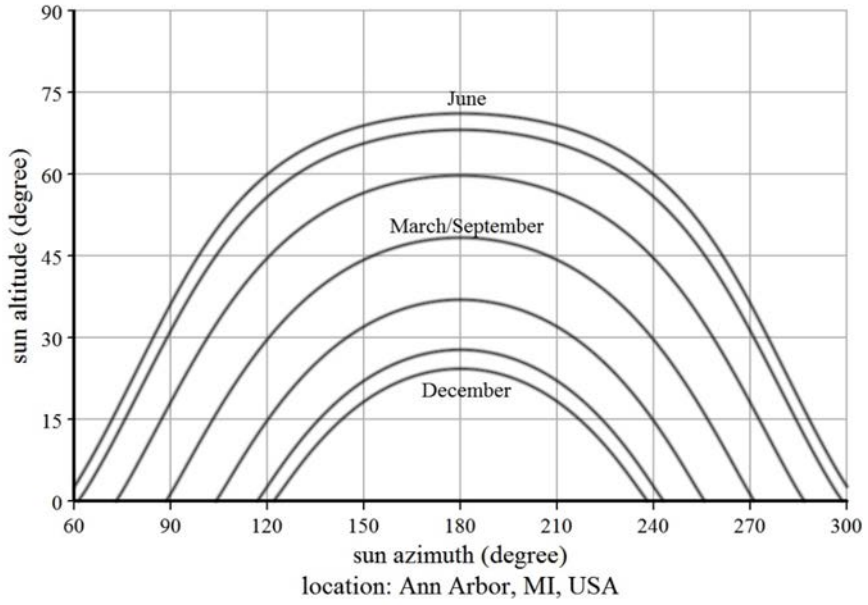

Figure 4.22 Solar altitude vs. solar azimuth (Ann Arbor, MI, USA)

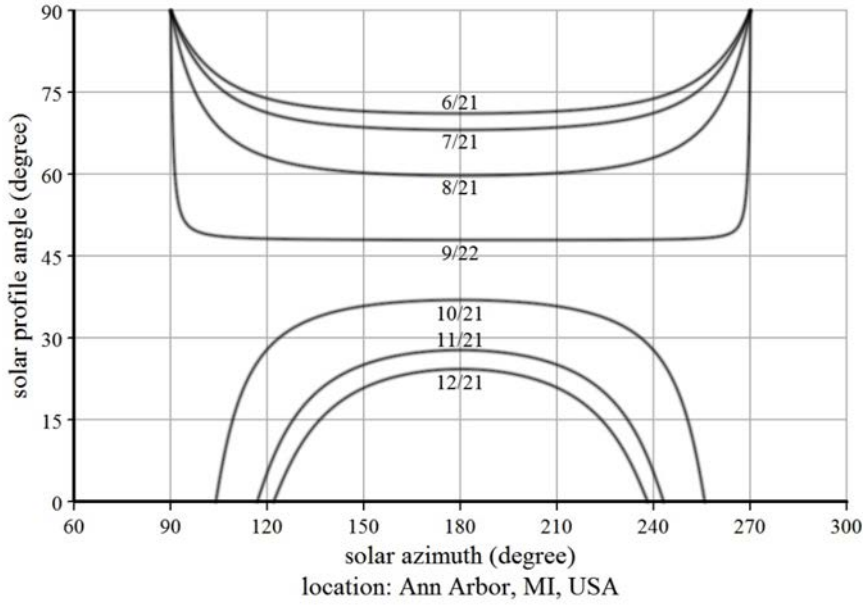

Figure 4.23 Solar profile angle (Ann Arbor, MI, USA)

4.8 Definition of angles

The tilt angle is the angular distance between the z-vector and the normal vector of the louver surface. The sign of the tilt angle is that of the cross product of the surface normal and the *z*-vector ($\vec{n} \times \vec{z}$). In other words, when the outer edge of the slat is higher than the inner edge, the slat angle is positive. Tilting up rotates the louver slat so that the tilt angle increases. Its direction is clockwise when the rotation is observed from the east (see Figure 4.24).

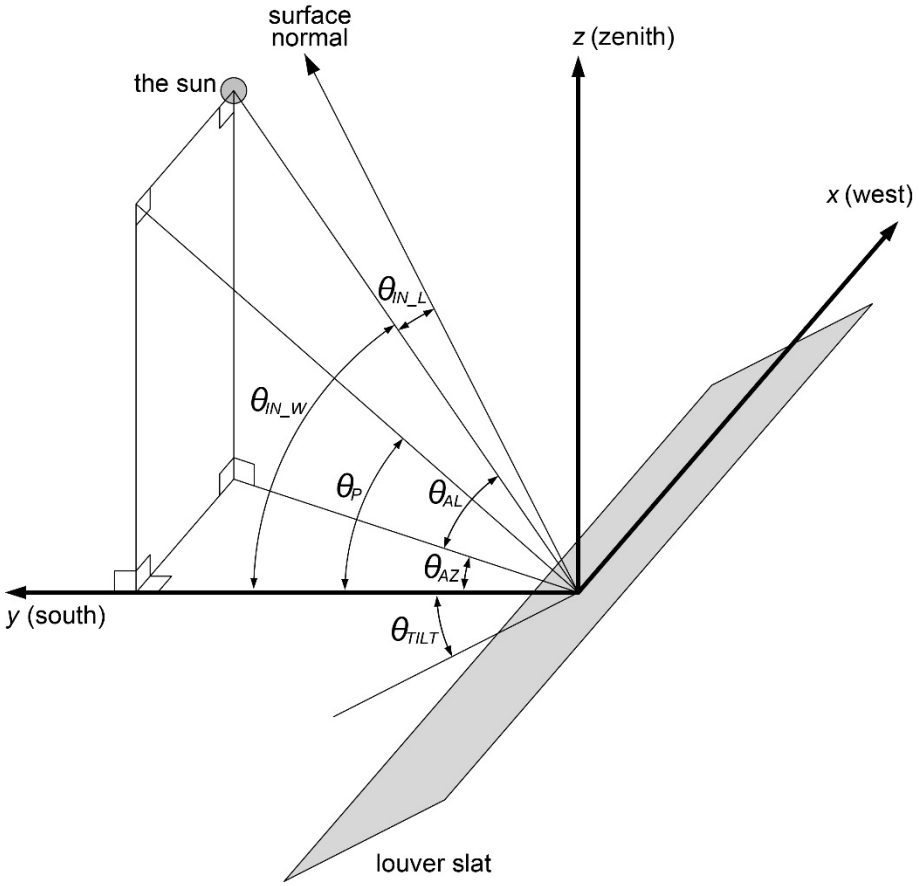

Figure 4.24 Angles dependent on sun position and slat tilt angle

The solar profile angle (θ_P) is the angle from the y-vector to the sun vector projected on the *yz* plane. It ranges between zero and 90 degrees. It is valid while the sun altitude is non-negative and the sun azimuth from the South is between -90 and +90 degrees. It is calculated using the following equation:

$$\theta_P = \tan^{-1}\left(\frac{\tan(\theta_{AL})}{\cos(\theta_{AZ})}\right) \tag{7}$$

The sunlight incident angle on the louver, θ_{IN_L}, is calculated using the following equation:

$$\theta_{IN\_L} = \cos^{-1}\left(\cos\left(\theta_{TILT} + \frac{\pi}{2}\right) * \cos(\theta_{AL}) * \cos(\theta_{AZ}) + \sin(\theta_{TILT} + \pi/2) * \sin(\theta_{AL})\right) \quad (8)$$

The sunlight incident angle on the south wall, θ_{IN_W}, is calculated using the following equation:

$$\theta_{IN\_W} = \cos^{-1}(\cos(\theta_{AL}) * \cos(\theta_{AZ})) \quad (9)$$

4.8.1 Effect of the direct component of daylight

Daylight consists of a direct component (sunlight) and an indirect component. The indirect component consists of a diffuse component from the sky and a reflected component from the ground. The direct component on a plane facing the sun is termed the direct normal component.

The direct component depends on the direct normal component and its incident angle on a surface. The indirect component consists of the diffuse sky component and the reflected component from the ground. The PV modules on the louver slats can be shaded by the adjacent upper slat. Therefore, the shaded portion is an additional factor of the direct component on the louver PV modules, and the shaded portion is considered for the obstructed slats below the unobstructed top slat. The ratio of the PV area receiving direct sunlight to the entire PV area, r_{DIRECT}, is based on the following equation:

$$r_{DIRECT} = \text{minimum}\left(1, \frac{2}{\cos(\theta_{TILT}) * \tan(\theta_P) - \sin(\theta_{TILT})}\right) \quad (10)$$

The minimum function is used to limit the ratio below the theoretical maximum, 1, which occurs when the entire PV area receives direct sunlight. The equation is a specific instance of the general equation

$$r_{DIRECT} = \text{minimum}\left(1, \frac{H}{W} * \frac{1}{r_{PV}} * \frac{1}{\cos(\theta_{TILT}) * \tan(\theta_P) - \sin(\theta_{TILT})}\right) \quad (11)$$

where H is the slat spacing, W is the slat depth, and r_{PV} is the ratio of the PV area to the slat area. For the test device, the slat depth and the slat spacing are the same (H/W=1). The outer half of the slat is coated with PV modules (r_{PV} = 0.5).

Let the direct component on the louver PV with regard to the direct normal sunlight be PV_{L_DIRECT}, which depends on the incident angle on the louver slat and the portion of the louver PV area exposed to the sun. Therefore, its equation is as follows:

$$PV_{L\_DIRECT} = \cos(\theta_{IN\_L}) * r_{DIRECT} \quad (12)$$

Replacing r_{DIRECT} with the equation 11 results in the following equation:

$$PV_{L\_DIRECT} = \text{minimum}\left(\cos(\theta_{IN\_L}), 2 * \cos(\theta_{AL}) * \cos(\theta_{AZ})\right) \quad (13)$$

This equation can be broken down into two cases: the louver PV modules are fully exposed to the sunlight (r_{DIRECT} =1), or the PV modules are partially shaded (r_{DIRECT} <1). If the PV modules are fully shaded, the direct component has no effect on the output of the PV modules. When no PV modules are shaded, the direct component incident on the modules follows the cosine law ($\cos(\theta_{IN\_L})$). Otherwise, it depends on the sun altitude and the sun azimuth ($2 * \cos(\theta_{AL}) * \cos(\theta_{AZ})$). In this case, the direct component on the louver PV is independent of the slat tilt angle because the gain from the change of the sunlight incident angle is identical to the loss from the change of the PV area exposed to the sun, and vice versa. The ratio of slat spacing to slat depth (H/W) and the ratio of PV area to the slat area (r_{PV}) are the additional factors of the general equation for the shaded-PV case. The general equation is as follows:

$$PV_{L\_DIRECT} = \frac{H}{W} * \frac{1}{r_{PV}} * \cos(\theta_{AL}) * \cos(\theta_{AZ}) \quad (14)$$

When no PV modules are shaded, minimizing the sunlight incident angle maximizes the direct component on the PV modules. The slat angle minimizing the sunlight incident angle is perpendicular to the sun profile angle. In other words, the direct component on the louver PV is at maximum when $\theta_{TILT} = \theta_P - \pi/2$. The maximum PV_{L_DIRECT} is

$$\cos(\theta_{IN\_L}) = \cos(\theta_{AL}) * \cos(\theta_{AZ}) / \cos(\theta_P) \quad (15)$$

In sum, the maximum ratio of the direct component on the louver PV to the direct normal sunlight is $2 * \cos(\theta_{AL}) * \cos(\theta_{AZ})$ when the louver PV modules are partially shaded, or $\cos(\theta_{AL}) * \cos(\theta_{AZ}) / \cos(\theta_P)$ otherwise.

4.9 Analog to digital converter (ADC) settings

Resolution

The resolution of each sample was 12 bits (4,096 steps). The ADC of ATmega16, the microcontroller of the wireless nodes used for the experiments, has a 10-bit resolution. However, only the eight most significant bits (MSBs) of the ten bits are guaranteed to be accurate (Atmel Corportation, 2010); thus, only 256 steps are available for each sample. For measurement of light level ranging between 0 and 100,000 lux, for example, each step represents 391lux, which is unsuitably large for experimental and research purposes. To increase the resolution, the oversampling method was used. Averaging 16 consecutive samples increases the resolution

from 8 bits to 12 bits. ADC noise reduction mode, which is a function supported by the ADC, was used for higher accuracy. During the noise reduction mode, other functions of the microcontroller are temporarily disabled while the ADC is active.

Sampling frequency

Each wireless sensor node can acquire 300 samples per second. The microcontroller on the wireless node has 1MHz of system clock frequency generated by the internal resistor-capacitor (RC) oscillator. The system clock frequency can be configured at up to 16MHz. At such a high frequency, however, the microcontroller consumes approximately ten times more electricity than it does at 1MHz. System clock frequency lower than 1MHz is also possible, but it should be fast enough to perform mathematical computations for adaptive control. In this research, a PC performed such computations, but the computation speed of a microcontroller is important for PC-less applications. Thus the system clock of the microcontroller was set to 1MHz out of consideration for energy consumption and computation capacity. Because ADC on the microcontroller is most accurate at input clock frequency between 50 kHz and 200 kHz (Atmel Corporation, 2010), ADC clock frequency was set to 62.5 kHz using the internal ADC prescaler (1/16) of the microcontroller. Because a single-ended conversion takes 13 ADC cycles, the ADC can perform 4,807 (62,500/13) conversions per second. Due to oversampling, 16 conversions are needed for each sample, which results in a sampling rate of 300 samples per second.

The PVIS control system in this research acquires samples from 16 ADC channels every five seconds. The sampling interval could be longer than five seconds for control purposes, but a short interval was used to enable cross-checking during data analysis.

4.9.1 ADC Channel allocation

There are sixteen ADC channels in the PVIS control system. The system has two wireless nodes, each of which has an ADC with eight channels. Two channels are assigned to PV cells. Two others are assigned to wide-range light sensors. The other twelve channels are assigned to narrow-range light sensors: three for work plane illuminance, three for wall illuminance, four for window luminance, and two for wall luminance. Of the sixteen channels, six are used for PVIS control. The others are used for data cross-checking and analysis. Table 4.4 gives detailed descriptions of the sensors assigned to the channels.

Sensor type	Measurement	Orientation	Location	Used for control
PV cell	PV output current	Vertical	South wall	-
		Same as slats	Louver slat	O
Light sensor (wide range)	Exterior illuminance	Vertical	South wall	O
	Window illuminance	Vertical	0.3m from window, height=1.2m	-
Light sensor (narrow range)	Interior illuminance (work plane illuminance)	Horizontal	1.5m from window, height=0.8m	-
			3.0m from window, height=0.8m	O
			4.5m from window, height=0.8m	-
	Interior illuminance	Vertical	East wall, height=1.2m	-
			West wall, height=1.2m	-
			Rear wall, height=1.2m	-
	Window luminance	Vertical	1.5m from window, height=1.2m	-
			3.0m from window, height=1.2m	-
			4.5m from window, height=1.2m	-
			Rear wall, height=1.2m	O
	Wall luminance	Vertical	East side of the window, height=1.2m	O
			West side of the window, height=1.2m	O

Table 4.4 ADC channel allocation

4.10 Communication between a wireless control node and a PC

Message structure

Six-byte messages are used for communication between the wireless nodes and a PC. The messages begin with two bytes of start of message identifier. The identifier is similar to those of Preamble and Start of Frame Delimiter (SFD) in the Ethernet frame. The remaining four bytes differ depending on the direction of communication. For messages from a PC to wireless nodes,

the destination node number (1Byte), command (1Byte), and command parameters (2Bytes) follow the start of message identifier. For those from a wireless node to a PC, the message comprises the source node number (1Byte), ADC channel number (1Byte), and ADC channel data (2Bytes) (see Tables 4.5 and 4.6). Because ZigBee protocol performs checksum (IEEE Computer Society, 2006), there is no additional checksum in the message.

PC software program

A software program was used for the communication between a PC and the wireless nodes (see Figure 4.25). The program included data acquisition, slat angle control, optimal control algorithms, and an ANN. The slat angle control functions allowed manual override, which was useful in testing the motor control system and aligning louver slats to the horizontal position at the beginning of each experiment. The program also calculated the sun position.

Byte order	1	2	3	4	5	6
Length in byte	2		1	1	2	
Description	Start of message identifier		Destination node ID	Command	Command parameters	

(a) From PC to node

Byte order	1	2	3	4	5	6
Length in byte	2		1	1	2	
Description	Start of message identifier		Source node ID	Channel number	Channel measurement data	

(b) From node to PC

Table 4.5 Structure of messages from PC to node (a) and from node to PC (b)

Category	Command name	Parameter	Description
Motor control	Go to angle	Target angle	Rotate slats to target angle
	Tilt up by a step	-	Rotate slats by 0.6 degrees
	Tilt down by a step	-	Rotate slats by -0.6 degrees
	Lock/Unlock	-	Disable/Enable motor control
ADC	Enable/Disable	-	Enable/Disable ADC
	Enable/Disable channel	Channel number	Enable/Disable an ADC channel
	Enable/Disable auto-trigger	-	Enable/Disable cyclic sampling
	Sampling interval	Target interval	Modify sampling interval

Table 4.6 PC-to-node command list

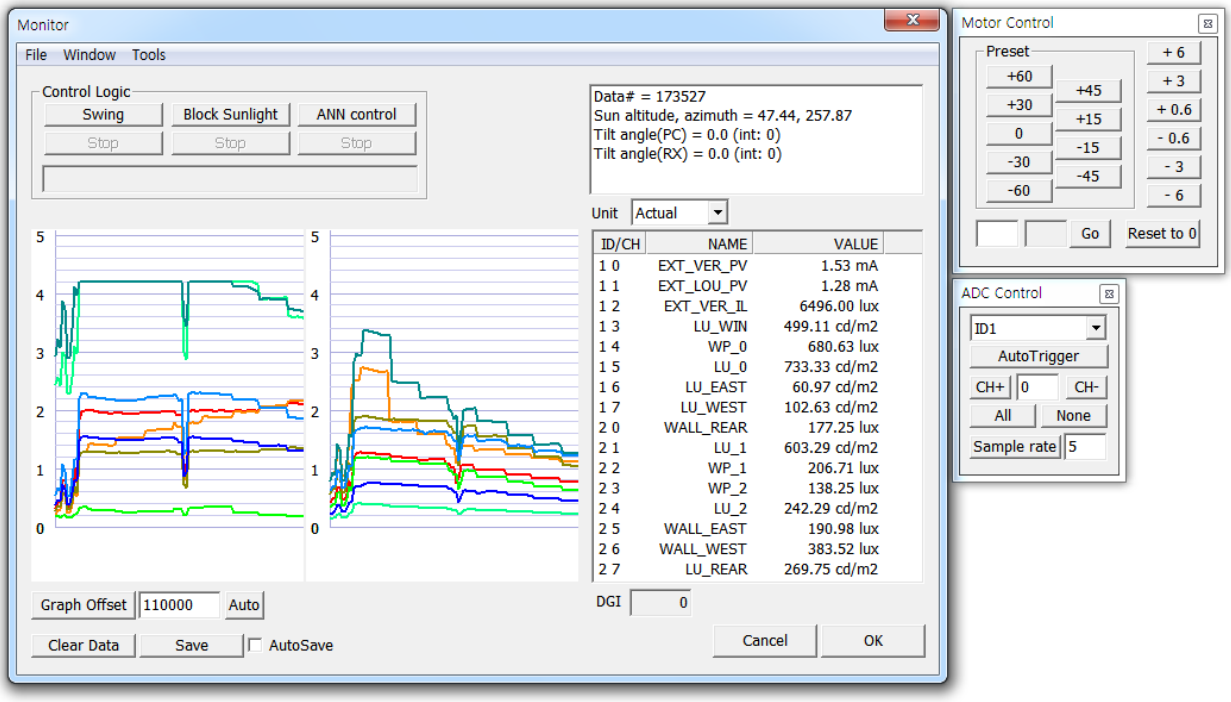

Figure 4.25 Data acquisition and motor control program

CHAPTER 5: ANALYSIS AND RESULTS

The main goal of this chapter is to evaluate the performance of the optimal control methods. Measurements of electricity output, interior light level, and glare provide an estimated performance of a PVIS. The experiment results discussed in this chapter are specific to the physical configurations and the location of the test building, but general strategies for controlling PV integrated shading devices can be inferred from the analysis of the experimental results.

5.1 Structure of this chapter

Section 5.2 describes the results of experiments using the three optimal control methods. The control methods are compared to each other in section 5.3, which investigates the effect of the constraining factors. The effects of the independent variables (exterior daylight level, sun position, and slat tilt angle) are described in sections 5.4 and 5.5. Section 5.4 discusses the effect of the uncontrollable variables: exterior daylight level and sun position. Section 5.5 describes the effect of the controllable variable: the slat tilt angle. It also discusses the effects of solar incident angle on the louver surfaces and partial shading on the louver PV coating. Solar incident angle and partial shading on PV depend on the combination of sun position and slat tilt angle. The accuracy of ANN-based optimal slat angle is discussed in Section 5.6. Finally, Section 5.7 describes the ANN training results.

5.2 Results of ANN-driven slat angle control

This section describes the results of ANN-driven slat angle control for three different control objectives.

5.2.1 Results of experiments using the PV-only method

The results of the PV-only control method are discussed in terms of PV output, work plane illuminance, and DGI. The PV-only method is one of the three optimal control methods. It seeks to maximize the louver PV output without considering visual comfort. The electricity output from the PV modules on the louver controlled using this method was compared to that of a wall-mounted PV module.

The experiment was conducted on 4/5/2012, when the sky was cloudy in the morning and almost clear in the afternoon. The exterior vertical illuminance indicating the daylight availability fluctuated between 9:30am and 12:00pm. The light sensor was shaded by the window frame between 10:30am and 11am. The low sensor reading during the period was due to the shadow on the sensor (see Figure 5.3). Because the exterior vertical illuminance was proportional to the wall PV output, its time-series data was omitted where the wall PV output was given. The exterior vertical illuminance charts for the other control methods appear in Appendix D.

The average electric current of the louver PV between 8am and 6pm was 17.25 mA, while that of the wall PV was 12.46 mA. The louver PV generated 38.4% more electricity than the wall PV. Because the PV modules were partially shaded by the window frame between 9:20am and 11:10am, and after 4:40pm, the louver PV output during the four hours after the solar noon (12:37pm-4:37pm) was also compared to the wall PV output to eliminate the effect of the

shadow. During the latter period (4 hours), the average electric current of the louver PV and the wall PV was 24.65 mA and 16.66 mA, respectively (see Figure 5.1). The louver PV generated 47.9% more electricity than the wall PV. These results demonstrate that PV panels installed on louvers can generate almost 50% more electricity than those mounted on south-facing walls on a clear day in spring and fall. Because PV output depends on sunlight incident angle, this difference varies according to the sun position. It increases during summer, when the solar incident angle on the south wall is greater than that on the louver tilted perpendicularly to the sunlight profile angle. The difference during winter is smaller than that during spring and fall for the same reason. The sunlight incident angle on the louver could have been decreased further, but the combined effect of the direct and the indirect components of daylight caused the maximum PV output to occur at a slat angle lower than one minimizing the solar incident angle (see Figure 5.2). Section 5.5 discusses the effect of the sunlight incident angle in more detail.

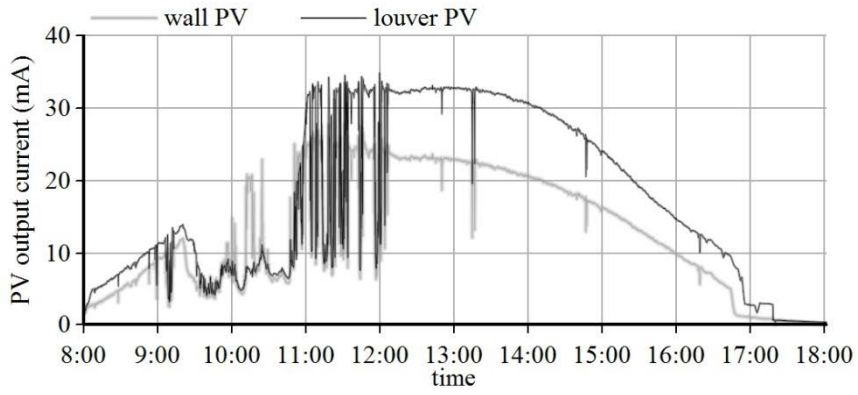

Figure 5.1 Output current of the louver PV (black) and the wall PV (gray) (PV-only method, 4/5/2012)

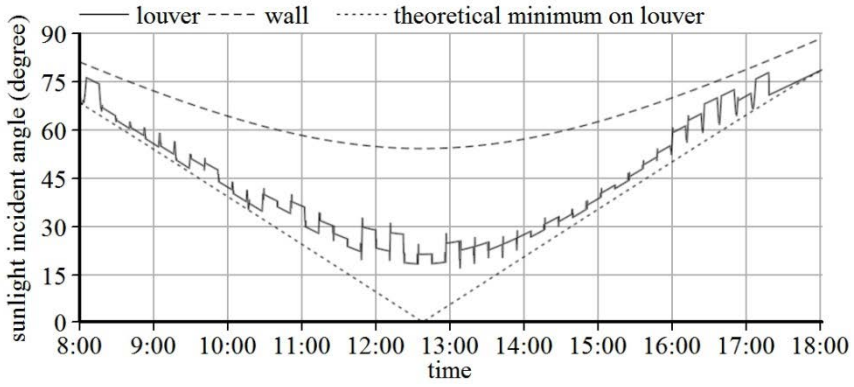

Figure 5.2 Sunlight incident angles on the louver and the south wall (4/5/2012)

Period (hour)	Average I_L (mA)	Average I_W (mA)	Ratio (I_L/ I_W)
8- 9	7.14	5.07	1.41
9-10	8.88	7.29	1.22
10-11	9.40	10.57	0.89
11-12	25.16	19.45	1.29
12-13	32.13	22.90	1.40
13-14	31.84	21.71	1.47
14-15	27.60	18.45	1.50
15-16	19.12	13.00	1.47
16-17	10.23	5.76	1.78
17-18	1.13	0.50	2.24
8-18	17.26	12.47	1.38

Table 5.1 Hourly PV output of the louver and the south wall (PV-only method, 4/5/2012)

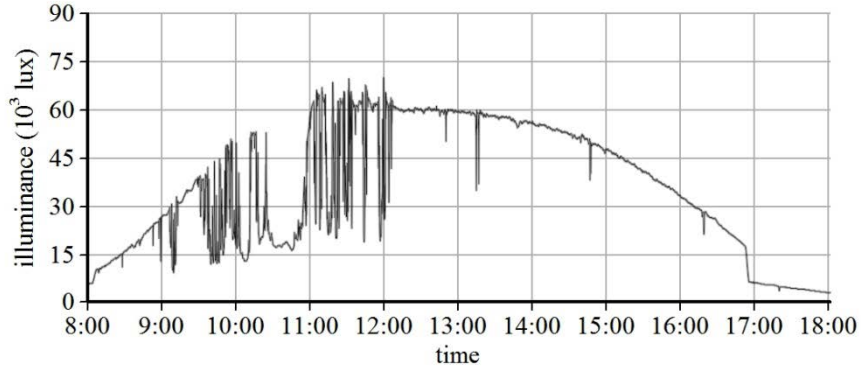

Figure 5.3 Exterior vertical illuminance (4/5/2012)

Except in five samples (25 seconds), the work plane illuminance was below the acceptable level. Measured light levels were above 400 lux in only 12.7 percent of the total samples during the ten hours of measurement (10.9 percent were between 400 and 450 lux; 1.8 percent were between 450 and 500 lux) (see Figures 5.4-5). The light levels were so low because most of the daylight was used to generate electricity. To avoid an unacceptable interior light level, work plane illuminance must be a criterion in the control objective. The experiment results of the PV+WP method, which includes such a criterion, are discussed in the next section (5.3).

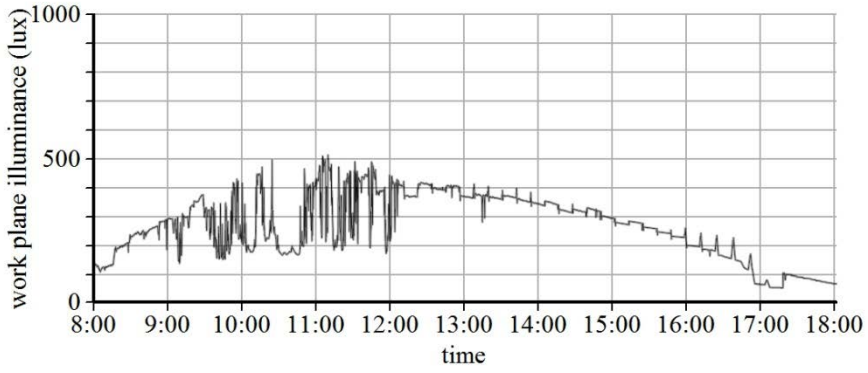

Figure 5.4 Work plane illuminance (PV-only method, 4/5/2012)

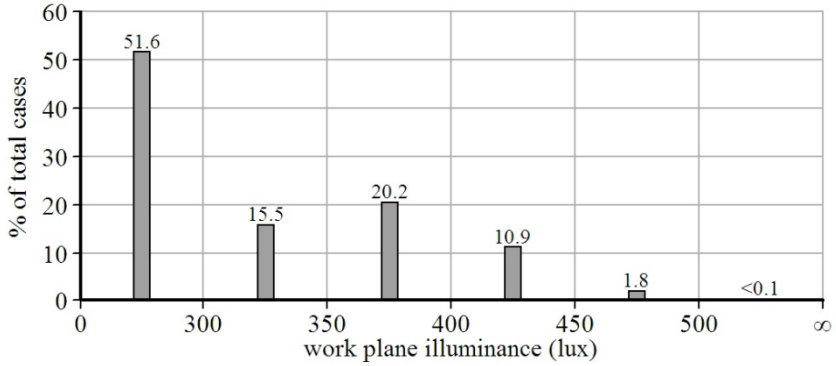

Figure 5.5 Work plane illuminance distribution (PV-only method, 4/5/2012)

DGI remained within the comfortable range during the entire time span; it stayed below 22, the threshold between comfort and discomfort (see Figure 5.6). The ratio of the background luminance to the window luminance was higher than the threshold of discomfort (see Figure 5.7). In other words, the luminance difference between the window and the background around the window was small enough not to cause glare.

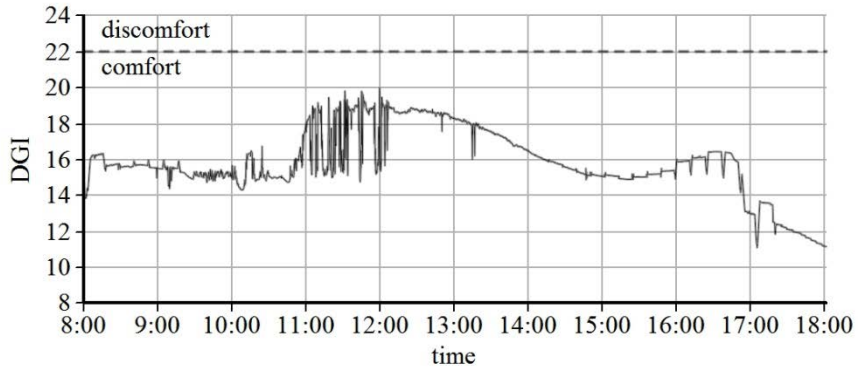

Figure 5.6 DGI: PV-only method (4/5/2012)

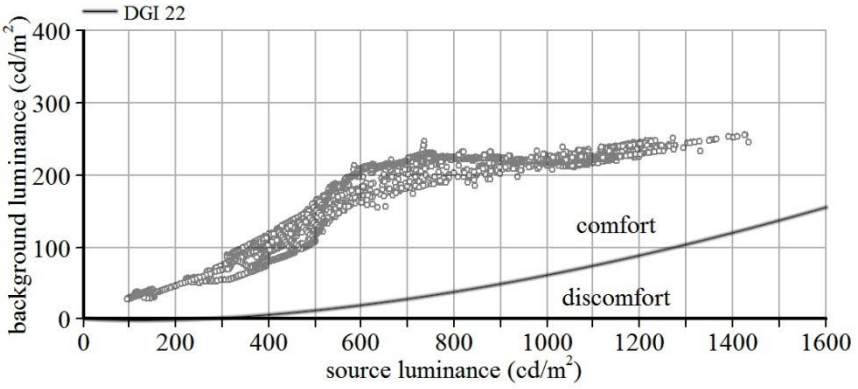

Figure 5.7 Distribution of the factors of DGI: source luminance and background luminance (PV-only method, 4/5/2012)

The slat tilt angle stayed within a narrow range (between -45 and -60 degrees) most of the time (see Figure 5.8), primarily because of the combined effect of the direct and indirect components of the solar radiation. The slats were set to the horizontal position after 5:20pm because the exterior daylight levels were below the threshold level of 5,000 lux.

A control cycle consists of the ANN-based angle control, the trial-and-error control to find an actual optimum, and a 10-minute idle period. The length of a cycle depends on the number of 3-degree step angle adjustments, each of which takes at least 10 seconds.

For the PV-only method, there were 47 cycles between 8:00am and 5:17pm (9 hours and 17 minutes), when the angle control was active. A cycle took 11.9 minutes on average. There were 378 step angle adjustments. There were 116 angle adjustments to the estimated optimum (30.7% of all angle adjustments). The other 262 adjustments (69.3%) were made by the trial-and-error control that moved the slat angle from the estimated optimum to the actual optimum. Every trial-and-error adjustment was made to increase the louver PV output; no other criteria were used. To increase the work plane illuminance, 120 adjustments were made. The average difference between the optimal angle acquired using the ANN and the actual optimal angle based on the trial-and-error control was 6.5 degrees. Out of 47 cycles, the difference for 35 (74.5%) cycles was smaller than or equal to 6 degrees (see Figures 5.9 and 5.10). In Figures 5.8 and 5.9, the flat lines represent the 10-minute idle periods between slat angle controls, and the slat angle controls appear as spikes.

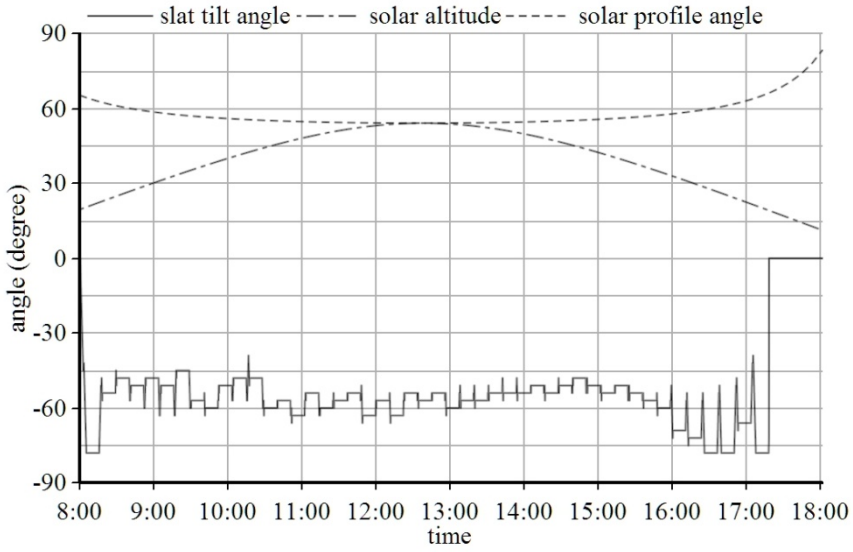

Figure 5.8 Slat tilt angle and the sun position (PV-only method, 4/5/2012)

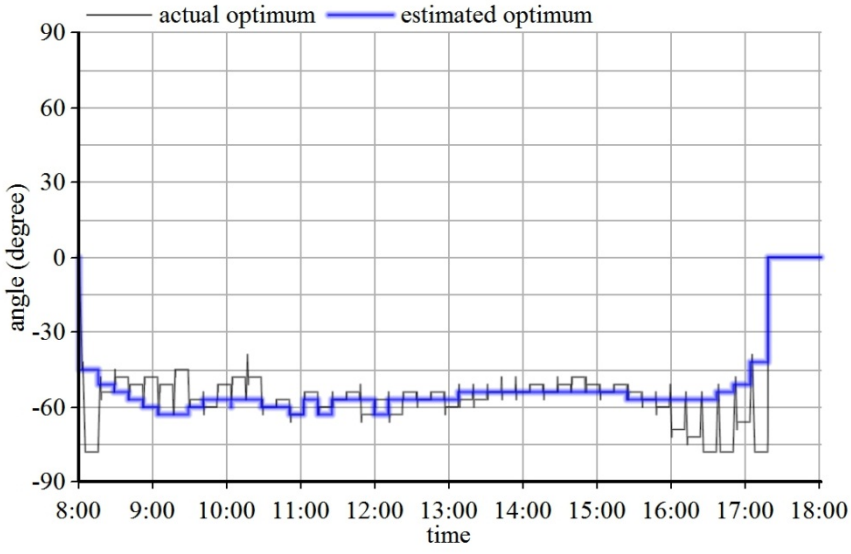

Figure 5.9 Actual and estimated optimal slat angle (PV-only method, 4/5/2012)

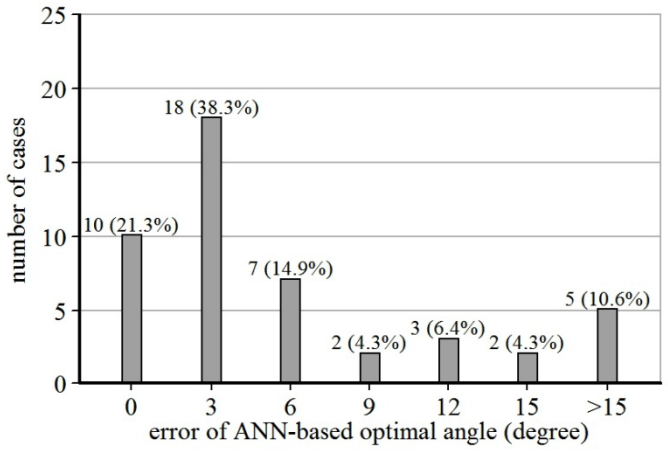

Figure 5.10 Difference between estimated optimal angle acquired using the ANN and actual optimal angle acquired by the trial-and-error control (PV-only method, 4/5/2012)

5.2.2 Results of experiments using the PV+WP method

As discussed in Section 5.2.1 on the PV-only method, maximizing the louver PV output without considering the work plane illuminance leads to an unacceptable light level on the work plane in certain cases. The PV+WP method seeks to prevent unacceptable light levels by including work plane illuminance as a control criterion in addition to electricity output from the PV cells.

The average electric current of the louver PV was 15.70mA, which is 16.5% higher than that of the wall PV, 13.48mA. Between 12:37pm and 4:37pm (four hours after the solar noon), the average electric current of the louver PV and the wall PV was 22.74mA and 16.87mA, respectively (see Figure 5.11 and Table 5.2). The louver PV produced 34.8% more electricity output than the wall PV. The ratio of the louver PV output to the wall PV output was 13.1% lower, in terms of the wall PV output, than that of the PV-only method described in Section 5.2.1. The PV output was lower because the louver angles were adjusted not only for PV electricity output but also for work plane illuminance. The work plane illuminance criterion caused the slat

angle to be tilted up from the maximum PV output angle, maintaining the work plane illuminance at the acceptable level.

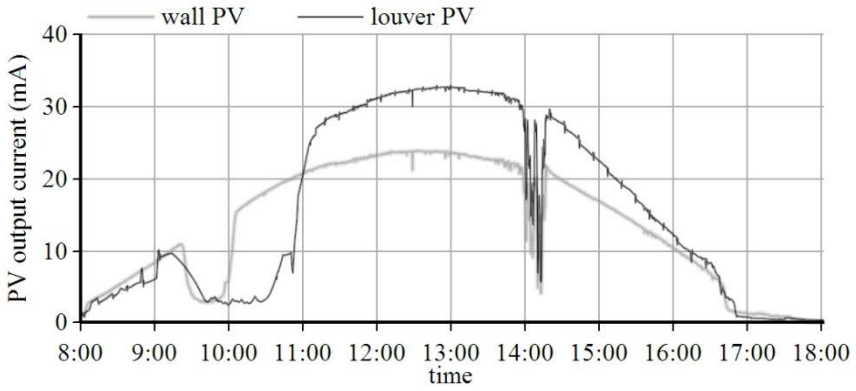

Figure 5.11 Output current of the louver PV (black) and the wall PV (gray) (PV+WP method, 4/7/2012)

Period (hour)	Average I_L (mA)	Average I_W (mA)	Ratio (I_L/ I_W)
8- 9	4.07	5.11	0.80
9-10	6.06	6.21	0.98
10-11	6.26	17.65	0.35
11-12	28.45	22.16	1.28
12-13	32.20	23.65	1.36
13-14	31.62	22.48	1.41
14-15	24.22	17.44	1.39
15-16	17.07	13.60	1.25
16-17	6.57	5.81	1.13
17-18	0.49	0.67	0.73
8-18	15.70	13.48	1.16

Table 5.2 Hourly PV output of the louver and the south wall (4/7/2012)

The work plane illuminance was kept close to the acceptable level (500 lux) whenever possible (see Figures 5.12-13). Out of 7,205 samples, 4,745 (65.9%) were above 500 lux. Due to the shadow on the sensor mentioned in section 5.4.6.1, a partial period between 12:37pm and 4:37pm, four hours after the solar noon, was also investigated. During the period, 2,074 of 2,880

samples (72.0%) were above 500 lux. 2,781 samples (96.6%) were above 450 lux. These results suggest that the control logic is capable of maintaining the work plane illuminance above a target value within an error of 50 lux. Therefore, setting the target illuminance to 550 lux would keep the work plane illuminance above 500 lux, the acceptable level.

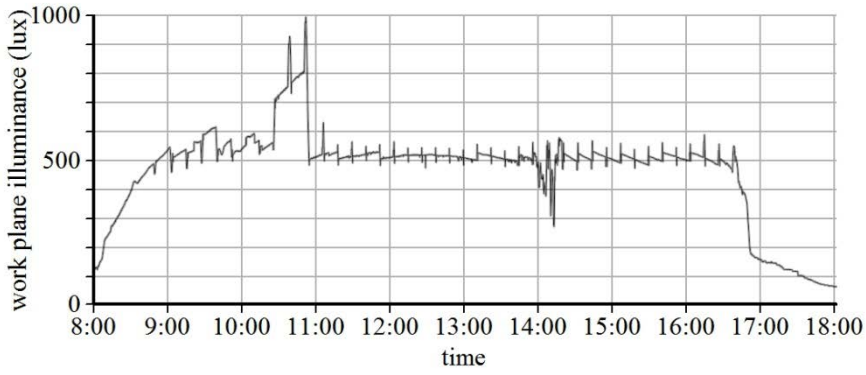

Figure 5.12 Work plane illuminance: PV+WP method (4/7/2012)

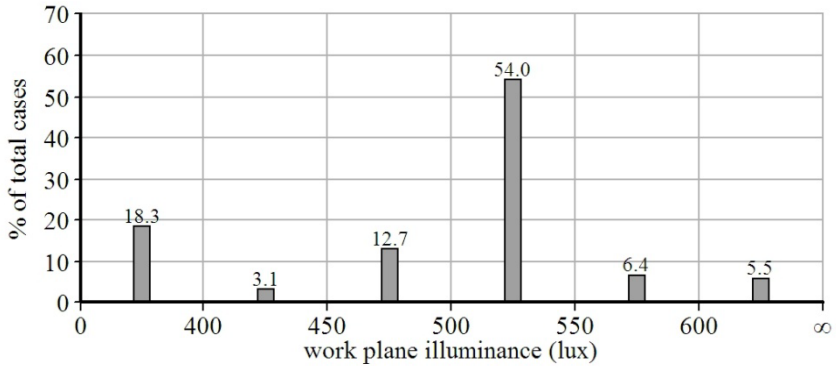

Figure 5.13 Distribution of work plane illuminance: PV+WP method (4/7/2012 8am-6pm)

Although the DGI criterion was excluded from the control method, DGI was within the comfortable range during experiments using the PV+WP control method (see Figures 5.14-15). From 11am to 2pm, the slat angle stayed below zero while DGI was relatively high. During this

period, the PV criterion that maximizes the louver PV output led to the negative slat angle, which kept DGI at acceptable levels.

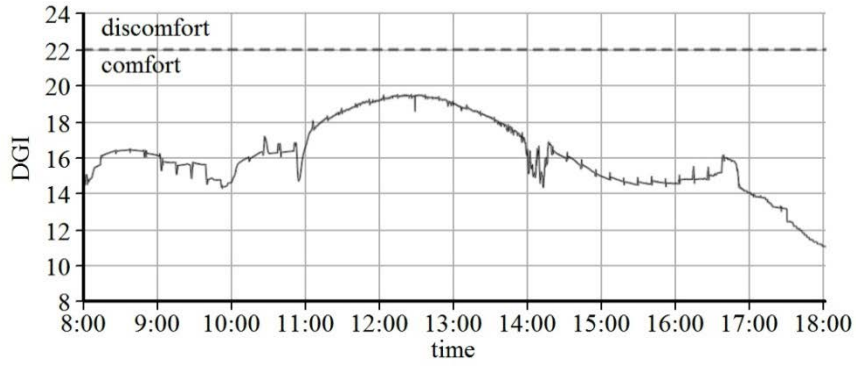

Figure 5.14 DGI: PV+WP method (4/7/2012)

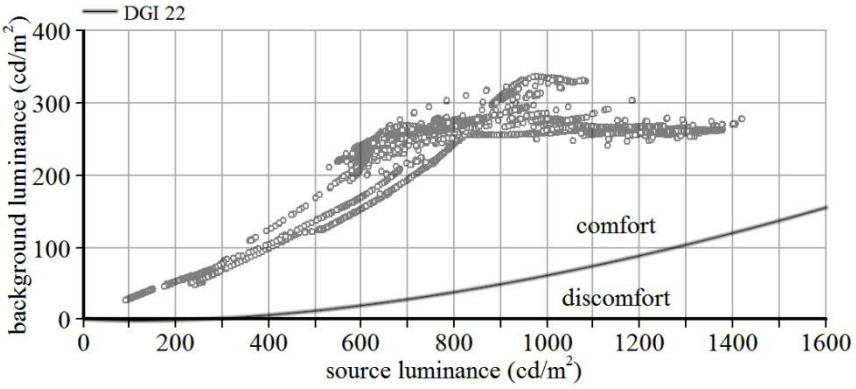

Figure 5.15 Distribution of the factors of DGI: source luminance and background luminance (PV+WP method, 4/7/2012)

The slat tilt angle was controlled to maximize PV output while maintaining the work plane illuminance above an acceptable level. The first step is to set the slat angle to the logically estimated optimal, which serves as the initial angle for the physical local search. The second step is the trial-and-error control, which adjusts the slat angle based on the actual measurements. The third step is to keep the adjusted slat angle for a certain duration (10 minutes) (see Section

4.3 for details). This step prevents too-frequent slat angle adjustment. These three steps were repeated between 8am and 6pm. If the sun was below the horizon or the exterior daylight level was low (<5,000 lux), the slat angle was set to 0, indicating no slat angle control was necessary (see Figure 5.16).

The average difference between the optimal angle acquired using the ANN and that acquired using trial-and-error was 4.9 degrees for the PV+WP method. Because the goal of the trial-and-error control is to find an actual optimum starting at the ANN-based estimated optimum, the small average difference indicates the accuracy of the ANN. There were 49 control cycles between 8:01am and 5:29pm (9 hours and 28 minutes), when the angle control was active. For 41 of the 49 cycles (83.7%), the difference was less than or equal to 6 degrees (Figures 5.17-18). A cycle took 11.6 minutes on average. There were 359 angle adjustments: 93 ANN-based adjustments and 266 trial-and-error adjustments. During the trial-and-error control, 146 adjustments were made to increase PV output when the work plane illuminance was above the acceptable level. To increase the work plane illuminance, 120 adjustments were made.

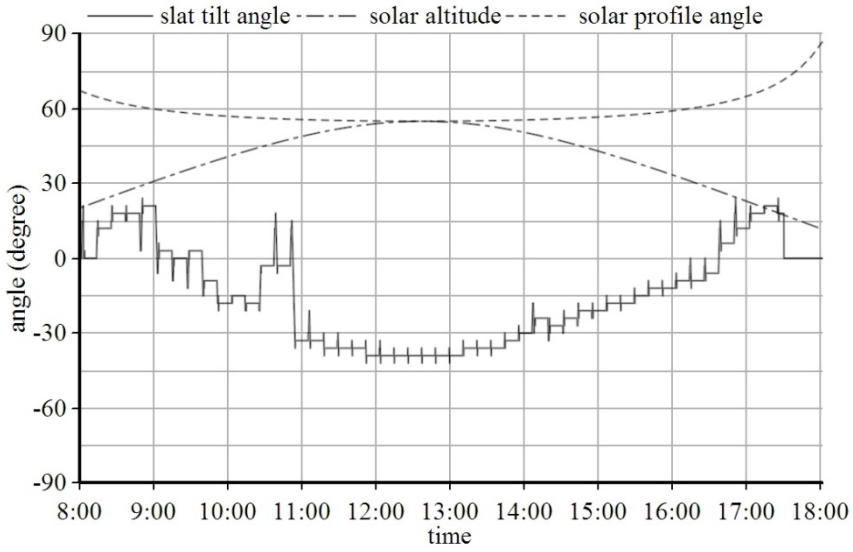

Figure 5.16 Slat tilt angle and sun position (PV+WP method, 4/7/2012)

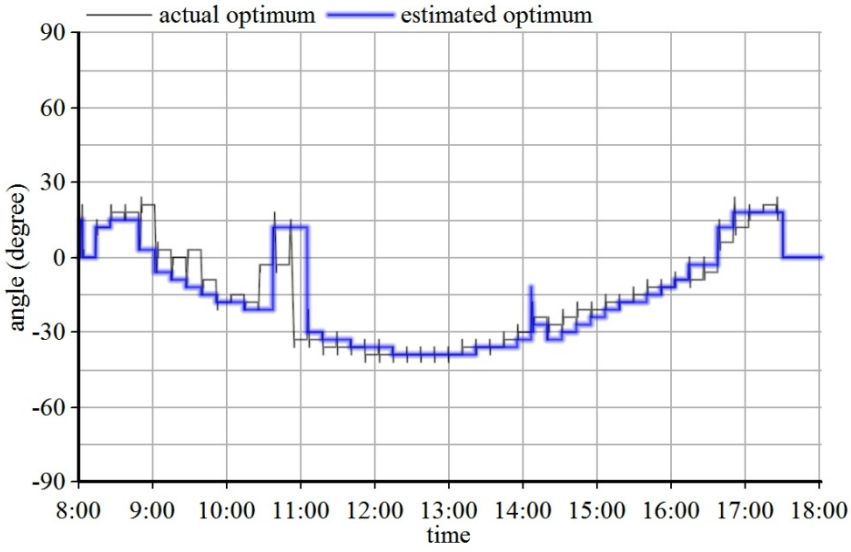

Figure 5.17 Optimal slat angle acquired using the ANN (thick line) and actual optimal slat angle acquired using the trial-and-error control (thin line) (PV+WP method 4/7/2012)

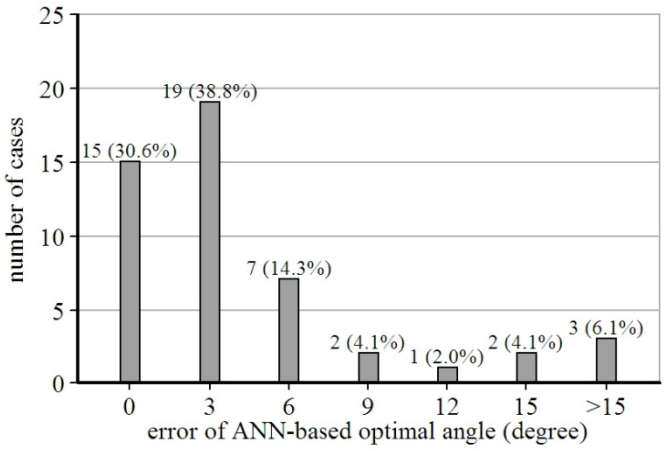

Figure 5.18 Difference between estimated optimal angle acquired using the ANN and actual optimal angle acquired using the trial-and-error control (PV+WP method, 4/7/2012)

The sky was almost clear on the day of the experiment. The sudden drop of the exterior vertical illuminance between 10:30am and 11:00am was due to the shadow of the window frame on the sensor. There was a short period of daylight fluctuation between 2:00pm and 2:20pm.

5.2.3 Results of experiments using the PV+WP+DGI method

In this control method, the daylight glare estimated by DGI had the highest priority. In other words, the controller attempted to lower DGI when it was greater than 22. The work plane illuminance had the second-highest priority. Only after these two criteria were satisfied did the controller attempt to maximize the louver PV output. As discussed in the previous section, the DGI criterion remained inactive (DGI < 22) (see Figure 5.22). Therefore, the results are identical to those of the PV+WP method.

The average electric current from the louver PV (15.78mA) was 17.8% higher than that from the wall PV (13.40mA) between 8am and 6pm. During the four hours after the solar noon, 12:37pm – 4:37pm, the average electric current of the louver PV and the wall PV was 23.46mA and 17.31mA, respectively. The louver PV's electric current was 35.6% higher than the wall PV's. These values (17.8% and 35.6%) are consistent with the corresponding values from the PV+WP method (16.5% and 34.8%) (see Figure 5.19).

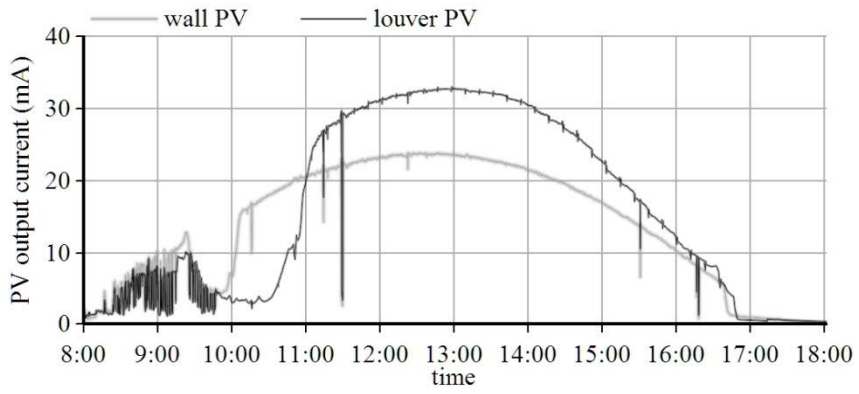

Figure 5.19 Output current of the louver PV (black) and the wall PV (gray) (PV+WP+DGI method, 4/8/2012)

During the 10 hours between 8am and 6pm, the work plane illuminance was higher than or equal to 500 lux for 6 hours, 1 minute and 20 seconds (60.2% of the total duration). Between 12:37pm and 4:37pm, the work plane illuminance was higher than or equal to 500 lux for 2 hours, 41 minutes and 50 seconds (67.4% of the period). It was 4.6% lower than the corresponding value of the PV+WP method. However, 99.7% of the samples during the period were above 450 lux, 3.1% higher than in the PV+WP method (see Figures 5.20-21). This difference resulted solely from different sky conditions; two control methods used the same ANN and the same algorithm. These results demonstrate that the control methods with the work plane illuminance criterion are

capable of maintaining the work plane illuminance above 450 lux (50 lux lower than the target illuminance) when there is no fluctuation in daylight level.

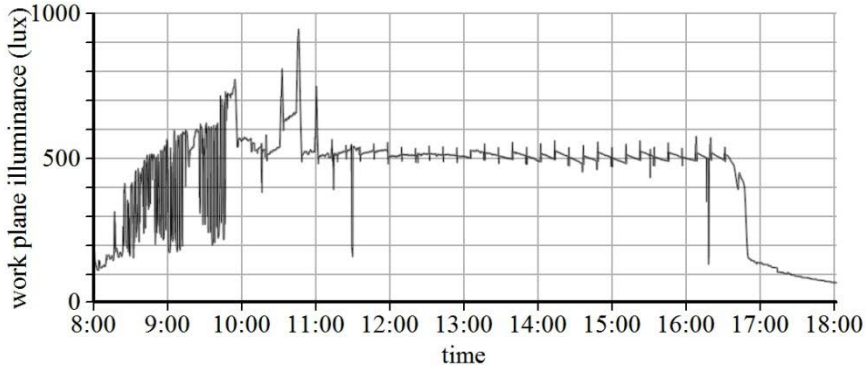

Figure 5.20 Work plane illuminance (PV+WP+DGI method, 4/8/2012)

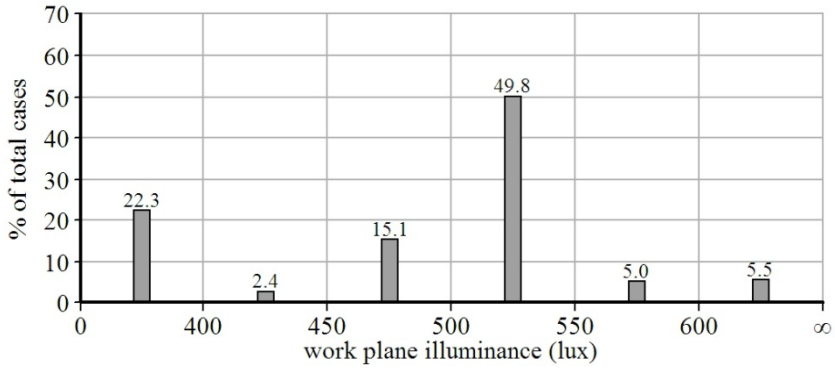

Figure 5.21 Error in work plane illuminance (PV+WP+DGI method, 4/8/2012)

The DGI result for the PV+WP+DGI method was identical to that for the PV+WP method. DGI remained within the comfortable range, staying below 22 during the entire time span (see Figure 5.22). The ratio of the background luminance to the window luminance was higher than the threshold of discomfort (see Figure 5.23).

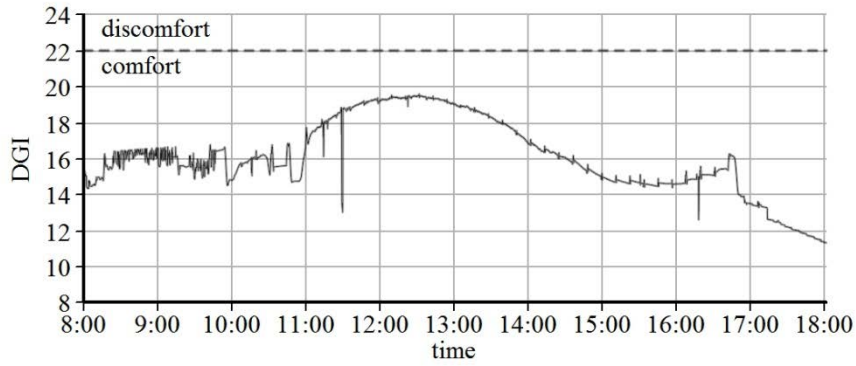

Figure 5.22 DGI (PV+WP+DGI method, 4/8/2012)

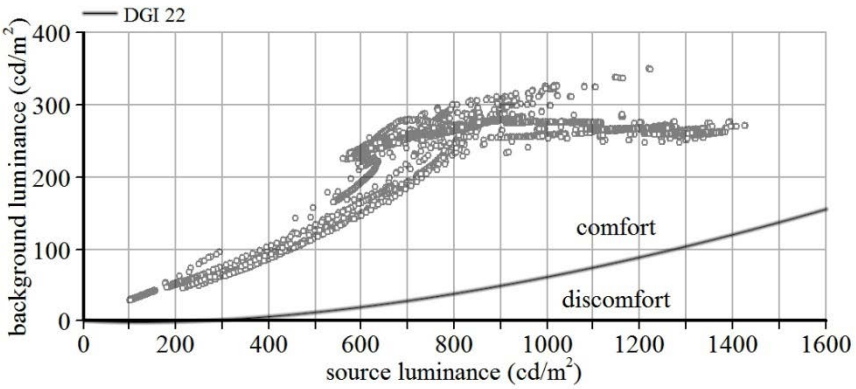

Figure 5.23 Distribution of the factors of DGI: source luminance and background luminance (PV+WP+DGI method, 4/8/2012)

There were 47 control cycles between 8:00am and 5:12pm (9 hours and 12 minutes), when the angle control was active. A cycle took 11.7 minutes on average. The slat tilt angle was adjusted 356 times; there were 98 ANN-based adjustments and 258 trial-and-error adjustments. During the trial-and-error control, 131 adjustments were made to increase PV output when the work plane illuminance was above the acceptable level. To increase the work plane illuminance, 127 adjustments were made. No adjustments were made to decrease DGI because it stayed within the acceptable range. The average difference between the estimated optimal angle and the actual

optimal angle was 4.5 degrees. In 37 out of 47 cycles (78.7%), the difference between the estimated optimal angle and the actual one was smaller than or equal to 6 degrees (see Figures 5.24-26).

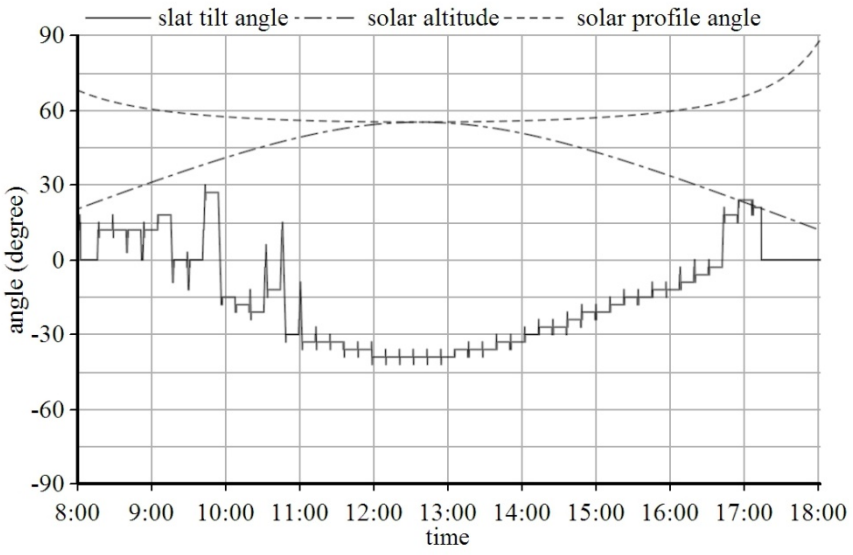

Figure 5.24 Slat angle and sun position (PV+WP+DGI method, 4/8/2012)

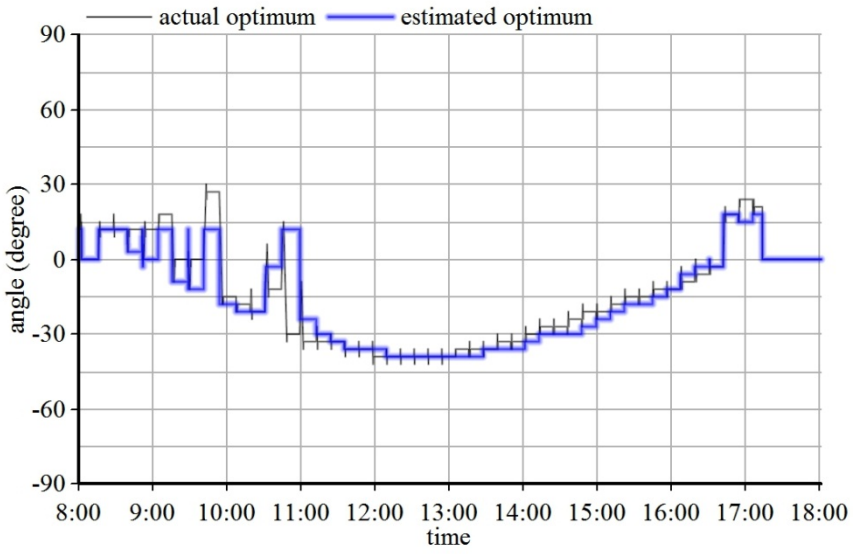

Figure 5.25 Actual and estimated optimal angle (PV+WP+DGI method, 4/8/2012)

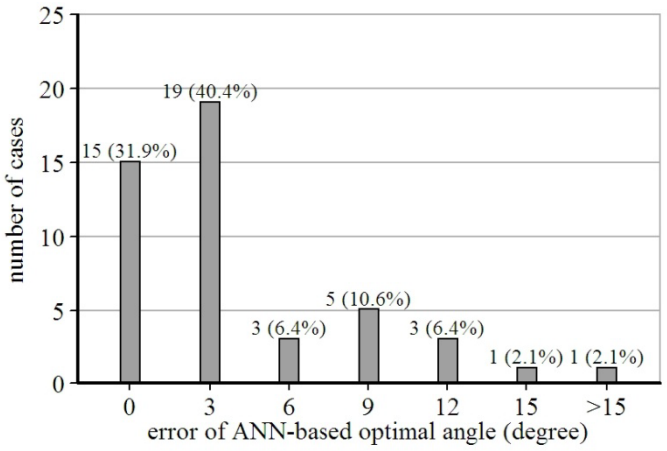

Figure 5.26 Difference between estimated optimal angle and actual optimal angle (PV+WP+DGI method, 4/8/2012)

5.3 Comparison of control methods

The effect of the work plane illuminance constraint is assessed by comparing the PV-only method and the PV+WP method. The comparison is based on the four hours after the solar noon (12:37pm-4:37pm, the gray area in Figure 5.27) to exclude from consideration most of the erroneous data and daylight fluctuation. The sensor error occurred due to the shadow on the sensor between 10:30am and 11am, and after 4:40pm. The performance of PVIS during the four hours before the solar noon was assumed to be identical to that of the four-hour period after the solar noon, because the sun position in the two periods is symmetric.

The work plane illuminance constraint decreased the louver PV output by 8.8%. For the PV-only method tested on 4/5/2012, the average output current of the louver PV was 24.67mA during the comparison period, 48% higher than the average wall PV output, 16.68mA. For the PV+WP method on 4/7/2012, the average louver PV output was 22.77mA, 35% higher than the average wall PV output, 16.89mA. For the PV+WP+DGI method on 4/8/2012, the average

louver PV output was 23.49mA, 36% higher than the average wall PV output, 17.33mA. The louver PV output was normalized using the wall PV output for comparison. Adopting the work plane illuminance constraint caused the normalized ratio of the louver PV to the wall PV to decrease from 1.48 (PV-only method) to 1.35 (PV+WP method). The decrease was 8.8% of the electricity output of the PV-only method. The gray area in Figure 5.26 highlights the difference between the louver PV output of the PV-only method and that of the PV+WP method between 12:37pm and 4:37pm. For the PV+WP+DGI method, the decrease was 8.4%, from 1.48 to 1.36.

Using the work plane illuminance criterion maintained the work plane illuminance at acceptable levels. In contrast, using the PV-only method, which excluded the daylight criterion, resulted in unacceptable light levels on the work plane. The average work plane illuminance of the PV-only method, the PV+WP method, and the PV+WP+DGI method was 300, 504, and 505 lux, respectively. For the PV-only method, the work plane illuminance was below 450 lux for the entire comparison period; it fell below 350 lux for 69% of the period. For the remaining 31% of the period, it was either between 350 and 400 lux (27% of the period) or between 400 and 450 lux (4% of the period). In contrast, using the other two methods (PV+WP and PV+WP+DGI), both of which include the work plane illuminance constraint, resulted in values above 500 lux for 72% and 67% of the period, respectively. In addition, the work plane illuminances of the two methods were above 450 lux for most of the comparison period (97% of the period for PV+WP and 99% for PV+WP+DGI) (see Figure 5.28).

DGI remained within the comfortable range for every control method tested. When DGI is below 22, the threshold between comfort and discomfort, daylight glare is considered acceptable.

During the experiments, all DGI values were below 20. For more than half of the experiment period, the daylight glare was deemed non-perceptible (DGI greater than 16 was considered perceptible). The duration of non-perceptible daylight glare for the PV-only method, the PV+WP method, and the PV+WP+DGI method was 51%, 58%, and 53% respectively. In the other cases, DGI was perceptible and acceptable (between 16 and 20) (see Figure 5.29).

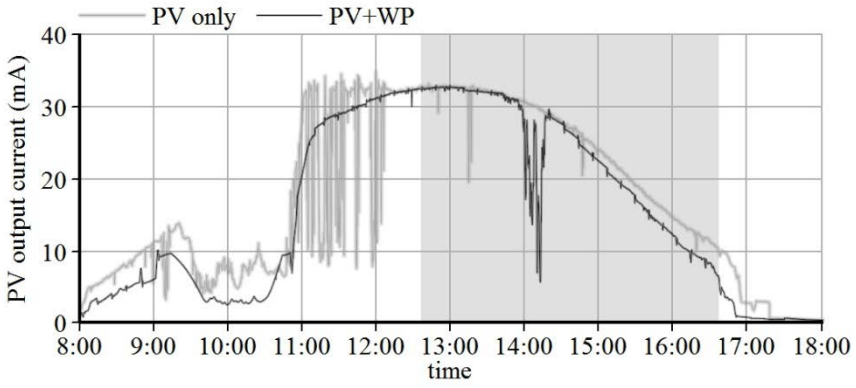

Figure 5.27 PV output current of PV-only method (gray) and PV+WP method (black)

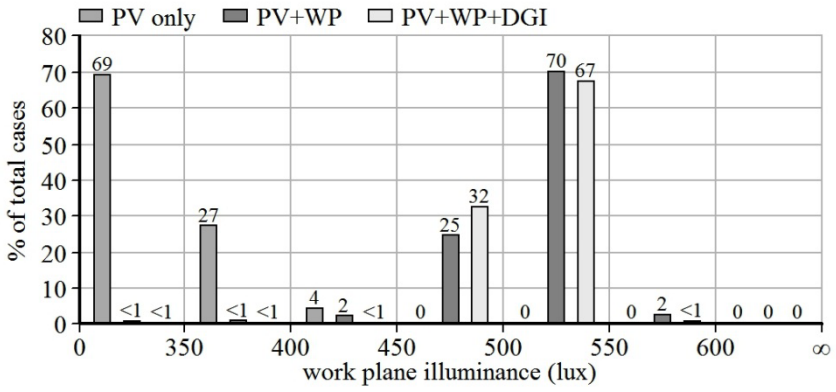

Figure 5.28 Distribution of work plane illuminance

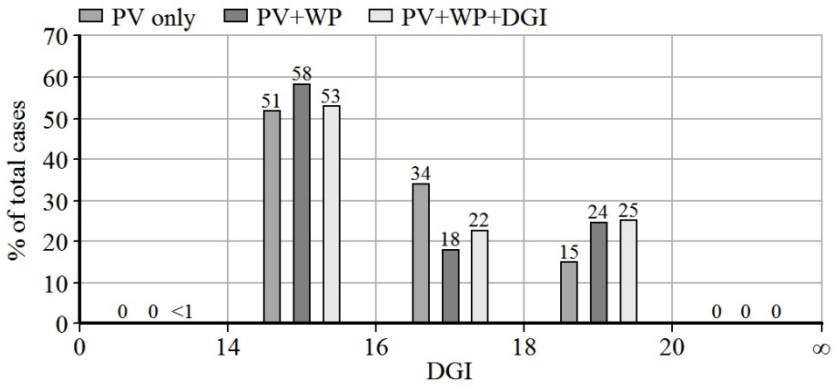

Figure 5.29 Distribution of DGI

The energy saving benefit of the PV+WP method is greater than that of the PV-only method. The total energy saving is the sum of PV electricity output and the reduction in electric lighting energy. For the PV-only method, the daily electricity output from the louver PV modules was 1.38kWh/day, which is 28.8% of the test building's estimated lighting energy demand, 4.8kWh/day (see Table 4.2). Because the work plane illuminance was below the acceptable level, there was no electricity saving from reducing artificial lighting. The electricity output was calculated based on the output of a single PV module of the scale model. The electricity output of the module after the solar noon was 532.6mWh. Because the output before the solar noon fluctuated, it was replaced with the output after the solar noon to represent a clear sky. The output was based on the PV output current measured every 5 seconds, the open circuit voltage (8V), and the fill factor of the PV module (0.65). The fill factor refers to the ratio of the maximum power of a PV module to the open circuit voltage (V_{OC}) multiplied by the short circuit current (I_{SC}). Therefore, for the PV-only method, the daily output of a single PV module on 4/5/2012 was estimated as 1.07Wh under a clear sky. After applying the total number of PV modules (36), the scale to the real building (1:6) to the PV output of the scale model, the daily

PV output of a full-scale building (1.38kWh/day) was acquired. The wall PV output of the full-scale building on the same day was 0.92kWh.

For the PV+WP method, the energy saving was at least 1.91kWh/day: 1.25kWh from the louver PV modules and 0.66kWh from electric lighting energy reduction. The total energy savings represented 39.7% of the test building's daily lighting energy demand. The duration of the work plane illuminance above 500 lux, 6.6 hours, was used instead of the duration above 450 lux (7.9 hours). Because the work plane was in the center of the room, the lighting energy saving for the southern half closer to the window was considered. In addition, the lighting energy demand was assumed to be evenly distributed throughout the day. This assumption was used to avoid over-estimating the electric lighting energy savings. Therefore, the energy conservation from natural lighting was at least 0.66kWh (6.6hours / 24hours * 12 m^2 * 0.2kWh/m^2). The energy saving of the PV+WP+DGI method was 1.88kWh (39.3% of daily lighting energy demand).

As discussed above, the total energy benefit of the control methods with the work plane illuminance criterion was greater than that of the method without it. Although the PV outputs of the PV+WP method and the PV+WP+DGI method were lower than that of the PV-only method, their energy savings from natural lighting led to higher overall energy savings. The daylight glare stayed within the comfort range, ensuring that the louver could be automatically controlled without the occupants manually overriding it in an attempt to reduce visual strain.

5.4 Effect of exterior daylight level

The electricity current from the wall PV was proportional to the exterior vertical illuminance. The output current in mA was approximately 0.04% of the exterior vertical illuminance in lux (the broken line in Figure 5.30). Some degree of non-linearity existed between the two factors.

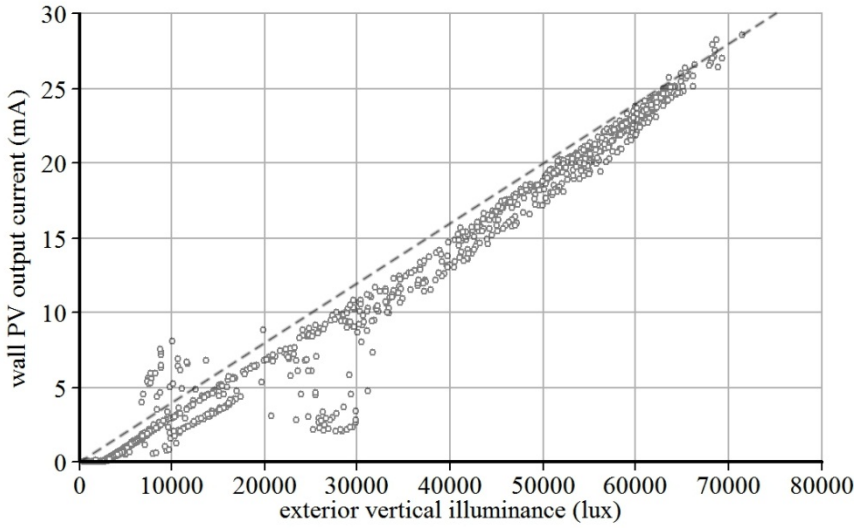

Figure 5.30 Exterior vertical illuminance vs. wall PV output current (3/24/2012~3/27/2012)

The work plane illuminance was proportional to the exterior vertical illuminance when the louver slats were fixed at a constant angle. The experiment data for two different slat angles (0 and -45 degrees) show this proportional relation (see Figures 5.31-32). Factors other than the exterior vertical illuminance also affected the work plane illuminance. These factors included the luminance distribution of the sky, the sun position, and sensor errors. However, the analysis excluded the effect of such factors on the work plane illuminance; instead, an ANN was used to represent the effect.

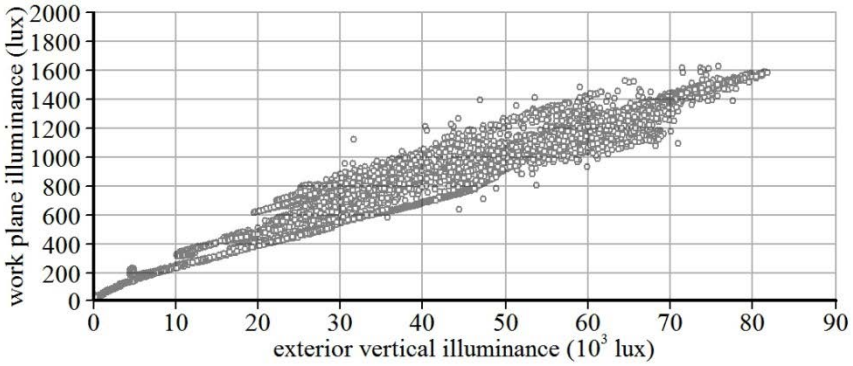

Figure 5.31 Work plane illuminance (slat angle = 0 degree, 2/28/2012)

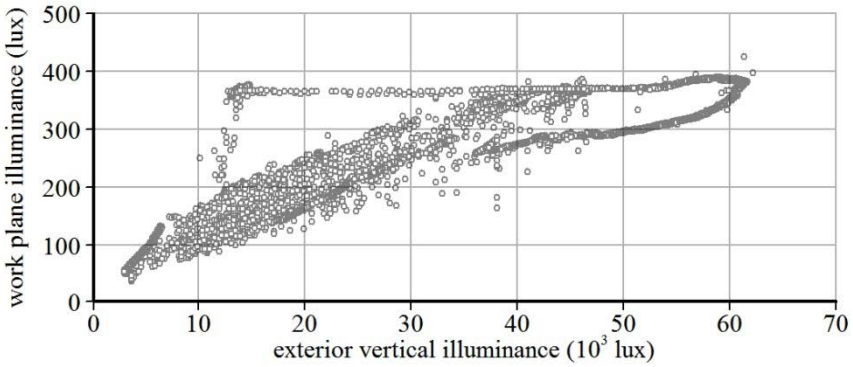

Figure 5.32 Work plane illuminance (slat angle = -45 degrees, 4/2/2012)

Higher DGI values were caused by a higher exterior vertical illuminance when the slat angle was constant. The experiment on 4/2/2012, when the slat angle was fixed at -45 degrees, is an example of this relation (see Figure 5.33). On that day, the peak DGI occurred around the solar noon (12:37pm), when the exterior illuminance was at maximum. However, the effect of the exterior vertical illuminance on DGI was non-linear.

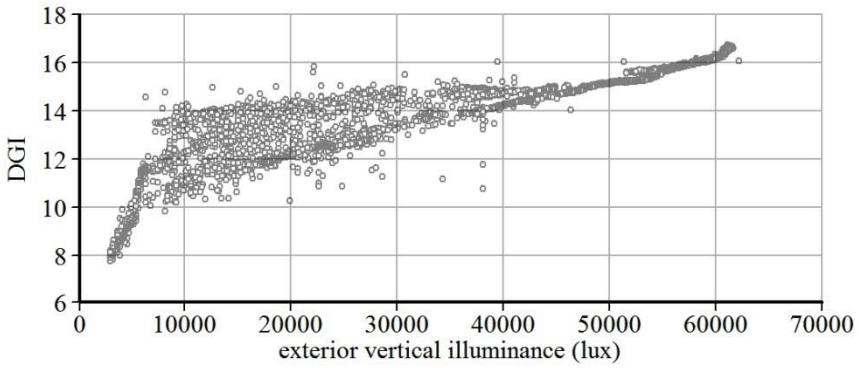

Figure 5.33 Exterior vertical illuminance vs. DGI (slat angle = -45 degrees, 4/2/2012)

5.5 Estimated PV output for the PV-only method

5.5.1 Self-shading of the louver on PV modules

With the exception of the uppermost slat, a louver slat can be shaded by the slat directly above it. Likewise, the PV modules on the louver can also be shaded. During the experiment period, April 5 to April 8, the effect of partial shading on the louver PV was insignificant. The regions of the slat angle causing partial shading (gray areas in Figure 5.34-36) existed before 9am and after 4pm, when the sun profile angle was greater than 60 degrees. However, the slat angle was within those regions for only a short time. The ranges of slat angle causing PV self-shading also appear in Appendix C.

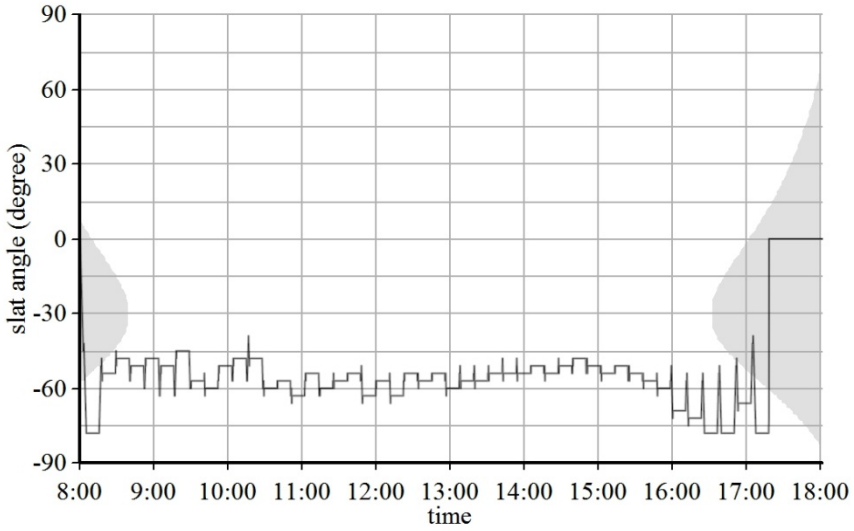

Figure 5.34 Range of slat angle causing PV self-shading (4/5/2012, PV-only method)

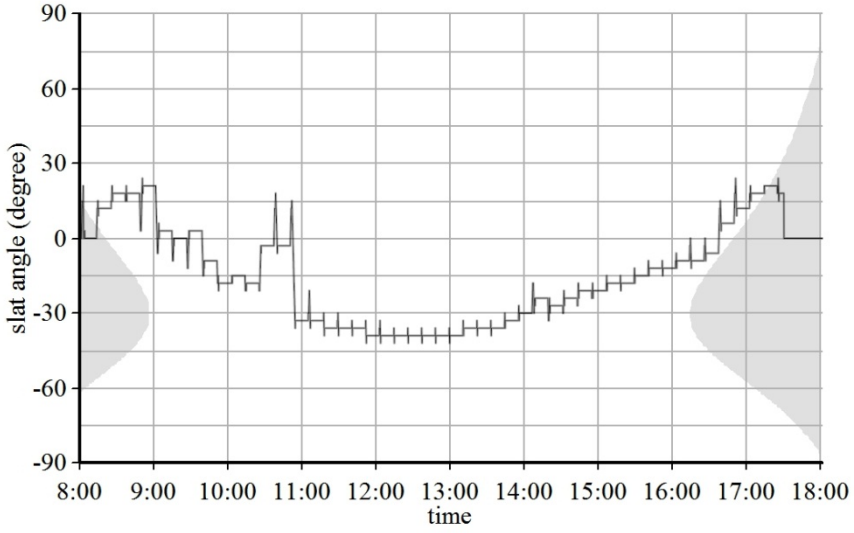

Figure 5.35 Range of slat angle causing PV self-shading (4/7/2012, PV+WP method)

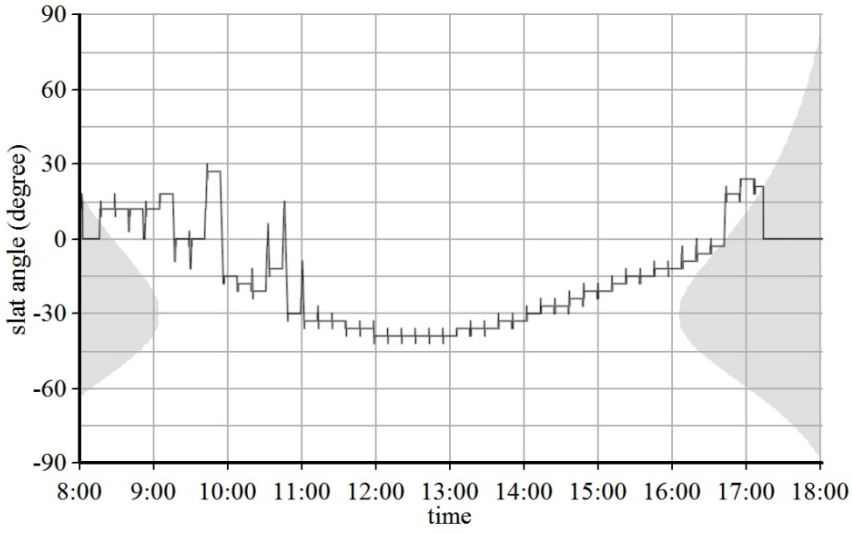

Figure 5.36 Range of slat angle causing PV self-shading (4/8/2012, PV+WP+DGI method)

5.5.2 Effect of the indirect component of solar radiation

The indirect component of daylight includes the diffuse component from the sky and the reflected component from the ground. The diffuse component was calculated based on the CIE standard clear sky model (Standard Sky Type 12) (CIE, 2003). The reflected component certainly existed, but it was excluded from the estimation of the indirect component due to its high dependence on ground conditions.

A fraction of the half-hemisphere is visible from a louver slat, while the entire half-hemisphere is visible from the south wall. The view from a louver slat is occluded by its adjacent upper slat. The visible sky area is dependent on the slat angle. The sky area visible from the center of a PV module on the louver slat tilted at two exemplar angles is illustrated in Figure 5.37 (+45 degrees) and Figure 5.38 (-45 degrees). The visible sky area decreases as the slat angle increases from -90 to 90 degrees, with an exceptional region between -15 and 0 degrees where the visible sky

area increases (see Figure 5.39). The illustrations are for ideal conditions, where no occluding objects exist in the view to the sky. In the experiments, however, the view to the sky was obstructed by trees and buildings.

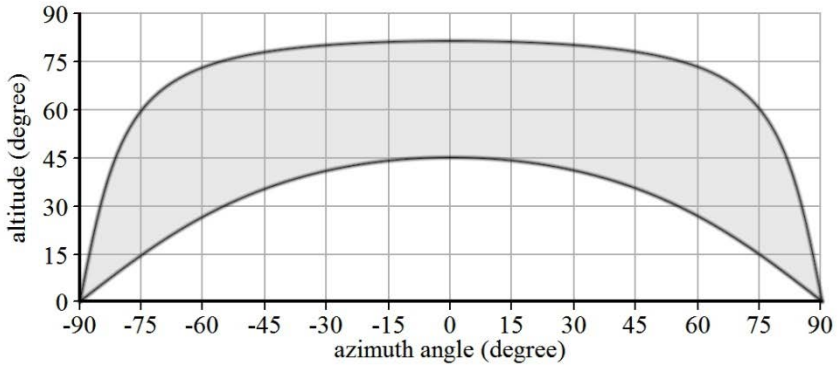

Figure 5.37 Sky area visible from the center of the louver PV module (slat angle = +45 degrees)

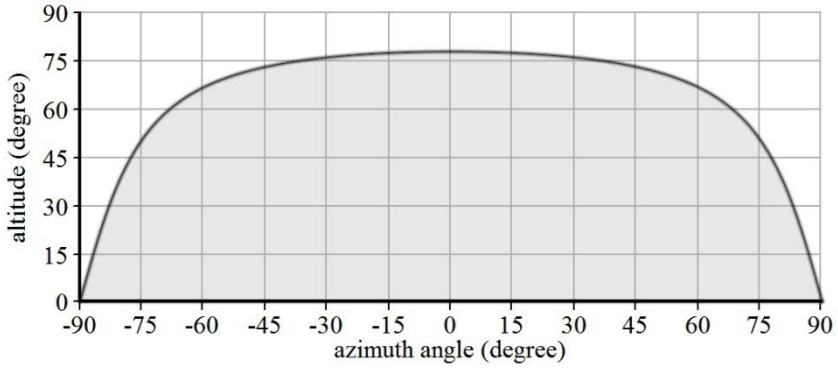

Figure 5.38 Sky area visible from the center of the louver PV module (slat angle = -45 degrees)

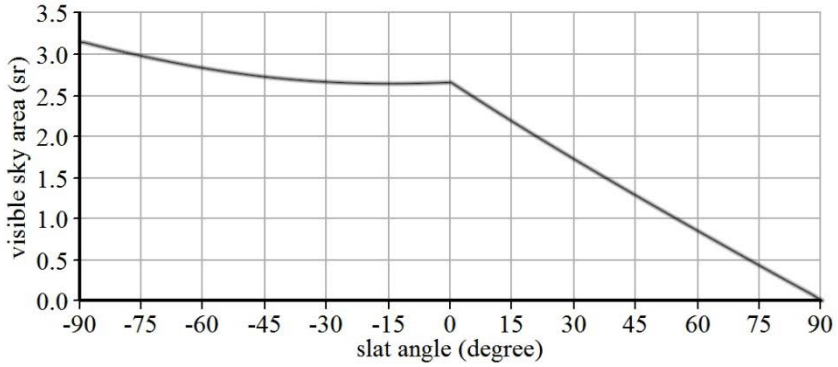

Figure 5.39 Slat angle vs. sky area visible from the center of a louver PV module

The solar radiation on a PV module also depends on the luminance distribution of the sky and the incident angle of sky luminance on the module. For a clear sky, the maximum diffuse component of solar radiation at the center of a PV module on an obstructed (non-top) slat occurs -56 degrees at the solar noon (see Figure 5.40). Because the sun path changes daily, this is an instance for the solar altitude of 50 degrees. For the overcast and the uniform sky, the diffuse component is independent of the sun position. The maximum diffuse component occurs at the slat angle of -56 degrees for the uniform sky (Figure 5.41) and -51 degrees for the overcast sky (Figure 5.42). The clear sky model was used to estimate the PV output in Sections 5.5.3 and 5.5.4.

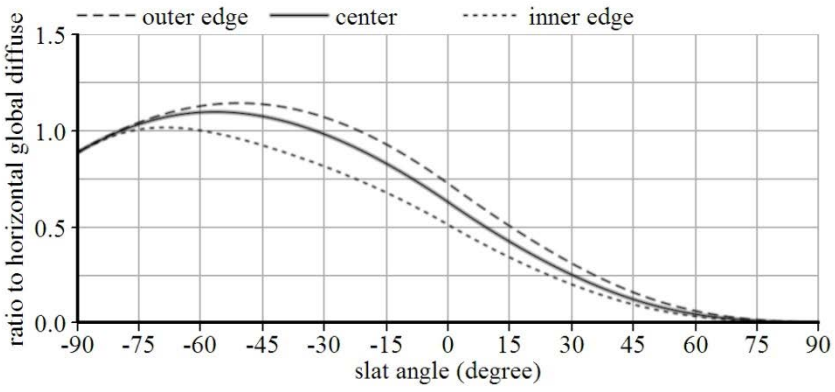

Figure 5.40 Ratio of the diffuse component of solar radiation on the louver slats to that on the horizontal surface under CIE clear sky model (maximum = 1.10 at -56 degrees) at the solar noon (solar altitude = 50 degrees)

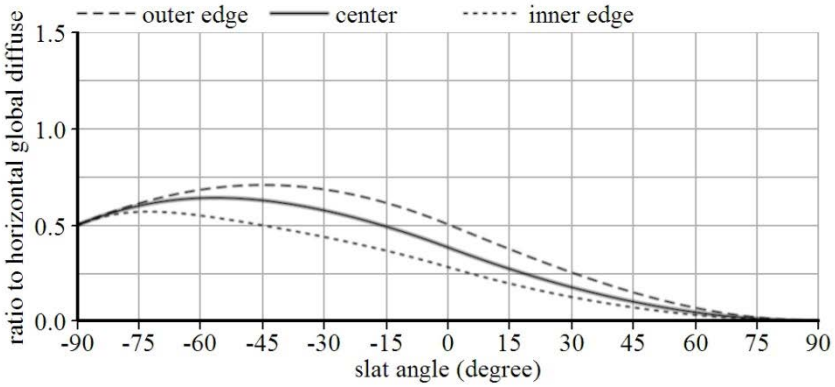

Figure 5.41 Ratio of the diffuse component of solar radiation on the louver slats to that on the horizontal surface under CIE uniform sky model (maximum = 0.64 at -56 degrees)

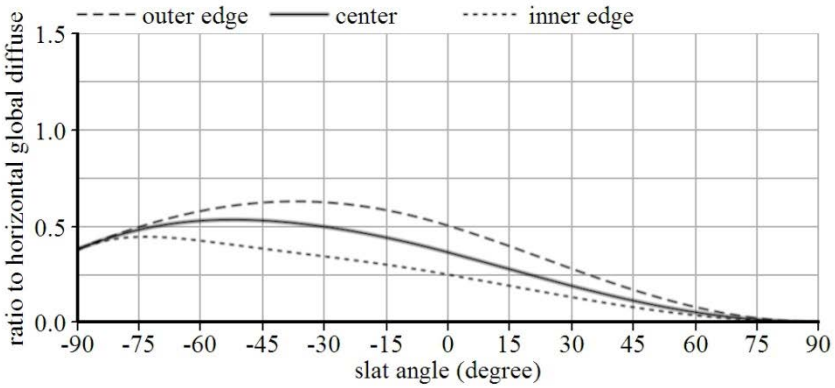

Figure 5.42 Ratio of the diffuse component of solar radiation on the louver slats to that on the horizontal surface under CIE overcast sky model (maximum = 0.53 at -51 degrees)

5.5.2.1 Results of PV output experiments

The maximum PV output occurred at the slat angle of -63 degrees. The slat angle was 23 degrees lower than the slat angle minimizing the sunlight incident angle, -40 degrees. It was close to the slat angle maximizing the diffuse component, -62 degrees. This was due to the

effect of the reflected component from the ground. The increase of PV output between 54 and 72 degrees was due to the solar radiation reflected by the surface of the adjacent slat. Figure 5.43 shows PV electricity output as a function of slat tilt angle under the clear sky conditions of March 25. Figures 5.44 and 5.45 show that the measured ratio of the louver PV output to the wall PV output coincides with the ratio of the direct component of solar radiation on the louver PV to that on the wall.

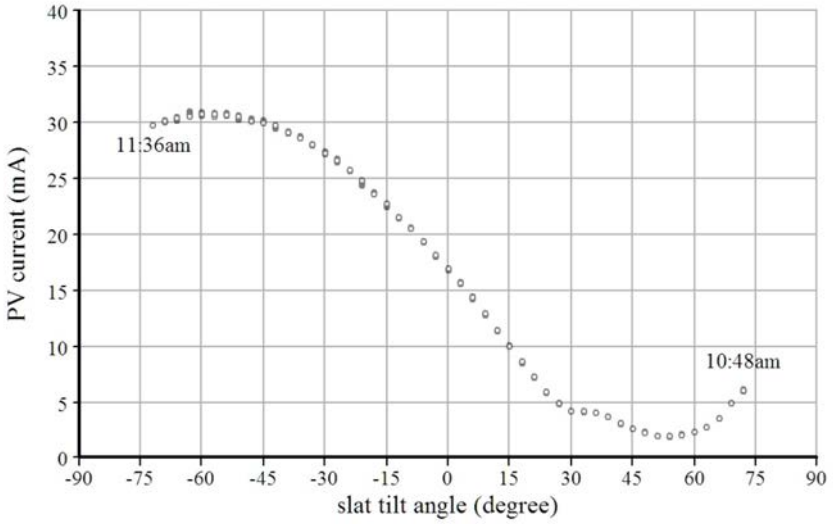

Figure 5.43 Slat tilt angle vs. louver PV output current (10:48am-11:36am, 3/25/2012)

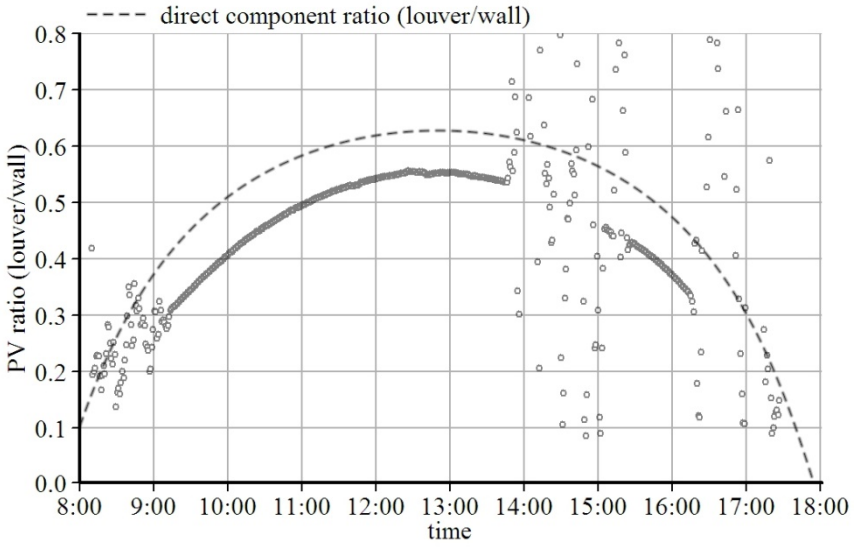

Figure 5.44 PV output ratio of the louver to the wall (dots) and direct component ratio (broken line) on a clear day before the spring equinox (slat tilt angle = 0 degrees, 2/6/2012)

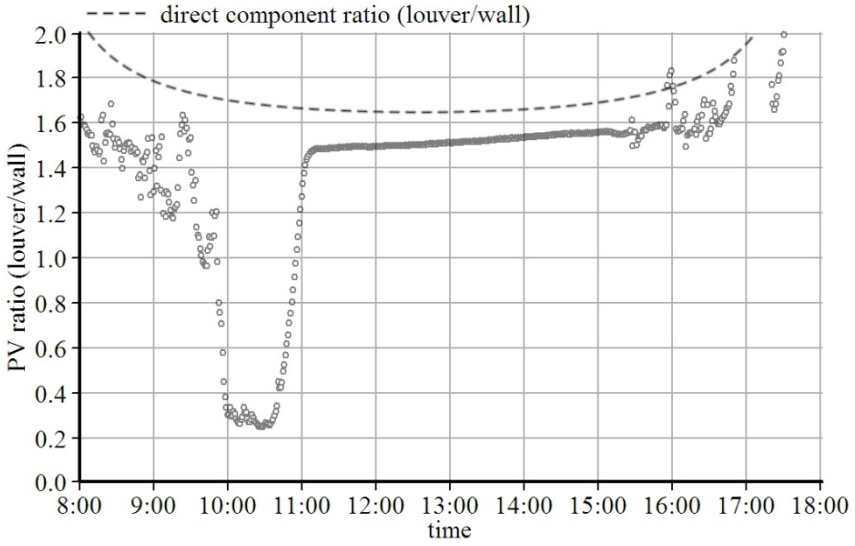

Figure 5.45 PV output ratio of the louver to the wall (dots) and direct component ratio (broken line) on a clear day after the spring equinox (slat tilt angle = -45 degrees, 4/2/2012)

5.5.3 Estimation of optimal slat angle for maximum louver PV output

The estimated slat angle for maximum louver PV output was determined based on the effect of the slat angle and the sun position on the direct and indirect solar irradiances on the louver PV modules. Because the contribution of the indirect component to the PV output varies depending on the sky conditions, it is difficult to estimate the exact angle of maximum PV output. Therefore, the slat angle maximizing the direct component is used as an alternative solution. Maximizing the direct component when it is dominant would result in a PV output close to the actual maximum. Unless the louver PV modules are shaded, the slat angle minimizing the sunlight incident angle is used. The angle is equal to the solar profile angle minus 90 degrees ($\theta_{TILT} = \theta_P - \pi/2$). When the modules are shaded, the slat angle has no effect on the PV output (see equations 13 and 14 in Section 4.8.1). Therefore, the slat angle closest to that maximizing the diffuse component was used. The angle is limited to the range in which the self-shading on the louver PV occurs.

The slat angle maximizing the diffuse component on the obstructed louver PV modules is between -65 and -55 degrees. The maximum level of the diffuse component is at solar noon, and the minimum is at sunrise and sunset. Although the diffuse component does exist before sunrise and after sunset, it is excluded due to its insignificant contribution to the PV output. The slat angle of the maximum diffuse component is between -65 and -64 degrees in winter (12/21), between -62 and -59 degrees in spring and fall (3/21 and 9/21), and between -59 and -55 degrees in summer (6/21) (see Figures 5.46). These angles are based on clear sky conditions.

As discussed above, the slat angle maximizing the louver PV output exists between that maximizing the direct component of solar radiation and that maximizing the indirect component.

Because the reflected component of the indirect component is highly dependent on ground conditions and thus unpredictable, the diffuse component is used as approximation the indirect component. The ranges of the slat angle of maximum PV output are shown in Figure 5.47 (April 5) and Figure 5.48 (December 21).

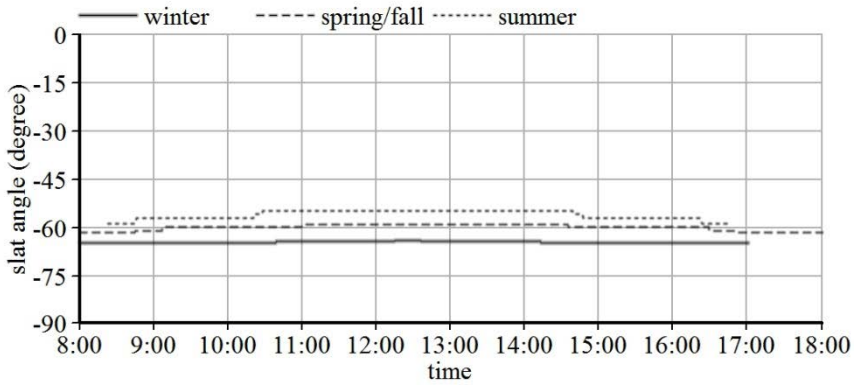

Figure 5.46 Slat angle of maximum diffuse component of solar radiation (-65 to -64 degrees in winter, -62 to -59 in spring/fall, -59 to -55 in summer)

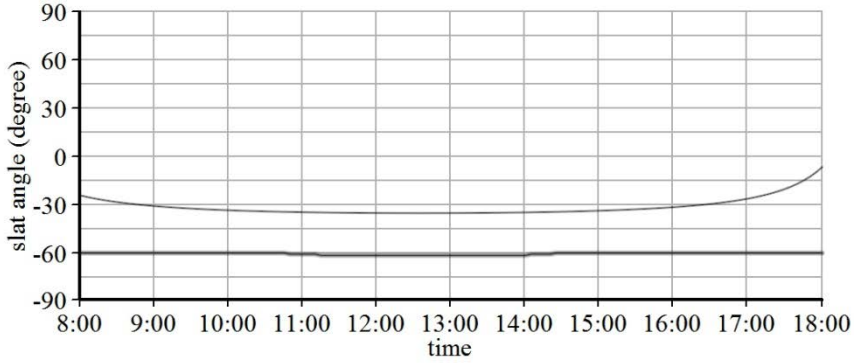

Figure 5.47 Slat angle of minimum solar incident angle (thick line) and slat angle of maximum diffuse component of solar radiation (thin line) (4/5/2012)

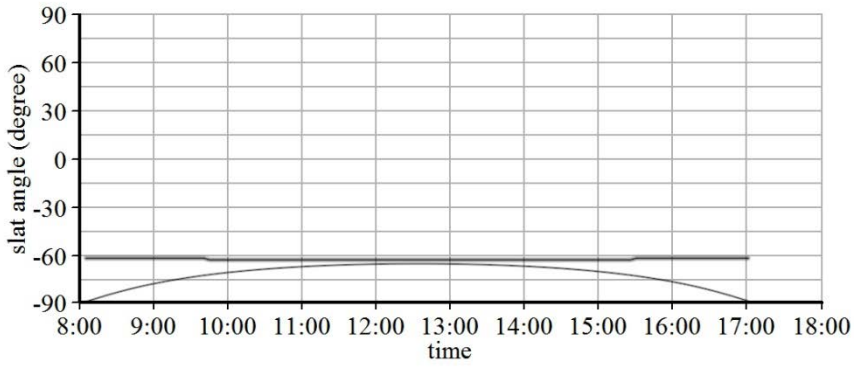

Figure 5.48 Slat angle of minimum solar incident angle (thick line) and slat angle of maximum diffuse component of solar radiation (thin line) (12/21/2012)

5.5.4 Estimated PV output for the PV-only method

The louver PV output controlled to the estimated optimal angle is greater than the wall PV output. The estimated optimal angle is based on clear sky conditions because there is no significant difference in PV output under an overcast or cloudy sky. The change of the solar radiation due to the change of the sun path, which contiuously varies in a yearly cycle, needs to bo considered. The average indicates the upper limit of the electricity output from the louver PV and the wall PV. The direct components of the solar radiation on the obstructed and the unobstructed slats in Table 5.1 are relative to the direct normal component of the solar radiation (see also Appendix B). For example, on 12/21, the direct component on the louver PV is 82.6% of that on the sun-tracking surface and 6% higher than that on the wall PV (77.7% of the direct normal). On that day, the louver PV modules were exposed to direct sunlight for 9 hours and 1 minute. The sun azimuth from the south was between -90 and 90 degrees, and the sun altitude was between 0 and 90 degrees during that experiment period. The period is limited by the solar altitude before the spring equinox and after the fall equinox, and by the solar azimuth between the spring equinox and the fall equinox. Because the top slat is unobstructed, its values are also calcuated and

compared to values of the other obstructed slats. Over the course of a year, the direct component on the PV modules on an obstructed slat is, on average, 39% higher than that on a wall PV with the same area. The decrease in the direct component resulting from partial shading is 13% (from 0.753 of the unshaded top slat to 0.658 of the other slats).

Date	Louver slat		Wall	Louver/wall		Duration of sunlight (hour:min)
	Obstructed	Unobstructed		Obstructed	Unobstructed	
1/21	0.797	0.797	0.732	1.09	1.09	9:33
2/21	0.716	0.716	0.598	1.20	1.20	10:48
3/21	0.642	0.642	0.424	1.51	1.51	11:54
4/21	0.648	0.748	0.324	2.00	2.31	10:10
5/21	0.486	0.825	0.243	2.00	3.40	8:47
6/21	0.422	0.853	0.211	2.00	4.04	8:12
7/21	0.488	0.824	0.244	2.00	3.38	8:48
8/21	0.653	0.744	0.327	1.99	2.28	10:13
9/21	0.640	0.640	0.426	1.50	1.50	11:56
10/21	0.720	0.720	0.604	1.19	1.19	10:44
11/21	0.798	0.798	0.753	1.09	1.09	9:31
12/21	0.826	0.826	0.777	1.06	1.06	9:01
Average	0.658	0.753	0.474	1.39	1.59	9:55

Table 5.3 Direct component on louver and wall with regard to direct normal component

The diffuse component on the obstructed PV modules is at least 10% higher than that on the wall PV modules. The louver PV output from the diffuse sky is higher than the wall PV by 10% in winter, 15% in spring and fall, and 29% in summer when the louver slats are controlled to the estimated angle for the PV-only method described above (see Table 5.4 and Figure 5.49).

Date	Louver/wall	
	Obstructed	Unobstructed
1/21	1.11	1.13
2/21	1.15	1.18
3/21	1.15	1.24
4/21	1.23	1.33
5/21	1.28	1.35
6/21	1.29	1.37
7/21	1.28	1.35
8/21	1.22	1.32
9/21	1.15	1.23
10/21	1.15	1.18
11/21	1.11	1.13
12/21	1.10	1.11
Average	1.17	1.22

Table 5.4 Ratios of diffuse components on louver to those on south wall

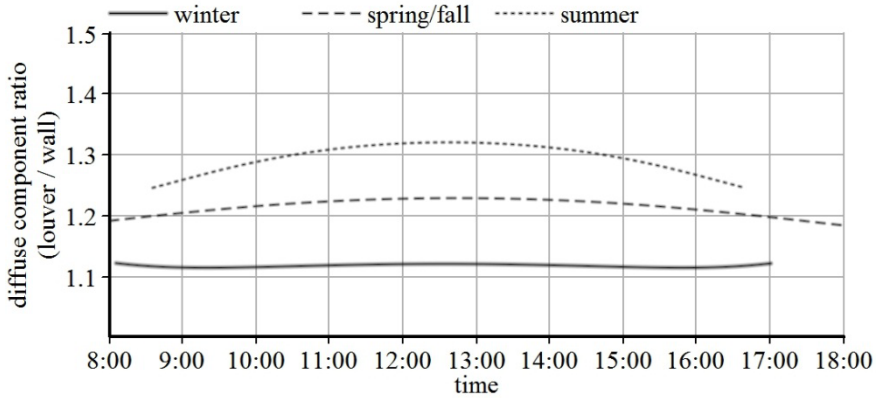

Figure 5.49 Ratio of the diffuse component of the solar radiation on the louver slats to that on the south wall

5.5.5 Effect of PV coating fraction

The disadvantage of self shading can be reduced by decreasing the PV coating fraction to the slat depth. For example, the yearly average direct component on the PV modules on an obstructed slat with regard to the direct normal component increases from 0.658 to 0.722 when the PV portion of the slat depth decreases from 0.5 to 0.3. The PV fraction of 0.3 is selected for

comparison because no shading on the louver PV modules occurs at solar noon on the summer solstice when the PV coating fraction is smaller than 0.322, which is the cosine value of the solar altitude at the moment. Table 5.5 lists the average direct component on the PV module of various PV fractions. Note that at the PV coating fraction of 1.0, the direct component on the PV modules on an obstructed slat is identical to that on the south wall (see the last entry of Table 5.5). This means that installing PV modules on the entire louver surface has no advantage over using the wall PV in terms of PV output.

The PV coating fraction has little effect on the the diffuse component on louver PV modules, as Table 5.6 shows.

PV coating fraction	Direct component on obstructed slat (ratio to direct normal)	Ratio of obstructed slat to unobstructed slat	Ratio of obstructed slat to wall
0.1	0.746	0.991	1.574
0.2	0.737	0.978	1.554
0.3	0.722	0.958	1.523
0.4	0.691	0.917	1.458
0.5	0.658	0.873	1.387
0.6	0.622	0.826	1.313
0.7	0.591	0.784	1.246
0.8	0.557	0.739	1.174
0.9	0.520	0.690	1.096
1.0	0.474	0.629	1.000

Table 5.5 Effect of PV coating fraction on the direct component of solar radiation on PV modules on an obstructed slat

PV coating fraction	Diffuse component on obstructed slat (ratio to horizontal)	Ratio of obstructed slat to unobstructed slat	Ratio of obstructed slat to wall
0.1	1.048	0.995	1.177
0.2	1.043	0.990	1.171
0.3	1.040	0.987	1.168
0.4	1.043	0.990	1.172
0.5	1.038	0.985	1.166
0.6	1.030	0.977	1.156
0.7	1.028	0.976	1.155
0.8	1.013	0.961	1.138
0.9	0.997	0.946	1.120
1.0	0.973	0.924	1.093

Table 5.6 Effect of PV coating fraction on the diffuse component of solar radiation on PV modules on an obstructed slat

5.6 Evaluation of ANN-based optimal angle

The estimated optimum was an approximation of the actual optimum; it served as the starting point for the physical local search. Without a predicted optimum, a physical global search, which can cause visual strain and inefficient louver PV control, must be performed instead of a local search. An accurate estimation of the optimal angle reduces the slat angle range of the physical local search, resulting in fewer angle adjustments and higher louver PV productivity.

According to the experiment results, the estimated optimal angle based on the ANN was close to the actual optimum. The average error of the ANN-based optimal angle for the PV only, the PV+WP, and the PV+WP+DGI methods was 6.5, 4.9, and 4.5 degrees, respectively. Therefore, the experiment results suggest that an accurately trained ANN can be used alone to control the slat angle, and that the trial-and-error control is unnecessary.

5.7 ANN training results

The ANN training data were collected using the swing control between 3/24 and 3/27/2012. The training period spanned ten hours (between 8am and 6pm) of each day. Section 4.5 describes the training data collection method using the swing control. Two of the four days were almost clear (3/25 and 3/26). The other two days were rainy (3/24) or partly cloudy (3/27). Figure 5.50 shows the exterior vertical illuminance representing daylight availability on 3/25/2012. Appendix A contains the exterior vertical illuminance graphs for the other days.

The ANN used for the experiment produced a close representation of the training data. The actual sensor measurements and the ANN-estimated values of the louver PV output (Figure 5.51), the work plane illuminance (Figure 5.52), and DGI (Figure 5.53) for 3/25/2012 are shown. The average error of the ANN for the entire training period was 1.11 mA (PV output), 54.6 lux (work plane illuminance), and 0.868 (DGI). To capture the effect of outliers, rooted mean squared error (RMSE) was also examined; the ANN error was 1.71 mA, 94.1 lux, and 1.28. The distribution of the ANN errors during the entire training period appears in Figure 5.54 (PV output), Figure 5.55 (work plane illuminance), and Figure 5.56 (DGI).

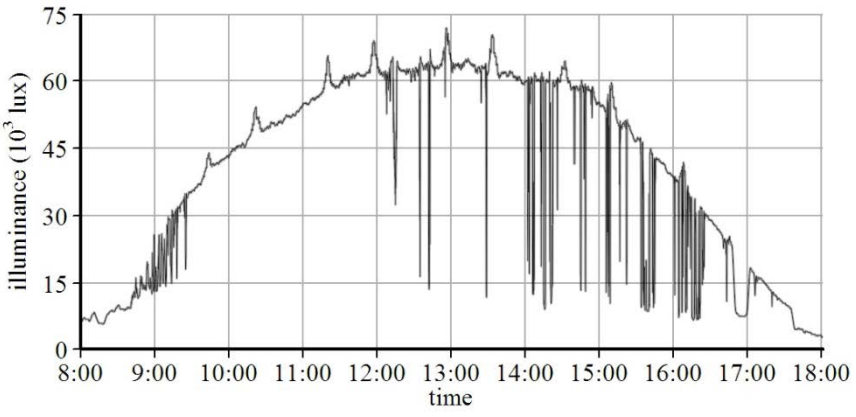

Figure 5.50 Exterior vertical illuminance on the second day of the ANN training period (3/25/2012)

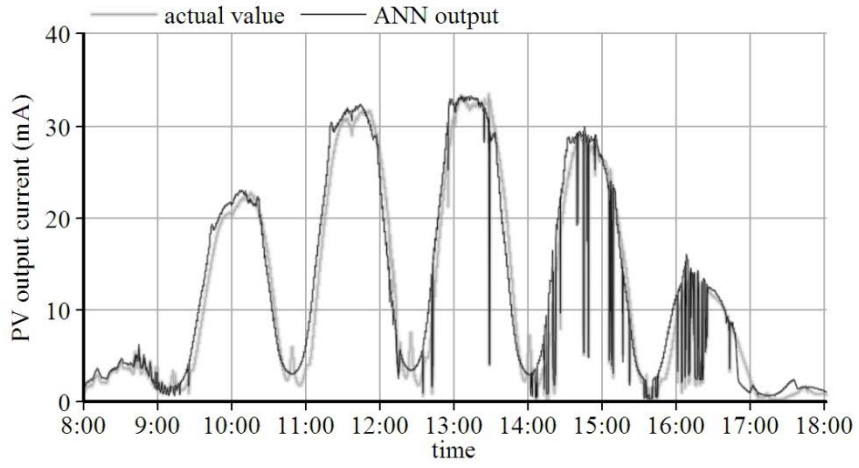

Figure 5.51 Measured (gray) and ANN-based (black) louver PV output (3/25/2012)

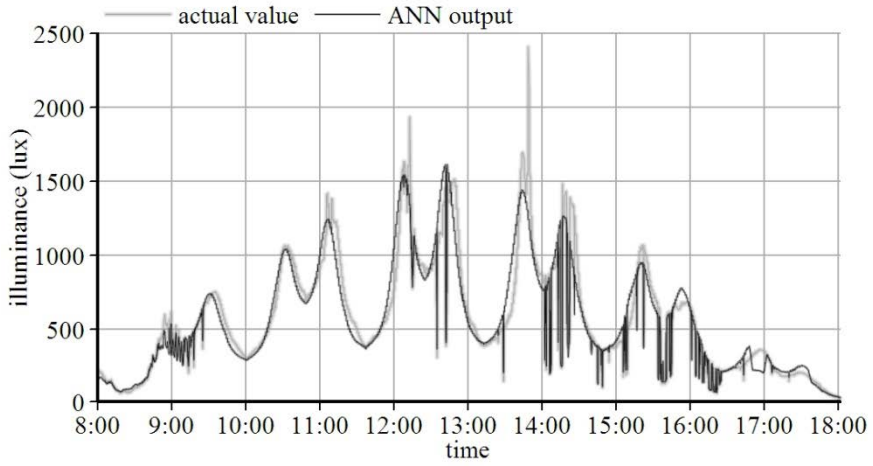

Figure 5.52 Measured (gray) and ANN-based (black) work plane illuminance (3/25/2012)

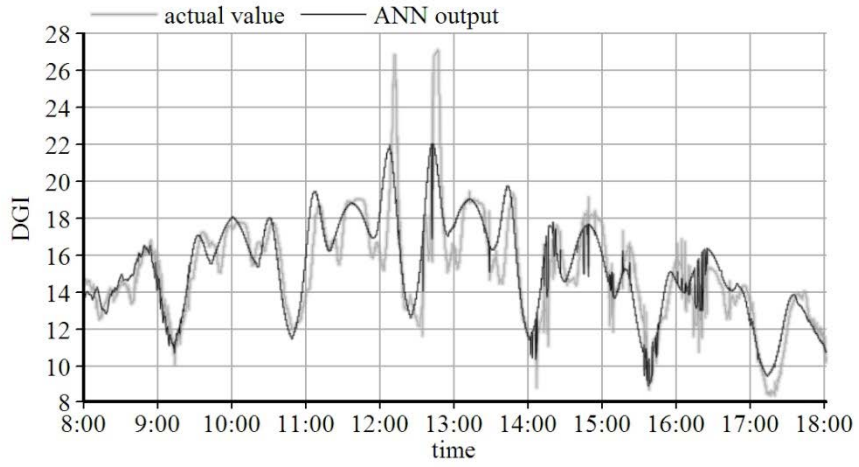

Figure 5.53 Measured (gray) and ANN-based (black) DGI (3/25/2012)

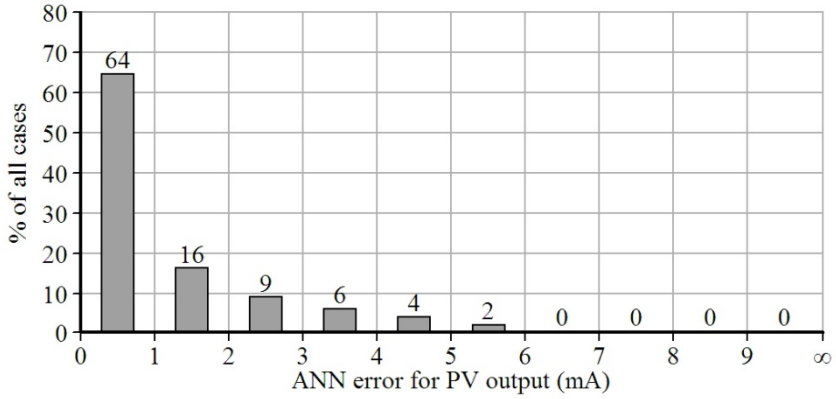

Figure 5.54 Distribution of ANN errors for PV output (3/24/2012~3/27/2012)

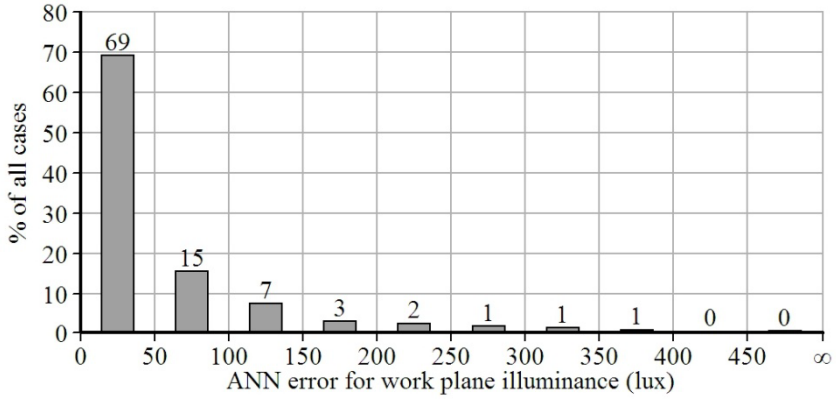

Figure 5.55 Distribution of ANN errors for work plane illuminance (3/24/2012~3/27/2012)

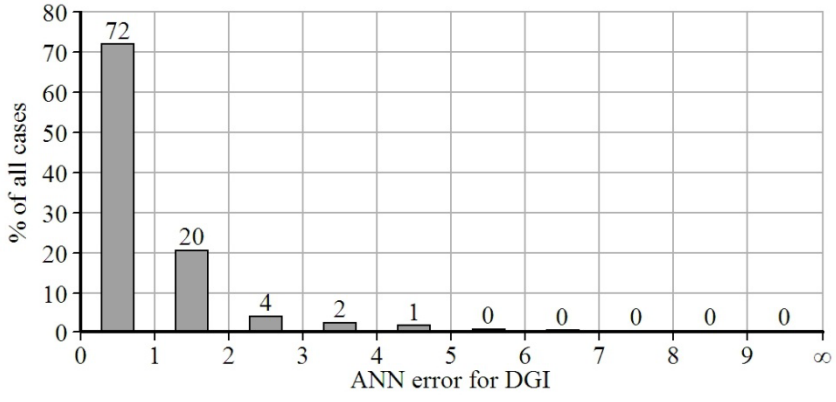

Figure 5.56 Distribution of ANN errors for DGI (3/24/2012~3/27/2012)

CHAPTER 6: CONCLUSIONS

This study investigated the framework for developing PVIS control methods and evaluated the performance of PVIS controlled using three different methods. The major findings were based on the experiments for quantitative evaluation of the PVIS control methods. Simulations were also conducted to test the validity of the experiment results and to evaluate the effect of PV self-shading and PV coating fraction. The PVIS design recommendations presented in this chapter are based on the findings.

6.1 Findings

This study investigated the performance of PVIS in terms of PV electricity output and visual comfort. Three control methods were devised and tested experimentally. The three methods had different optimization objectives and constraints: 1) to maximize the louver PV output without considering visual comfort (PV-only), 2) to maximize the louver PV output while maintaining an acceptable level of work plane illuminance (PV+WP), and 3) to maximize the louver PV output while maintaining an acceptable level of work plane illuminance and daylight glare (PV+WP+DGI).

PV output

The louver PV module generated more electricity than the wall-mounted PV module in all three control methods. The PV module on a louver slat controlled by the PV-only method generated

48% more electricity than the wall module. The PV+WP method and the PV+WP+DGI method resulted in 35% and 36% more electricity, respectively. The results for the PV-only method support the hypothesis that a PV module on an adjustable louver slat can generate more electricity per PV area than a wall-mounted module. Simulations of the irradiation on the louver PV and the wall PV also support this hypothesis. According to the simulations, however, the output of the PV modules installed on the entire surface of a louver slat would be similar to that of the wall PV output due to partial shading of the louver PV. Therefore, installing PV modules on the sunny area closer to the outer edge of louver slats is essential if the louver PV is to be more productive than the wall PV.

The louver PV outputs of the PV+WP and the PV+WP+DGI methods were lower than that of the PV-only method by 8.8% and 8.4%, respectively. The use of the work plane illuminance criterion caused the decrease by leading the system to use more solar radiation for natural lighting than for electricity conversion. The PV-only method, which aimed to maximize the louver PV output, always resulted in an unacceptably low work plane illuminance.

Work plane illuminance

For the control methods with visual comfort criteria (the PV+WP and PV+WP+DGI methods), the work plane illuminances were close to the acceptable level (500 lux) with an error of 50 lux. The duration above 450 lux for the PV+WP method was 7.86 hours a day, and that for the PV+WP+DGI method was 7.53 hours in the experiments conducted between 4/5/2012 and 4/8/2012. During the four hours after the solar noon, the work plane illuminance was above 450 lux for 95% of the period in the PV+WP method, and 99% in the PV+WP+DGI method. These

results indicate that setting the target work plane illuminance at a level higher than required, for instance to 550 lux, can effectively achieve an acceptable light level on the work plane.

DGI

While the louver PV output was being maximized, DGI always remained within the comfort range. This indicates that, for the given louver dimensions tested in this study, meeting the PV criterion simultaneously fulfills the daylight visual comfort requirement. In other words, a slat angle adjustment that increased the louver PV and blocked sunlight provided acceptable levels of DGI. In contrast, increasing the work plane illuminance usually resulted in higher levels of daylight glare.

Because the DGI criterion was practically inactive, the PV+WP method and the PV+WP+DGI method resulted in the same louver slat angles.

Total energy benefit

The energy benefit of PVIS using the PV+WP method was 1.91kWh/day, which represents 39.7% of the test building's daily lighting energy demand. 1.25kWh (26.0% of daily lighting energy demand) came from the electricity production of the louver PV modules, and 0.66kWh (13.7%) came from decreased use of electric lighting due to daylight admission. The energy benefit of the PV-only method was smaller than that of the PV+WP and the PV+WP+DGI methods: 1.38kWh/day, which amounts to 28.8% of the building's daily lighting energy demand.

ANN

Using ANN for PVIS control yielded reasonably accurate results. For the PV-only method, the average error of the ANN-based optimal angle was 6.5 degrees. For the PV+WP and the PV+WP+DGI methods, the average error was 4.9 and 4.5 degrees, respectively. The errors of the estimated optimum were determined based on the actual optimum found by the trial-and-error control that followed each ANN-based slat angle control. These results show that the actual optimum existed within two step angle adjustments from the optimum estimated by the ANN. The error of the estimated optimum was corrected by the trial-and-error control, which performed a physical local search using the scale model starting from the estimated optimum.

An ANN should be trained to accurately take into account the effects of slat angle, exterior light level, and sun position on PV output, work plane illuminance, and DGI. Training data must be filtered to exclude erroneous sensor measurements. An exterior illuminance sensor should be installed at a location where it can represent daylight availability on louver PV modules. It is advisable to use multiple sensors to avoid obtaining incorrect information about daylight availability due to local shading on the sensors. In addition, exterior light sensors should be installed where the effect of the reflected sunlight from the louver does not exist.

The trial-and-error control can be omitted when the ANN-based optimal angle is accurate enough for practical use. When the trial-and-error control is used, large angular changes of the slat angle may occur, especially during daylight fluctuation. The number of angle adjustments in a control cycle should be limited to prevent visual strain due to a large slat angle change.

The ANN parameters were determined through a sensitivity study. The learning rate of the ANN used for experiments was 0.01, and the momentum was 0.9. The ANN had two hidden layers, each of which had five neurons. Four variables were used for the input layer: the slat tilt angle, the exterior vertical illuminance, the solar altitude, and the solar azimuth. Three variables (the louver PV output, the work plane illuminance, and DGI) were used for the output layer.

Recommendations

The PV+WP+DGI method is suitable for PVIS control for maximum energy conservation. The PV-only method should be used whenever it is not necessary to consider visual comfort—for example, when a space is unoccupied.

The PV coverage ratio should be determined according to building location (especially latitude) and the corresponding yearly sun profile angle change to avoid self-shading of the PV surfaces.

6.2 Directions for future research

The experiments should be expanded to provide better support for the conclusions drawn in this study. Conducting experiments in the winter and the summer would give more accurate estimations of PVIS performance. The PV self-shading effect can be experimentally investigated during the summer, when such an effect is significant. Using an ANN trained during a different season and seeing how it adapts to the new environment would be also informative. In addition, experimentally identifying the effect of the constants in this study (e.g., PV coating fraction) would help in designing a PVIS.

Finally, the slat angle control algorithm needs to be improved, especially for daylight fluctuation. In the control methods used in this study, the ANN used the daylight level measured immediately before its feed-forward process. The ANN error was corrected by the trial-and-error control. However, the trial-and-error control can also be incorrect during daylight fluctuation. Therefore, future research should develop a better method of determining a slat angle during periods of daylight fluctuation.

APPENDICES

APPENDIX A: Exterior vertical illuminance during the ANN training period (3/24/2012~3/27/2012)

3/24/2012

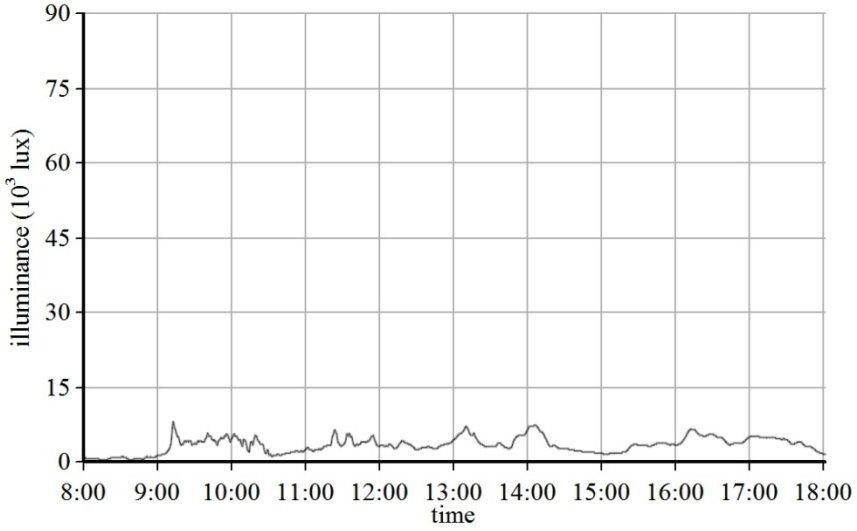

3/25/2012

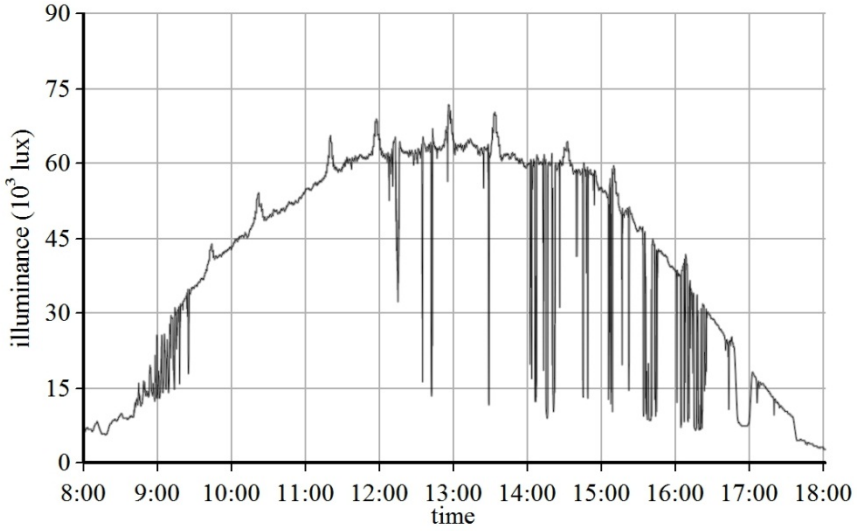

3/26/2012

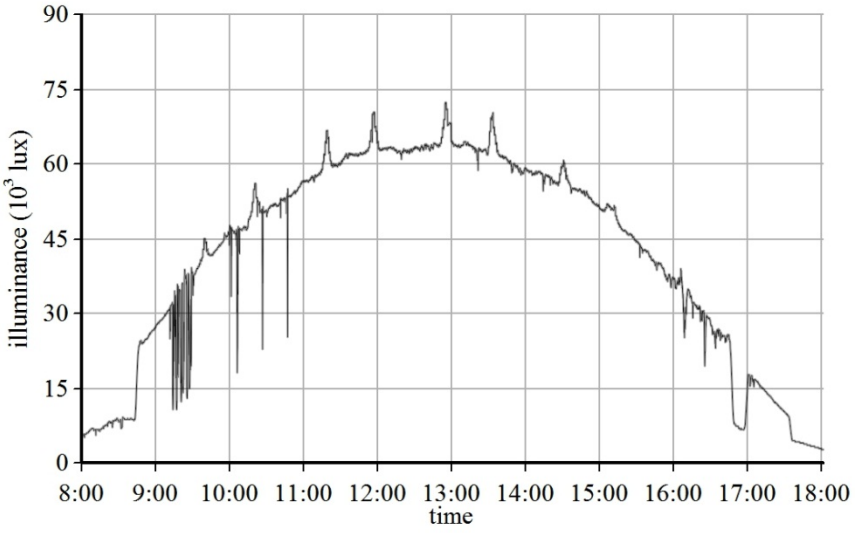

3/27/2012

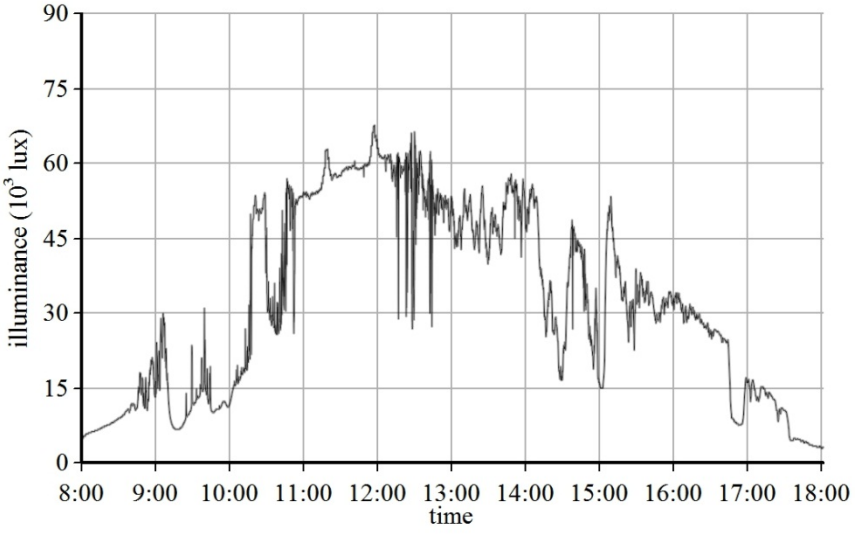

APPENDIX B: Estimated direct component of daylight on the louver PV and the wall PV with regard to the direct normal component

December

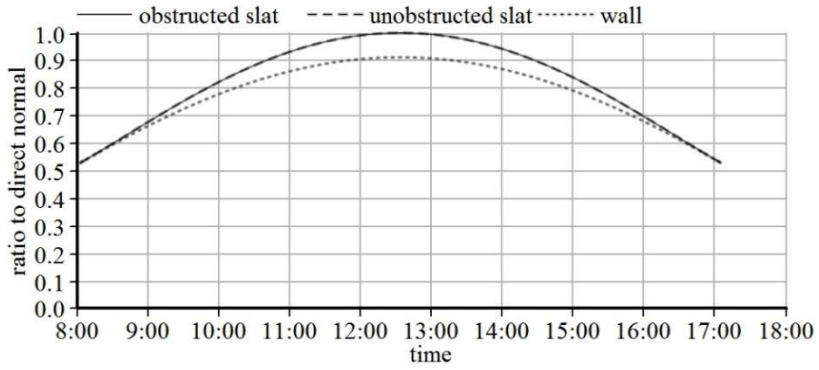

January

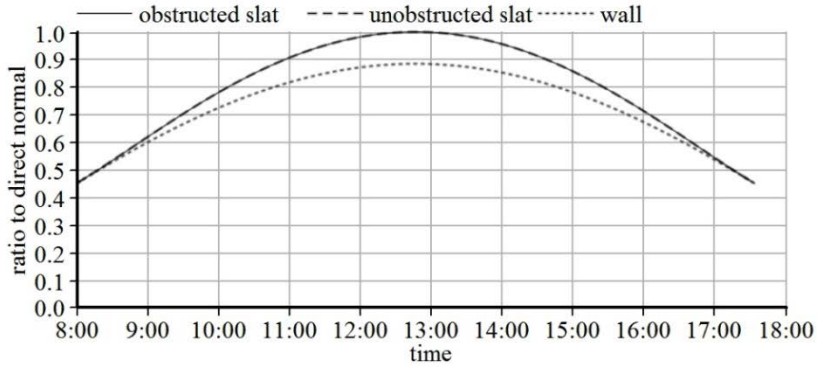

February

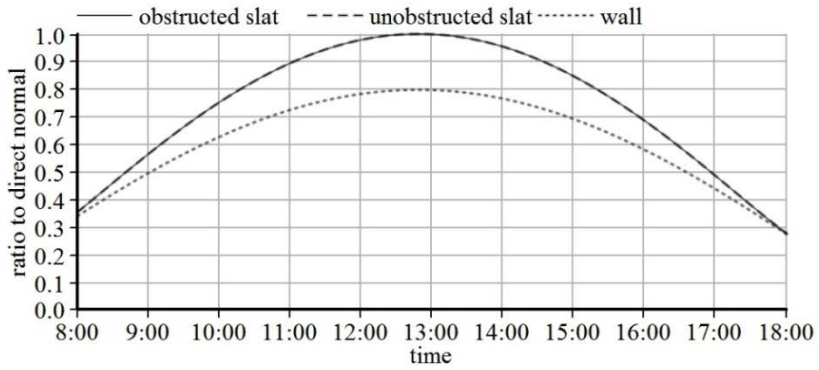

March

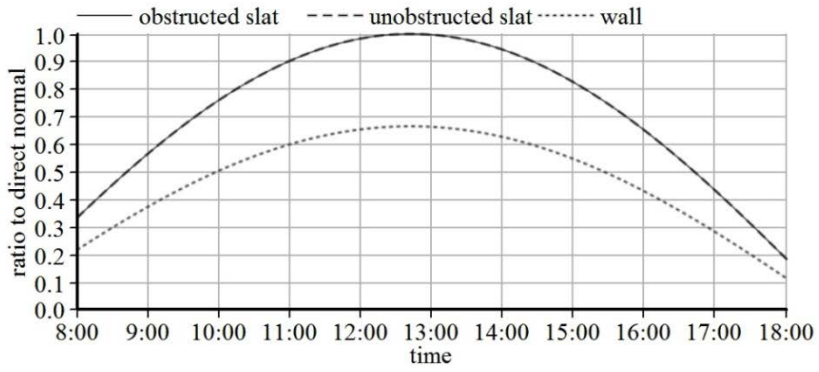

April

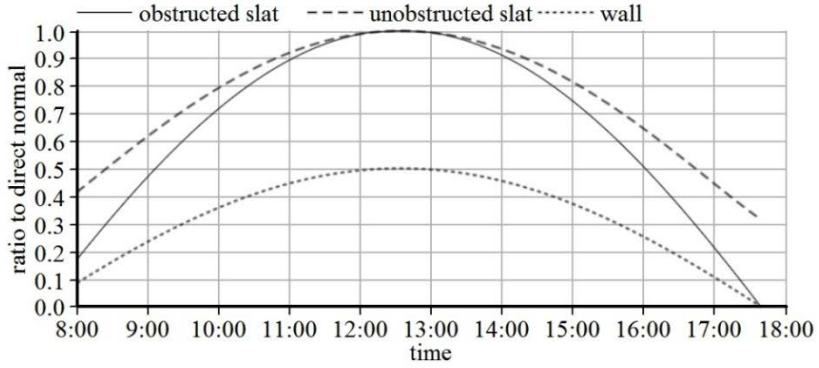

May

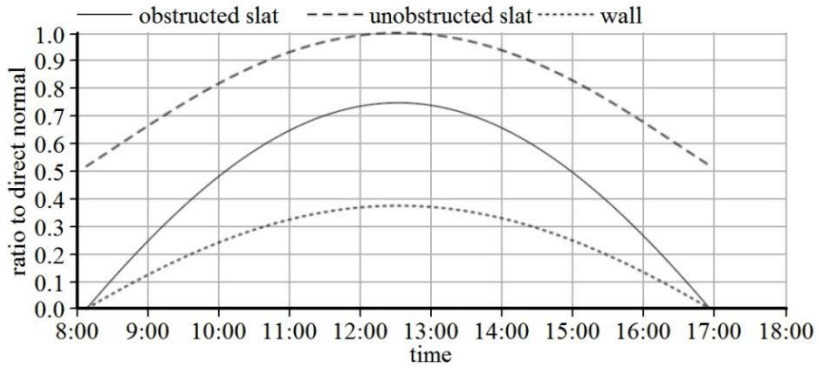

June

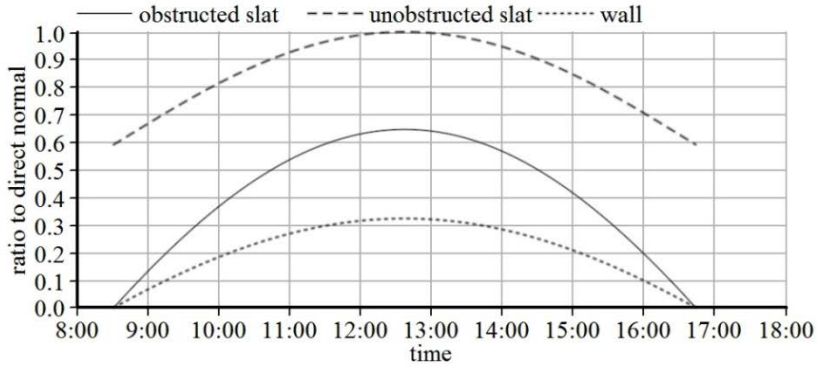

APPENDIX C: Slat angle region of PV partial shading and direct sunlight into interior space

December

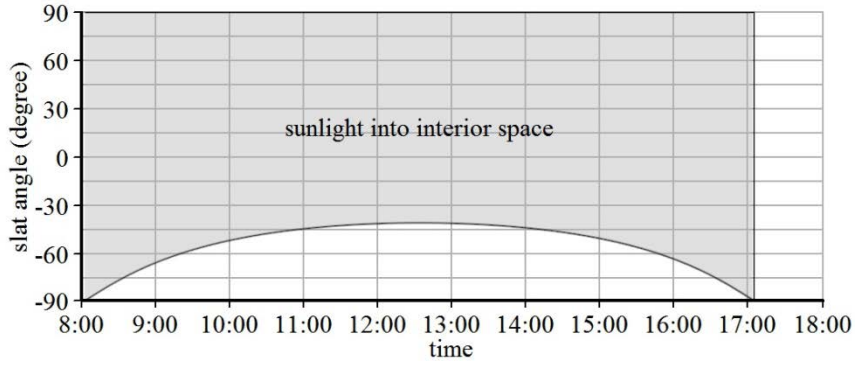

January

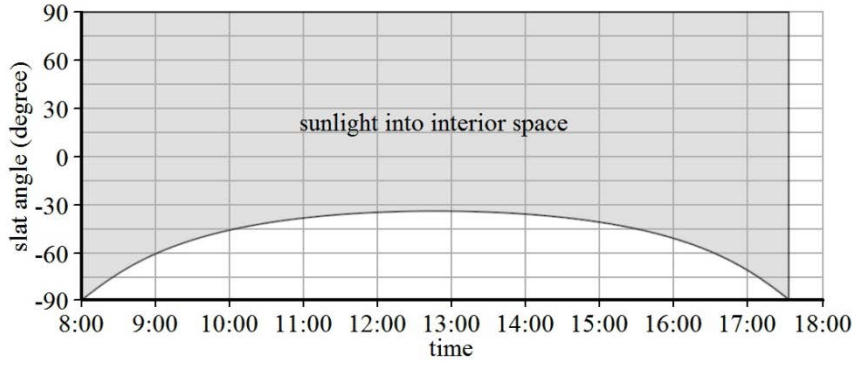

February

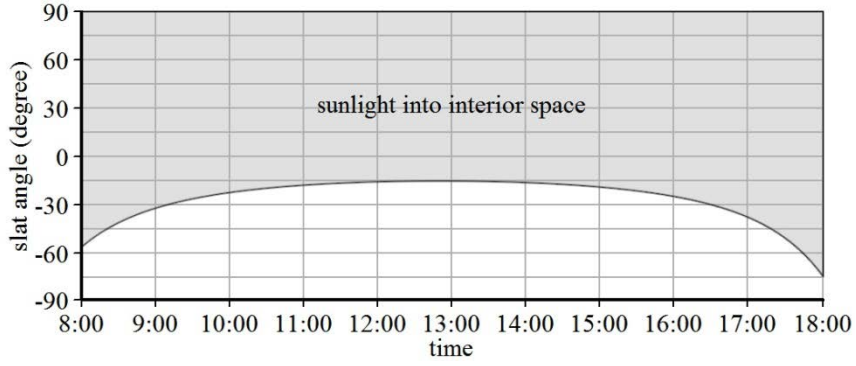

March

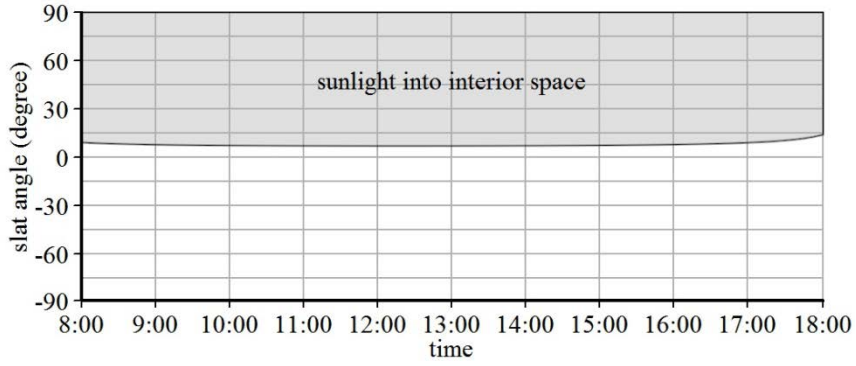

April

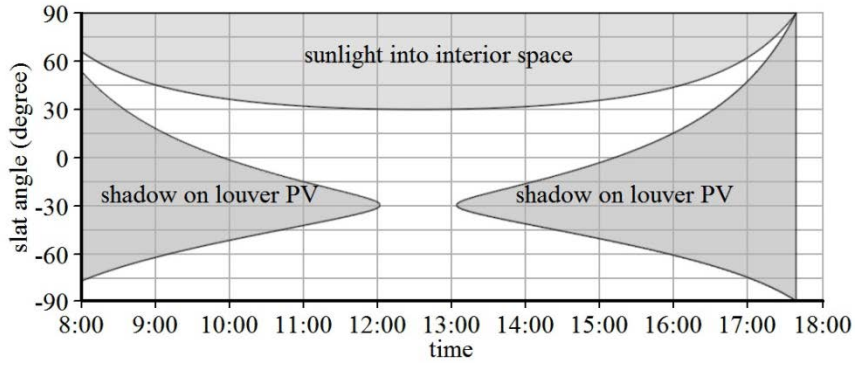

May

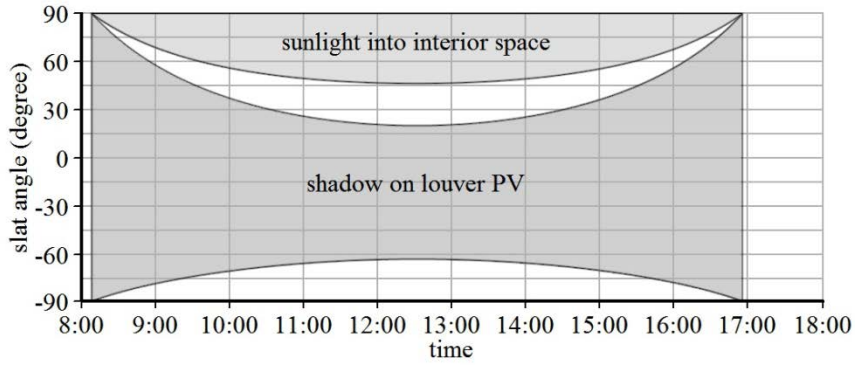

June

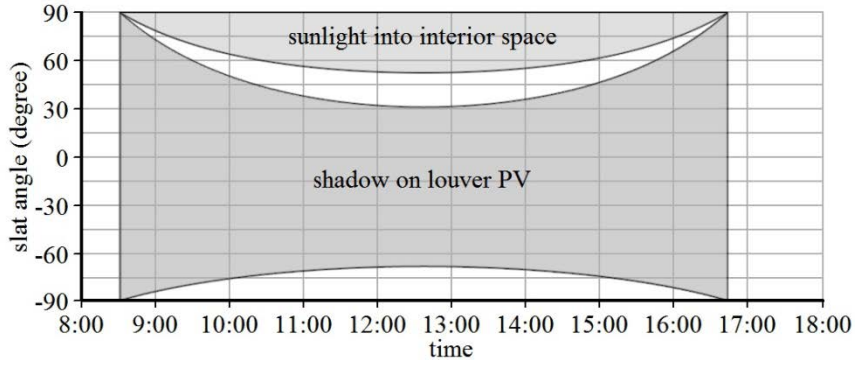

APPENDIX D: Exterior vertical illuminance during the optimal control method experiments

PV only method (4/5/2012)

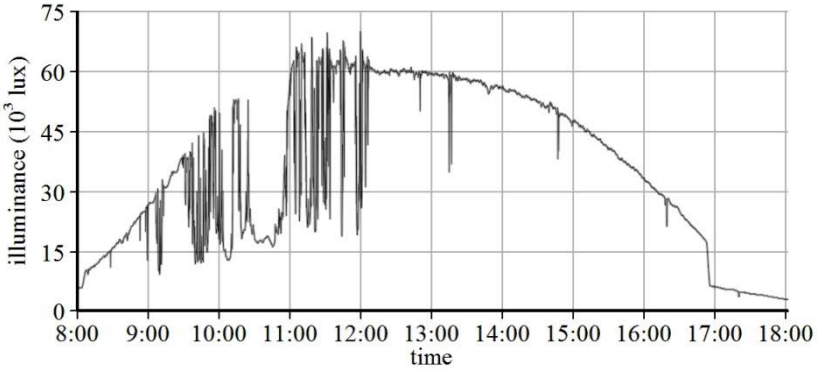

PV+WP method (4/7/2012)

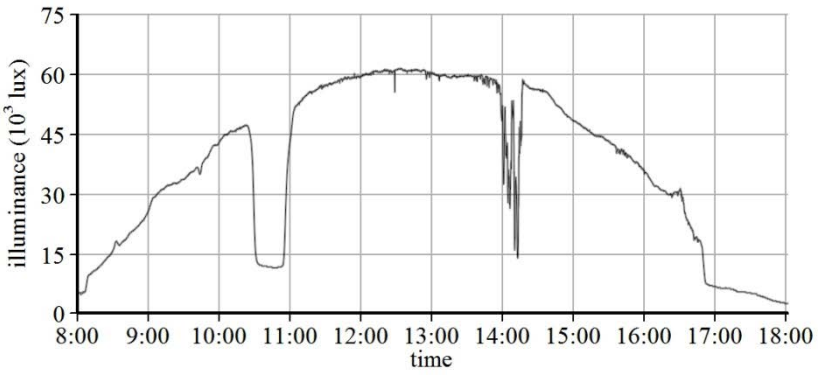

PV+WP+DGI method (4/8/2012)

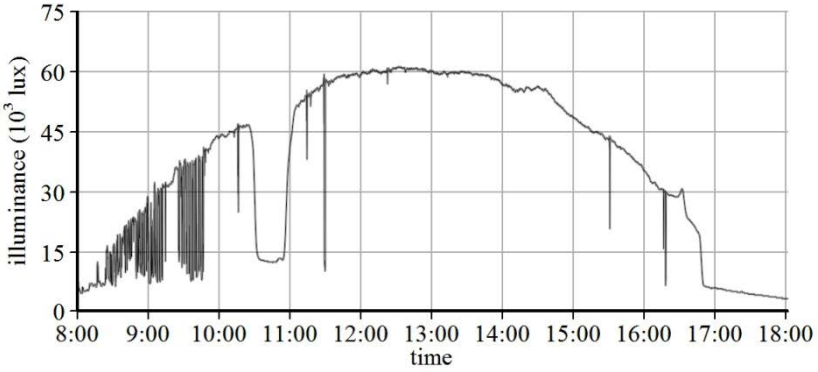

REFERENCES

Archer, M. D., & Hill, R. (2001). *Clean electricity from photovoltaics*. London: Imperial College Press.

Atmel Corporation. (2010). *ATmega16/ATmega16L datasheet.* Retrieved from http://www.atmel.com/Images/doc2466.pdf

Boyce, P., Hunter, C., & Howlett, O. (2003). The benefits of daylight through windows. *Troy, New York: Rensselaer Polytechnic Institute*.

Brendel, R., Werner, J. H., & Queisser, H. J. (1996). Thermodynamic efficiency limits for semiconductor solar cells with carrier multiplication. *Solar energy materials and solar cells*, *41*, 419-425.

Chen, C., Duan, S., Cai, T., & Liu, B. (2011). Online 24-h solar power forecasting based on weather type classification using artificial neural network. *Solar Energy*, *85*(11), 2856-2870.

CIBSE. (2000). *TM25 Understanding building photovoltaics*. London: The Chartered Institution of Building Services Engineers.

CIE. (2003). *Spatial distribution of daylight – CIE standard general sky.* Commision Internationale de l'Eclairage.

Edwards, L., and Torcellini, P. (2002). *A literature review of the effects of natural light on building occupants*. Golden, CO: National Renewable Energy Laboratory.

Fanney, A. H., Dougherty, B. P., & Davis, M. W. (2002). Performance and characterization of building integrated photovoltaic panels. In *Photovoltaic Specialists Conference, 2002. Conference Record of the Twenty-Ninth IEEE* (pp. 1493-1496). IEEE.

Fisekis, K., Davies, M., Kolokotroni, M., & Langford, P. (2003). Prediction of discomfort glare from windows. *Lighting Research and Technology*, *35*(4), 360-369.

Galasiu, A. D., Atif, M. R., & MacDonald, R. A. (2004). Impact of window blinds on daylight-linked dimming and automatic on/off lighting controls. *Solar Energy-Journal of the International Solar Energy Society*, *76*(5), 523-544.

Galasiu, A. D., & Veitch, J. A. (2006). Occupant preferences and satisfaction with the luminous environment and control systems in daylit offices: a literature review. *Energy and Buildings*, *38*(7), 728-742.

Golden, R. M. (1996). *Mathematical methods for neural network analysis and design*. Cambridge, Mass.: The MIT Press.

Green, M. A., Emery, K., Hishikawa, Y., & Warta, W. (2011). Solar cell efficiency tables (version 37). *Progress in photovoltaics: research and applications*, *19*(1), 84-92.

Hachem, C., Athienitis, A., & Fazio, P. (2011). Parametric investigation of geometric form effects on solar potential of housing units. *Solar Energy*, *85*(9), 1864-1877.

Hopkinson, R. G. (1963). *Architectural Physics: Lighting*. London: H. M. Stationery Office.

IEEE Computer Society. (2006). *IEEE Standard 802.15.4-2006 (Revision of IEEE Standard 802.15.4-2003)*. New York, NY: IEEE

Ihm, P., Nemri, A., & Krarti, M. (2009). Estimation of lighting energy savings from daylighting. *Building and Environment*, *44*(3), 509-514.

Inoue, T. (2003). Solar shading and daylighting by means of autonomous responsive dimming glass: practical application. *Energy and buildings*, *35*(5), 463-471.

Ishaque, K., & Salam, Z. (2011). A comprehensive MATLAB Simulink PV system simulator with partial shading capability based on two-diode model. *Solar Energy*, *85*(9), 2217-2227.

James, P. A. B., Jentsch, M. F., & Bahaj, A. S. (2009). Quantifying the added value of BiPV as a shading solution in atria. *Solar Energy*, *83*(2), 220-231.

Kalogirou, S. A. (2001). Artificial neural networks in renewable energy systems applications: a review. *Renewable and sustainable energy reviews*, *5*(4), 373-401.

Kalogirou, S. A., & Bojic, M. (2000). Artificial neural networks for the prediction of the energy consumption of a passive solar building. *Energy*, *25*(5), 479-491.

Kazmerski, L. L. (1997). Photovoltaics: a review of cell and module technologies. *Renewable and sustainable energy reviews*, *1*(1), 71-170.

Kim, J. J., & Gerow, J. (2013). Feasibility of Zero Energy Homes. In *ICSDEC 2012: Developing the Frontier of Sustainable Design, Engineering, and Construction* (pp. 877-884). ASCE.

Kim, J. J., Jung, S. K., Choi, Y. S., & Kim, J. T. (2010). Optimization of photovoltaic integrated shading devices. *Indoor and Built Environment*, *19*(1), 114-122.

Kolokotsa, D., Rovas, D., Kosmatopoulos, E., & Kalaitzakis, K. (2011). A roadmap towards intelligent net zero- and positive-energy buildings. *Solar energy*, 85(12), 3067-3084

Leather, P., Pyrgas, M., Beale, D., & Lawrence, C. (1998). Windows in the Workplace Sunlight, View, and Occupational Stress. *Environment and Behavior*, 30(6), 739-762

Li, D. H. W., Lam, T. N. T., & Wong, S. L. (2006). Lighting and energy performance for an office using high frequency dimming controls. *Energy Conversion and Management*, *47*(9), 1133-1145.

Lin, G. H., & Carlson, D. E. (2000). Photovoltaics in the year 2025. *International journal of hydrogen energy*, *25*(9), 807-811.

Ma, R. H., & Chen, Y. C. (2011). BIPV-powered smart windows utilizing photovoltaic and electrochromic devices. *Sensors*, *12*(1), 359-372.

Maniccia, D., Rutledge, B., Rea, M. S., & Morrow, W. (1999). Occupant use of manual lighting controls in private offices. *Journal of the Illuminating Engineering Society*, *28*(2), 42-56.

Moon, J. W., & Kim, J. J. (2010). ANN-based thermal control models for residential buildings. *Building and Environment*, *45*(7), 1612-1625.

Mozer, M. C. (1998). The neural network house: An environment that adapts to its inhabitants. In *Proc. AAAI Spring Symp. Intelligent Environments* (pp. 110-114).

Murdoch, J., Harrold, R., & Goldsbury, C. J. (Eds.). (1996). *IESNA lighting ready reference: a compendium of vision & optical control, light source tables, illuminance recommendations, calculation data, energy management considerations, cost analysis methods, selection procedures, definitions.(3rd ed.)*. New York, NY: Illuminating Engineering Society of North America.

National Oceanic & Atmospheric Administration. (2014, July 29). *Solar calculation details.* Retrieved from http://www.esrl.noaa.gov/gmd/grad/solcalc/calcdetails.html

National Renewable Energy Laboratory. (2014, July 29). *PVWatts calculator.* Retrieved from http://pvwatts.nrel.gov/pvwatts.php

National Renewable Energy Laboratory. (2013, February 19). *Solar cell efficiency chart.* Retrieved from http://www.nrel.gov/ncpv/images/efficiency_chart.jpg

Nicol, F., Wilson, M., & Chiancarella, C. (2006). Using field measurements of desktop illuminance in European offices to investigate its dependence on outdoor conditions and

its effect on occupant satisfaction, and the use of lights and blinds. *Energy and Buildings*, *38*(7), 802-813.

Nielsen, M. V., Svendsen, S., & Jensen, L. B. (2011). Quantifying the potential of automated dynamic solar shading in office buildings through integrated simulations of energy and daylight. *Solar Energy*, *85*(5), 757-768.

Radhi, H. (2010). Energy analysis of façade-integrated photovoltaic systems applied to UAE commercial buildings. *Solar Energy*, *84*(12), 2009-2021.

Rea, M. S. (1984). Window blind occlusion: a pilot study. *Building and Environment*, *19*(2), 133-137.

Reed, R. D., & Marks, R. J. (1999). *Neural smithing: supervised learning in feedforward artificial neural networks*. Cambridge, Mass.: The MIT Press.

Reinders, A. H. M. E., van Dijk, V. A. P., Wiemken, E., & Turkenburg, W. C. (1999). Technical and economic analysis of grid-connected PV systems by means of simulation. *Progress in Photovoltaics: research and applications*, *7*(1), 71-82.

Reinhart, C. F. (2004). Lightswitch-2002: a model for manual and automated control of electric lighting and blinds. *Solar Energy*, *77*(1), 15-28.

Reinhart, C. F., & Voss, K. (2003). Monitoring manual control of electric lighting and blinds. *Lighting Research and Technology*, *35*(3), 243-258.

Roisin, B., Bodart, M., Deneyer, A., & D'herdt, P. (2008). Lighting energy savings in offices using different control systems and their real consumption. *Energy and Buildings*, *40*(4), 514-523.

Roman, E., Martinez, V., Jimeno, J. C., Alonso, R., Ibanez, P., & Elorduizapatarietxe, S. (2008). Experimental results of controlled PV module for building integrated PV systems. *Solar Energy*, *82*(5), 471-480.

Rubin, A. I., Collins, B. L., & Tibbott, R. L. (1978). *Window blinds as a potential energy saver: A case study*. US Department of Commerce, National Bureau of Standards.

Schoen, T. J. N. (2001). Building-integrated PV installations in the Netherlands: examples and operational experiences. *Solar energy*, *70*(6), 467-477.

Stamenic, L., Smiley, E., & Karim, K. (2004). Low light conditions modelling for building integrated photovoltaic (BIPV) systems. *Solar Energy*, *77*(1), 37-45.

Texas Instruments. (2003). *OPT101: Monolithic photodiode and single-supply transimpedance amplifier*. Retrieved from http://www.ti.com/product/opt101

US Energy Information Administration. (2003). *Commercial Buildings Energy Consumption Survey (CBECS).* Retrieved from http://www.eia.gov/consumption/commercial/

Vine, E., Lee, E., Clear, R., DiBartolomeo, D., & Selkowitz, S. (1998). Office worker response to an automated venetian blind and electric lighting system: a pilot study. *Energy and buildings*, *28*(2), 205-218.

Yang, H., Zheng, G., Lou, C., An, D., & Burnett, J. (2004). Grid-connected building-integrated photovoltaics: a Hong Kong case study. *Solar energy*, *76*(1), 55-59.

Yoo, S. H. (2011). Simulation for an optimal application of BIPV through parameter variation. *Solar Energy*, *85*(7), 1291-1301.

Yoo, S. H., & Manz, H. (2011). Available remodeling simulation for a BIPV as a shading device. *Solar Energy Materials and Solar Cells*, *95*(1), 394-397.

Yoon, J. H., Song, J., & Lee, S. J. (2011). Practical application of building integrated photovoltaic (BIPV) system using transparent amorphous silicon thin-film PV module. *Solar Energy*, *85*(5), 723-733.

Yun, G. Y., McEvoy, M., & Steemers, K. (2007). Design and overall energy performance of a ventilated photovoltaic façade. *Solar Energy*, *81*(3), 383-394.